12-2012

CO2 Injection Into a Deep Saline Aquifer: Porosity Measurements, Numerical Modeling, and Costs Associated with Uncertainty of Petrophysical Parameters

Michael John Gragg
mgragg1@utk.edu

To the Graduate Council:

I am submitting herewith a thesis written by Michael John Gragg entitled "CO2 Injection Into a Deep Saline Aquifer: Porosity Measurements, Numerical Modeling, and Costs Associated with Uncertainty of Petrophysical Parameters." I have examined the final electronic copy of this thesis for form and content and recommend that it be accepted in partial fulfillment of the requirements for the degree of Master of Science, with a major in Geology.

Edmund Perfect, Major Professor

We have read this thesis and recommend its acceptance:

Larry D. McKay, Peter J. Lemiszki

Accepted for the Council:
Carolyn R. Hodges

Vice Provost and Dean of the Graduate School

(Original signatures are on file with official student records.)

CO_2 Injection Into a Deep Saline Aquifer: Porosity Measurements, Numerical Modeling, and Costs Associated with Uncertainty of Petrophysical Parameters

A Thesis Presented for the Master of Science Degree
The University of Tennessee, Knoxville

Michael John Gragg
December 2012

Acknowledgments

I would first like to thank my wife, Gretchen, for her unending support through the years of education that have brought me here. She has encouraged me, taken care of our boys, and at times completely supported us financially. Without her none of this would have been possible. I would also like to thank my two boys, Elijah and Yohan, for the joy that they bring into my life. Also, my parents, John and Elizabeth, deserve a huge thank you for supporting my interests and me as I was growing up.

Dr. Edmund Perfect has been a wonderful advisor and holds an enormous amount of my gratitude for his guidance and patience over the past few years. From the first time I visited with him, over a year before starting graduate school, he has been helpful and kind, directing me through the transition from undergraduate to graduate student. I would also like to thank Chu-Lin "Mike" Cheng for all of his help with the STOMP simulator, for sharing his expertise, advice, teakettle, and for helping me find answers to my many questions. Ken Christle also deserves a huge thank you for helping run some of the STOMP simulations over the summer of 2012 and helping to trouble shoot when problems arose. Thanks also to my committee members, Dr. Larry McKay and Dr. Peter Lemiszki, for their timely replies to my questions and many helpful suggestions. Thanks to Dr. Colin Sumrall and Will Atwood for providing training and use of the NextEngine 3D desktop laser scanner. I would also like to thank the faculty and graduate students of the Earth and Planetary Sciences Department at UT for making my time in Knoxville so enjoyable.

My funding, for which I am eternally grateful, has come from the University of Tennessee, Knoxville, Earth and Planetary Sciences Department and from the Tennessee Division of Geology.

Abstract

Anthropogenic levels of atmospheric greenhouse gases, particularly carbon dioxide (CO_2) have increased rapidly over the last several decades and coincide with rising temperatures globally. One possible solution is to capture CO_2 before it is released into the atmosphere by large point sources, such as fossil fuel power plants. Once captured, the CO_2 can be condensed and transported to a storage facility. Of the available options for storage of condensed CO_2, geologic sequestration in deep saline aquifers is considered the most viable option.

Porosity measurements were obtained for nearly 100 core samples of the Knox and Stones River groups from the middle Tennessee area as part of a larger project for the Tennessee Division of Geology, characterizing the potential for geologic CO_2 sequestration in Tennessee. Certain formations within these groups were found to exhibit higher porosity (higher storage potential) than others. Measured porosity values were quite low, ranging from 0.21 – 10.67 % with a median value of 1.21 %. These data can be used to aid in the decision-making process concerning possible geologic targets for geologic CO_2 sequestration in Tennessee.

A sensitivity analysis was also performed using a numerical model for geologic carbon sequestration (STOMP). Intrinsic permeability, porosity, pore compressibility, the van Genuchten residual liquid saturation, α and *m* parameters, and the Brooks and Corey residual liquid and gas saturations were varied independently and their influence on CO_2 storage was determined. Changes in costs based on the parameter variations were calculated to evaluate the relative importance of the various parameters. The most influential parameters were intrinsic permeability, the van Genuchten *m* parameter, and

the Brooks and Corey residual gas saturation. These results highlight the need for accurate measurement of intrinsic permeability and capillary pressure-saturation parameters in addition to more commonly measured properties like porosity.

Table of Contents

List of Tables

Table **Page**

List of Figures

Chapter 1 – General Introduction

Anthropogenic levels of atmospheric greenhouse gases, particularly carbon dioxide (CO_2), have increased rapidly over the last several decades and coincide with rising temperatures globally. According to Sundquist et al. (2008), CO_2 concentrations in the atmosphere have risen from around 280 ppm to over 380 ppm in the last 250 years, inducing measureable increases in global temperature. Concerns over regional air quality and global warming have resulted in the need to evaluate alternative methods for dealing with CO_2 and other airborne emissions from various sources. One possible alternative is to capture CO_2 before it is released into the atmosphere by large point sources such as fossil fuel power plants and cement operations. Once captured, the CO_2 can be condensed and transported to a storage facility. There are several options for storing condensed CO_2 including mineralization in the form of stable carbonates, deep ocean sequestration, and sequestration in geologic material at depth. Of these, geologic storage is considered the most viable option (Yang et al., 2010; Celia and Nordbotten, 2009). In order for site specific or regional investigations to take place a basic understanding of the available geologic reservoirs and their hydraulic and storage properties is required.

There are several options for deep geologic storage: depleted oil and gas reservoirs; unmineable coal seams; and deep saline aquifers. The technology for carbon capture and storage already exists and is currently implemented by the oil and natural gas industries for enhanced oil and natural gas recovery as well as for temporary storage of natural gas (Solomon et al., 2008; Pacala and Socolow, 2004). Carbon dioxide stored in unmineable coal beds can enhance coal bed methane extraction while sequestering the CO_2 through displacement of the methane (Klara et al., 2003). Finally, deep saline aquifers seem to be

the most attractive targets for carbon sequestration since they are normally unused due to high salinity, typically have high storage capacity, and are readily available (Yang et al., 2010; Pruess et al., 2003).

In order for a deep saline reservoir to function as a storage site the CO_2 must meet several requirements. One of these requirements is that the target unit is at a minimum depth of 800 meters (2625 feet). This ensures the best storage conditions by assuring that the CO_2 remains in a supercritical state at which CO_2 becomes dense like a liquid with gas-like viscosity, allowing a much higher mass of CO_2 to be stored in a given volume. Also, CO_2 must remain in the formation for many years. This is accomplished by several trapping mechanisms that operate on differing time and spatial scales. These mechanisms include structural and stratigraphic trapping, residual gas trapping, solubility trapping, and mineral trapping (Bradshaw et al., 2007). Structural and stratigraphic traps exist due to the geologic structures within the reservoir (folds, faults, etc.) and the buoyancy contrast between the CO_2 and surrounding brine. Residual gas trapping takes place as CO_2 becomes trapped in the pore space of the reservoir rock as the plume migrates away from the injection well. Over the course of many years, as the CO_2 migrates, it also begins to dissolve into the reservoir brine. This is known as solubility trapping. Over large time scales mineral trapping can become substantial as the CO_2 chemically reacts with the reservoir rock minerals and the brine. These trapping mechanisms are summarized in table 1, which was modified from Bradshaw et al. (2007).

This thesis focuses on geologic sequestration of CO_2 in deep saline aquifers and is divided into several sections. The first section centers around porosity measurements made for the Tennessee Division of Geology as part of a larger project (Subcontract

#32701-00962, Edison Record ID 28407) to estimate the potential for geologic carbon sequestration in Tennessee. This project involved nearly 100 core samples from the middle Tennessee area taken from the Knox and Stones River groups, consisting predominantly of carbonate rocks (limestones and dolostones with minor sandstones and shales). Measurements involved creating a three-dimensional scan of each core in order to obtain bulk volume data and weighing each sample under both oven-dry and water-saturated conditions in order to determine the porosity of each sample.

The overall goal of the first section was to characterize prospective geologic reservoirs in Tennessee. This goal can be broken down into two main objectives:

- Measurement of matrix porosity of rock cores from units of interest
- Identification of specific formations of high potential storage volume

The hypothesis for the project was simply that measured porosity values would be significantly higher for some formations than others.

The second section focuses on a sensitivity analysis of a numerical model for geologic carbon sequestration (STOMP), to examine the relative influence of input parameters on CO_2 storage. In this section multiple petrophysical input parameters were varied independently. The parameters investigated were intrinsic permeability, porosity, pore compressibility, the van Genuchten α parameter, the van Genuchten *m* parameter, the van Genuchten residual liquid saturation, the Brooks and Corey residual liquid saturation, and the residual gas saturation. The model outputs were analyzed to quantify the impact of geologic heterogeneity and measurement accuracy on injection costs.

The goal of this research was to examine the relative importance of different input parameters for numerical simulation of CO_2 storage in geologic reservoirs. This will help

future researchers focus on obtaining accurate estimates of parameters that have the greatest effect on the simulation while spending less time and money on those which are less significant. This study should help to:

- Identify parameters that have the greatest impact on simulation results (these influential parameters should therefore be most accurately estimated);
- Identify parameters that are less influential to the simulation results (these parameters could therefore be less accurately estimated);
- Demonstrate the usefulness of numerical models in predicting costs associated carbon dioxide capture and storage.

These objectives can be rewritten in the form of two hypotheses. First, that certain parameters, most likely intrinsic permeability and porosity, will show significantly more influence on model outputs than others. Second, that variations of influential parameters will result in significant changes in the cost of CO_2 injection.

The final section summarizes conclusions of the study and outlines possible directions for future work.

Chapter 2 – Determination of Porosity

2.1 Introduction

Porosity, defined as the ratio of void space within a rock to the total rock volume, is of great importance in regards to storage volume potential. This void volume is the basis for estimating the amount of a given substance, such as supercritical CO_2, that can be stored within a reservoir. There are multiple methods for measuring porosity including mercury intrusion porosimetry, gas expansion, computed tomography and the wet and dry weight method, described later in this chapter (Franklin, 1972; Goldstrand et al., 1995; Kazimierz et al., 2004).

Because porosity is a basic petrophysical parameter required for modeling injection of CO_2 into an aquifer, an estimate of porosity is required before beginning any simulation. Estimates of porosity can come from the literature or from some form of measurement. For example, some researchers have used computed tomography to estimate porosity changes due to different CO_2 injection rates (Izgec et al., 2005). Others have used geophysical data from injection wells calibrated to porosity measurements from core samples to determine inputs for numerical models of the Frio Brine Test pilot site in Texas, USA (Sakurai et al., 2005; Doughty et al., 2008). Similarly, Gupta et al. (2008) measured porosity for the Rose Run and Copper Ridge Formations in the Ohio River Valley from geophysical logs and from core samples using mercury injection. Conversely, in their analysis of basin-scale storage potential, Szulczewski and Juanes (2009) estimated the porosity of the Fox Hill sandstone in the Powder River Basin using the only available published estimate. Recently, Koperna et al. (2012) used geophysical data as well as core samples to determine porosity of the Paluxy sandstone at the SECARB Anthropogenic Test R&D site near Bucks, Alabama, USA.

In more theoretical approaches an estimation of porosity is used with the assumption that this value falls within an acceptable range of porosity values, typically between 10% and 20% (Pruess et al., 2002). Regardless of the methods used, an estimation of porosity is absolutely necessary for simulating geologic sequestration of CO_2 in saline aquifers.

Simply put, an understanding of the petrophysical properties of available geologic reservoirs is necessary for any regional or site-specific study to take place. To that end, porosity measurements on core samples were made as part of a larger project through the Tennessee Division of Geology to characterize the potential for geologic carbon storage in Tennessee. These porosity values are needed to evaluate the volume of CO_2 that can be stored within a given geologic formation

The overall goal of the project was to characterize prospective geologic reservoirs in Tennessee. This goal was broken down into several objectives:

- Measurement of matrix porosity of rock core from units of interest
- Identification of specific formations of high potential storage volume

The hypothesis for the project was simply that measured porosity values would be significantly higher for some formations than others.

For this first study the Knox (K) and Stones River (SR) groups, west of the Cumberland Plateau-Valley and Ridge province boundary, were considered to be the most promising storage assessment units (SAU) in Tennessee (see figure 1). Little to no data currently exists for the rock units of interest within the study area, making basic measurements, such as porosity, extremely valuable. Part or all of the K-SR SAU's, which consists predominantly of carbonate rocks (limestones and dolostones with minor sandstones and shales), was sampled from six separate cores: Dupont geohydrological

survey well (Humphreys County), 4-44-309 basement test (Smith County), 04-31-1 (Davidson County), CA-5 (Clay County), Exxon CU-30 (Cannon County), and 2-50-1 (Overton county). Tests were conducted to determine the porosity of the samples, which give insight into the storage potential of deep saline aquifers between the eastern front of the Cumberland Plateau and the Mississippi River in Tennessee.

2.2 Methodology

2.2.1 Core Sampling

Sampling of the Dupont and 4-31-1 cores was done at the Tennessee Division of Geology storage facility in Waverly, Tennessee. The 4-44-309 basement core was sampled in the Department of Earth and Planetary Sciences on the University of Tennessee - Knoxville campus. For these cores the Stones River group samples and the Knox group samples were taken at approximately 23 and 46 meter intervals, respectively. These sampling intervals were chosen in order to sample all formations within the groups and limit the number of samples to approximately 100 due to cost restraints. The CA-5, Exxon CU-30, and 2-50-1 cores were sampled at the Tennessee Division of Geology Ellington storage facility in Nashville, Tennessee. These cores were sampled at roughly 30 meter intervals, again providing a sampling of all formations but limiting the number of samples taken. Preference was given to previously broken sections of core in order to minimize damage. However, if no broken pieces were present near the desired depth, or if the core was crushed, then the core was broken manually and a sample was extracted. A total of 97 samples were collected; 35 from the Dupont core taken in Humphreys County, Tennessee covering both the Stones River and Knox groups (348-1696 meters depth), 28 from the 4-

44-309 core taken in Smith County, Tennessee which also covered the Stones River and Knox groups (87-1116 meters depth), 8 from the CA-5 core taken in Cannon County, Tennessee which covered a portion of the Stones River group (101-328 meters depth), 9 from the Exxon CU-30 core taken in Jackson County, Tennessee which covered most of the Stones River group (206-441 meters depth), 11 from the 2-50-1 core taken in Overton County, Tennessee covering portions of the Stones River and Knox groups (439-724 meters depth), and 6 from the 4-31-1 core taken in Davidson County, Tennessee, which covered a portion the Knox group (442-670 meters depth). Figure 2 shows samples from the Exxon CU-30 core, which was similar to most of the other core samples.

2.2.2 Measurements and Calculations

Bulk volume measurements of rock samples were made using a NextEngine Desktop 3D Scanner (NextEngine Inc., Santa Monica, Ca, USA) (see figure 3). This method, described by Rossi and Graham (2010), was preferred because of the irregular and angular nature of the samples, making caliper measurements of bulk volume impractical (see figure 2). Using a modified version of the method described by Goldstrand et al. (1995), samples where first dried at 105°C for 24 hours, expelling any pore water present while not affecting the water of hydration within the minerals. The drying time was significantly longer than that employed by Goldstrand et al. (1995), which was only one hour. We found that the longer drying time expelled a greater amount of water and thus resulted in a more accurate estimation of the actual porosity of each sample. The oven-dried samples were weighed using a scale with an accuracy of 0.01 grams. Samples were allowed to cool completely and were then submerged in water within a vacuum desiccator. The samples were left under

vacuum (~24 mmHg) for 17 hours to minimize possible errors, pointed out by Goldstrand et al. (1995) and Dorsch (1997), related to incomplete saturation. Following removal from the desiccator, any excess water was removed from the surface with a damp wipe and samples where again weighed with an accuracy of 0.01 grams. The difference between the dry and saturated weights represents the mass of water within the pores of the sample. Using the following equation and the known density of water, porosity (ϕ) values were calculated as:

$$\phi = \frac{V_v}{V_b} = \left[\frac{(M_s - M_d)}{(\rho V_b)}\right] * 100 \quad (1)$$

where V_v is the volume of void space, V_b is the bulk volume measured using the laser scanner, M_s is the saturated mass, M_d is the oven-dry mass, and ρ is the density of water, assumed to be 1 g cm^{-3}.

2.3 Results and Discussion

2.3.1 Reproducibility

Tests were conducted on cylindrical Berea sandstone cores (25.5 mm in diameter by 51.3 mm long) to determine the reproducibility of the method used for calculating bulk volume and selected samples from the K-SR cores were used to determine the reproducibility of the drying and saturation methods. Berea core samples were used for the bulk volume tests in order to facilitate caliper measurements to compare with the NextEngine laser scanner measurements, as the irregular shape of the K-SR core samples made this impractical. Coefficients of variation (CV) were calculated for the volume and weight measurements, using the following equation:

$$CV = \left(\frac{\sigma}{\bar{x}}\right) * 100 \quad (2)$$

where σ is the standard deviation, and $\bar{x}$ is the mean value. In both cases the resulting CV's showed very little variation (Tables 2 and 3), suggesting that the methods employed were highly reproducible. The oven dry and vacuum-saturated weights used in the calculation of porosity had accuracies (expressed as CV's) of 0.03-0.05% and 0.19-0.24%, respectively (Table 2). The core volume data measured using the laser scanner had an accuracy (expressed as a CV) of 0.11% (Table 3). Since the Berea cores were regular cylinders it was also possible to determine their volume by making height and diameter measurements with digital calipers. The caliper volume measurements exhibited more variation than the laser scanner volume measurements (Table 3). According to a two-sample unequal variance t-test, the mean core volumes for the two methods were significantly different at the 95% confidence level. Assuming the mean core volume measured by the digital calipers is the true volume, yields a precision for the laser porosity measurements (expressed as a CV) of ~0.8%. Thus, the total error (due to both precision and accuracy) for the laser scanning volume measurements (expressed as a CV) is 0.91%. Based on the averages of the CV data presented in Tables 2 and 3, and assuming a zero precision error for the oven dry and vacuum-saturated weights, the total error (due to both precision and accuracy) for the laser scanning porosity measurements (expressed as a CV) was calculated to be ~ 1.2%.

2.3.2 Porosity within the K-SR SAU's

Although 97 samples were obtained, results for only 95 samples are presented because two of the samples fragmented during analysis resulting in loss of material. The

data were non-normally distributed and so the central tendency was described using median values. The median porosity value for all six cores was 1.21%. Porosity trends with depth are shown in Figures 4 - 8. Minimum, median, and maximum porosity values for core samples above and below the K-SR SAU minimum depth of 800 m are given in Table 4.

Porosity values for the different formations are summarized in Table 5. Porosity values for the Dupont core ranged from 0.31 to 6.29% with a median of 1.13%. Testing of the 4-44-309 core produced porosity values ranging from 0.21 to 10.67%, with a median of 1.24%. Porosity values for the 2-50-1 core ranged from 0.92 to 6.50%, with a median of 1.40%. For the CU-30 core, porosity values ranged from 0.40 to 1.27%, with a median of 0.94%. The CA-5 core porosity values ranged from 0.76 to 3.17%, with a median of 1.09%. For the 4-31-1 core, porosity values ranged from 0.98 to 5.32% with a median of 1.72%.

There are eight samples with porosity values above 5%. The sample with porosity of 10.67% is from a sandstone interval in the Mascot Dolomite of the Knox Group. This was the only sandstone sampled and the result may be representative of the sandstones that are known to occur throughout the Knox Group, which are prevalent in the lower part of the Chepultepec Dolomite and Mascot Dolomite. Two of the samples with relatively high porosity values contained small, but identifiable vuggy porosity. The remaining five samples with porosity values greater than 5% did not have any surface features that could explain the test result.

A Kruskal-Wallis test performed in SAS indicated significant differences between the median values in Table 5 at the 95% confidence level. Logarithmic transformation of the raw data facilitated an Analysis of Variance (ANOVA) in SAS. The results are reported as geometric mean values in Table 5. There were significant differences at the 95%

confidence level between the porosities of the different formations, with the Wells Creek and Murfreesboro formations having the highest and lowest geometric mean values, respectively.

2.3 Conclusions

Based on the results presented in Table 5, the Wells Creek, Mascot, and Kingsport formations appear to be the most suitable for geologic sequestration of carbon dioxide in terms of available matrix pore space. These formations have significantly higher porosity than the other formations, supporting our hypothesis. In order to fully characterize these units as potential reservoirs for CO_2 sequestration further measurements of other parameters must be made, most notably intrinsic permeability. Porosity values of approximately 2.0% are not usually considered adequate for large-scale storage projects and this should be taken into consideration before further investigation of the K-SR SAU takes place. However, the values presented here represent matrix porosity alone and do not take into account fractures and possible dissolution features that will contribute to total storage potential.

Chapter 3 – Numerical Modeling and Cost Estimates

3.1 Introduction

Attempts at modeling storage of CO_2 in geologic media span a wide range approaches and foci. Schnaar and Digiulio (2009) summarized the main processes considered in these models: multiphase flow and heat transport, reactive transport, and geochemical modeling. Multiphase flow models focus on phase transition behavior of CO_2, buoyancy contrasts between CO_2 and brine, solubility of CO_2 in brine, leakage through abandoned wells or faults, precipitation of salt in brine, and three-phase relative permeability relationships. Heat transport is an important process in CO_2 sequestration modeling because many transport mechanisms of CO_2 are temperature dependent, relating mainly to cooling due to decompression of supercritical CO_2. Reactive transport models can simulate mineral dissolution and precipitation and their associated changes to petrophysical parameters as well as aquifer acidification. Modeling of geochemical processes can provide insight into aquifer and caprock pressure buildup and possible fault reactivation as well as changes in petrophysical parameters such as porosity and permeability.

Numerical models have been used for many purposes applied to CO_2 sequestration. Simulation of geologic sequestration systems and site characterization allow for estimates of feasibility of potential reservoirs. Simulations of generic saline aquifers using geochemical and multiphase flow and heat transport models have been run by Pruess et al. (2003) to determine the capacity of CO_2 that can be stored given certain conditions. Birkholzer et al. (2009) investigated the probability of leakage through confining layers, the pressure buildup within a target aquifer, and how these processes affect groundwater

using a multiphase flow model. King et al. (2011) explored the possibility of sequestering CO_2 along side an enhanced oil recovery operation in the Conroe oil field in Texas, USA. Poiencot et al. (2012) investigated the feasibility of carbon sequestration under different transportation scenarios in the Florida Panhandle region using various cost models. Zhang and Agarwal (2012) introduced a method for the optimization of CO_2 sequestration design in deep saline aquifers by using a multiphase flow and heat transport model coupled with an optimization algorithm. Using their algorithm - simulator combination, Zhang and Agarwal (2012) found an optimized water-alternating-gas injection scheme and modeled it in both a vertical and horizontal injection well. Both scenarios showed reduction in the CO_2 impact area by 14% when compared with a strict CO_2 injection scheme.

Site-specific numerical simulations were conducted by Gupta et al. (2008) for the American Electric Power Mountaineer Power Plant in West Virginia using a multiphase flow and heat transport model to assess the storage capabilities of the Rose Run and Copper Ridge formations in the Ohio River Valley. The Sleipner Project off the Norwegian coast, which has been injecting CO_2 into a sandstone formation 700 meters below the North Sea floor since 1996, is another example (Kongsjorden et al., 1997; Eiken et al., 2011). Using a multiphase flow and heat transport model, Doughty (2010) investigated potential plume migration and behavior at a potential large-scale sequestration pilot test site in central California's San Joaquin valley. Carbon Sequestration will soon begin on a commercial-scale at an Archer Daniels Midland Company ethanol plant near Decatur, Illinois where CO_2 is captured from the fermentation process at the ethanol plant and injected underground into the Mount Simon sandstone at a rate of 1,100 tons per day (Frailey and Finley, 2010; Frailey et al., 2011). In western Kentucky, a sequestration test

project has shown that injection of supercritical CO_2 in the Knox is a viable storage option (Bowersox et al., 2011). Recently at the SECARB Anthropogenic Test site, capture of CO_2, transport, and subsequent sequestration is currently underway at a rate up to 550 tons per day (Koperna et al., 2012).

Numerical simulations have also been run in conjunction with monitoring at field sites where sequestration of CO_2 is already taking place. One such site is the Frio brine pilot project in Texas, USA. Injection of CO_2 at the site and the monitoring of its migration have provided additional information to fine-tune numerical models for simulating subsurface CO_2 sequestration (Sakurai et al., 2005; Doughty et al., 2008).

Dissolution and precipitation of minerals can be of concern because of changes in porosity, permeability, and other petrophysical parameters as well as leading to possible leakage through the caprock. André et al. (2007) modeled CO_2-saturated water and pure CO_2 injection into the Dogger aquifer of the Paris Basin, France, using a reactive transport – multiphase flow and heat transport model, concluding that highly reactive CO_2-saturated water increased porosity near the injection well due to dissolution of carbonates while pure CO_2 injection could possibly lead to mineral precipitation and porosity reduction near the injection well. Similarly, evolution of the caprock during and after injection of CO_2 into a saline aquifer was investigated using a reactive transport model by Gherardi et al. (2007). They found that when a CO_2-dominated phase entered the caprock, dissolution of calcite resulted in porosity enhancement while calcite precipitation occurred when a purely liquid phase was present, reducing porosity and enhancing the seal.

Some researchers have looked at the sensitivity of models to variability in petrophysical parameters due to heterogeneity when modeling geologic storage of CO_2.

Using a multiphase flow and heat transport model it was found that, through variation of capillary pressure and relative permeability, the amount of trapped CO_2 gas decreased when the ratio of vertical to horizontal permeability was increased (Mo and Akervoll, 2005). Juanes et al. (2006) studied the effects of relative permeability hysteresis, as did Mo and Akervoll (2005), and varying injection rates on CO_2 storage using a multiphase flow model. In another set of simulations using a multiphase flow model, researchers found that horizontal permeability had the largest effect on the amount dissolved CO_2 in the formation and, not surprisingly, residual gas saturation appeared to be the most influential parameter in determining the amount of residually trapped CO_2 (Sifuentes et al., 2009). A study done by Doughty (2010), mentioned above, varied residual gas saturation, permeability, and permeability anisotropy, and concluded that small changes in these parameters resulted in large shifts in the CO_2 gas plume migration. Han et al. (2011), using a multiphase flow model, investigated the changes in residual trapping of CO_2 due to variations in petrophysical parameters including vertical and horizontal permeability and porosity, as well as the density of the brine and the maximum residual gas saturation. Results indicated CO_2 residual trapping increased proportionally with horizontal and vertical permeability, brine density, and maximum residual gas saturation but decreased when porosity was increased (Han et al., 2011).

Variations in costs for carbon capture, transport, and storage have also been investigated. Cinar et al. (2008) modeled low- and high-permeability formations near and far from the CO_2 source, respectively. They found that even with the use of horizontal drilling and fracturing, the low-permeability formation had significant cost disadvantages despite a shorter transportation distance. McCoy and Rubin (2008) also found permeability

to be the most influential petrophysical parameter when using an engineering - economic model to evaluate different performance and cost scenarios for carbon sequestration. In another study, mentioned above, the costs associated with storage of CO_2 in conjunction with an enhanced oil recovery option in Texas were investigated (King et al., 2011). As previously noted, Poiencot et al. (2012) investigated the feasibility of carbon sequestration in the Florida Panhandle region as well as the associated costs given different transportation scenarios. Middleton et al. (2012) utilized an economic-engineering optimization model coupled with a performance and risk assessment model to look at how geologic uncertainty affected the costs of storage as well as the spatial distribution of the capture, transport, and storage infrastructure. In this study it was noted that geologic uncertainty produced wide ranges in infrastructure design as well as large fluctuations in storage costs. Heath et al. (2012) used a multiphase flow and heat transport model and geospatial averaging techniques to explore links in variations in costs with uncertainty associated with geologic heterogeneity and well injectivity. The authors concluded that, due to the wide variations in CO_2 storage costs due to heterogeneity in geologic properties, great care must be taken to ensure accurate descriptions of potential storage sites (Heath et al., 2012).

No other study that we are aware of has systematically varied a suite of petrophysical parameters required for numerical modeling of CO_2 sequestration and used the output to estimate fluctuations in cost as a result of heterogeneity or inaccurate measurement. By doing so, we will be able to determine the most influential parameters that should be most accurately measured in order to avoid erroneous conclusions based on unrealistic simulation outputs.

3.1.2 Objectives

In order to accurately model sequestration of carbon dioxide into underground reservoirs an understanding of the input parameters is necessary. Some parameters, such as porosity or intrinsic permeability, can be measured rather easily through drilling techniques or laboratory experiments, as was done by Gupta (2008), while other parameters, such as residual gas or liquid saturation, are more difficult to estimate. The accuracy of these parameters determines the validity of the model outputs.

For this study a parameter sensitivity analysis was performed by running multiple numerical simulations of CO_2 injection into a modeled confined saline aquifer and the various outputs were used to investigate shifts in costs associated with geologic uncertainty.

While several researchers have performed numerical simulations of carbon sequestration, typically many of the input parameters are rough estimates of the actual field conditions (Bacon and Murphy, 2011; Bacon et al., 2009; Gupta, 2008; Pruess et al., 2003). As a result, there is inherent variability between the estimated parameters and actual conditions on site.

The overall goal of this section is to describe the relative importance of different input parameters for numerical simulation of CO_2 storage in geologic reservoirs. The objective is to allow future researchers to focus on obtaining accurate estimates of parameters that have the greatest effect on the simulation while spending less time and money on those which are less significant. This study should help to:

- Identify parameters that have the greatest impact on simulation results (these influential parameters should therefore be most accurately estimated);

- Identify parameters that are less influential to the simulation results (these parameters could therefore be less accurately estimated);
- Demonstrate the usefulness of numerical models in predicting costs associated with carbon dioxide capture and storage.

These objectives can be rewritten in the form of two hypotheses. The first is that certain parameters, most likely intrinsic permeability and porosity, will show significantly more influence on model outputs than others. The second is that variations of influential parameters will result in significant fluctuations in the cost of injecting CO_2.

3.2 Methodology

Multiple simulations were carried out using the STOMP (Subsurface Transport Over Multiple Phases) computer code. The STOMP code was developed by the Hydrology group at the Pacific Northwest National Lab (PNNL) to model remediation technologies, simulating subsurface flow and transport. STOMP is available in several different versions including STOMP-CO2, which is specifically designed for modeling the injection of CO_2 into deep saline aquifers. This version operates under the main assumptions that isothermal conditions exist, there is no NAPL phase or dissolved oil, and that local thermodynamic equilibrium exists. The simulation makes numerical predictions for subsurface hydrogeologic flow in variably saturated porous media, solving the governing equations by the integral volume finite difference method and Newton-Raphson iteration (White and Oostrom, 2006).

The parameters tested in the simulations were porosity, intrinsic permeability, pore compressibility, the van Genuchten α, m, residual liquid saturation (equations 3 and 4), and

the Brooks and Corey residual gas and residual liquid saturations (equation 5). The residual gas saturation represents the CO_2 that becomes trapped in tiny pore spaces and cannot be displaced by the liquid phase once the gas plume has migrated through an area. Similarly, the residual liquid represents the liquid that becomes trapped in tiny pore spaces and cannot be displaced by the gas phase. At first it may seem odd to have two distinct residual liquid saturations instead of one. However, while the van Genuchten and Brooks and Corey residual liquid saturations can be coupled (i.e. the same value), in some cases they are treated as independent variables. This is acceptable because these parameters are typically determined by separate experiments (capillary pressure – saturation versus permeability/core flood). Consequently, it is conceivable that the two residual liquid saturations could be different values. The van Genuchten and Brooks and Corey equations implemented in STOMP are given below (White and Oostrom, 2006).

The van Genuchten model, containing the van Genuchten residual liquid saturation as well as the α and m parameters, describes the capillary pressure – saturation relation and is shown in equation 3 (van Genuchten, 1980):

$$\bar{S}_{lvG} = \left[1 + (\alpha h_{gl})^{1/(1-m)}\right]^{m} \quad ; \quad \bar{S}_{lvG} = \frac{S_l - S_{lrvG}}{1 - S_{lrvG}} \tag{3}$$

where $\bar{S}_{lvG}$ is the effective van Genuchten liquid saturation, α is a fitting parameter, h_{gl} is the gas-aqueous capillary head (m), m is a fitting parameter related to the pore size distribution, S_l is the residual saturation, and S_{lrvG} is the van Genuchten residual liquid saturation. The van Genuchten residual liquid saturation and m parameter are also found in the aqueous relative permeability relation, described here in equation 4 using the van

Genuchten capillary pressure – saturation relation along with the Maulem porosity distribution function (van Genuchten, 1980):

$$K_{rl} = \bar{S}_{lvG}{}^{0.5} \left\{ 1 - \left[1 - \bar{S}_{lvG}{}^{-(1/m)} \right]^{m} \right\}^{2} \quad (4)$$

where K_{rl} is the aqueous relative permeability. The Brooks and Corey residual liquid and gas saturation are shown in equation 5, describing the gas relative permeability relation using the Corey formulation:

$$K_{rg} = (1 - \hat{s})^2 \, (1 - \hat{s}^2) \, ; \quad \hat{s} = \frac{S_l - S_{lrC}}{1 - S_{lrC} - S_{grC}} \quad (5)$$

where K_{rg} is the gas relative permeability, $\hat{s}$ is the Brooks and Corey effective saturation, S_{lrC} is the Brooks and Corey residual liquid saturation, and S_{rgC} is the Brooks and Corey residual gas saturation.

A base scenario was created following Pruess et al. (2002) for simulating radial flow of supercritical CO_2 from an injection well into a deep saline aquifer. A 100 m thick, isotropic and homogeneous aquifer of 100 km radial extent (infinite acting) was modeled with supercritical CO_2 injected in the center of the infinite-acting domain at various rates for 10,000 days (approximately 27 years). The default aquifer temperature and pressure are adequate for maintaining a state of supercritical CO_2 (Table 6 and Figure 9). The multiple phases considered in this model were CO_2 and brine (15 wt. % salinity). There was a constant flux boundary in the west at the injection well, a constant head boundary in the

east opposite the injection well, and no-flow boundaries at the bottom and top of the model aquifer (Figure 10). Gravity and inertial effects were neglected and flow was assumed one-dimensional. One hundred grid cells were employed with spacing increasing exponentially with distance from the injection well. The input parameters for this model are listed in Table 6, with the bold-italicized parameter values varied in the following simulations. All of the other parameters were set at their default values. The parameter estimates served as starting points for the simulations. Parameters where then varied stepwise by a constant value within a reasonable range which included the default of the parameter. The range of variation depended upon the specific variable under investigation and attempted to encompass the majority of values used as inputs for other published modeling studies. However, the *m* parameter and intrinsic permeability values were not arbitrary. Values of *m* ranging from 0.426 to 0.772 were used by Cheng et al. (2011) to investigate variations in model output and were based on estimates of *m* by Cropper et al. (2011). This is a relatively small range, 0.346, but is appropriate for the parameter being tested. Conversely, intrinsic permeability can vary by orders of magnitude within a given region and should be modeled accordingly. In this case, values of intrinsic permeability correspond to the USGS class two for residual trapping (Brennan et al., 2010).

The model default values for each of the above mentioned parameters were varied separately in order to determine the sensitivity of the simulation to each variable, while holding all other parameters constant. In addition, eight simulations were run for each parameter estimate, corresponding to eight different CO_2 injection rates for most parameters (3.13, 6.25, 12.5, 18.75, 21.88, 25, 50, and 100 kg/s). Due to large variations in intrinsic permeability, additional injection rates were used for this parameter (0.10, 0.20,

0.41, 0.82, 1.63, 3.13, 6.25, and 150 kg/s) in order to ensure a modeled pressure close to the base scenario mean pressure. In total, this exercise involved conducting over 450 numerical simulations. For each parameter value, a plot of injection rate versus mean gas pressure within the aquifer was created. The mean aquifer pressure was calculated by adding the gas pressure at each grid cell and then dividing by the total number of grid cells. Using linear regression, a relationship between the injection rate and the mean gas pressure was calculated. From this relationship an injection rate associated with the mean gas pressure produced using the base scenario, 2.01×10^7 Pa, could be calculated for each parameter estimate. This injection rate was then used to calculate the cost per metric ton of CO_2 for each simulation. The capital cost for a single well was calculated from Ogden (2002) such that:

$$\text{Capital (\$/well)} = \$1.25 \text{ million} + \$1.56 \text{ million/km of depth} \quad (6)$$

Operation and maintenance for the well were assumed 4% of capital and the annual capital charge rate of 15% of the total capital, resulting in a yearly cost of $714,330 in 2001 USD (Heath et al., 2012). Assuming a yearly inflation rate of 1.023%, the yearly cost of operating the injection well would be $917,341 in 2012 USD. This value was then used as a rough estimate of the cost to operate the injection operation per year for a single well when calculating the costs per metric ton of CO_2.

In order to compare the variation of different properties normalization must be done to account for differences in scale and to eliminate units. For example, comparing the difference in cost for intrinsic permeability with the costs associated with variations of *m* may be unreasonable since the range of variation for the actual parameters are vastly

different and they contain different units. The normalized coefficient of variation for each parameter, which is a measure of the variability within the parameter values and the price per ton of CO_2, was computed as follows (see equations 7, 8, and 9) in order to compare variables with differing scales and units.

$$CV_p = \left(\frac{\sigma_p}{\bar{x}_p}\right) * 100 \quad (7)$$

$$CV_\$ = \left(\frac{\sigma_\$}{\bar{x}_\$}\right) * 100 \quad (8)$$

$$CV_n = \left(\frac{CV_\$}{CV_p}\right) * 100 \quad (9)$$

Where CV_P is the coefficient of variation for the parameter, σ_P is the standard deviation for the parameter values, $\bar{x}_P$ is the mean parameter value, $CV_\$$ is the coefficient of variation of the cost per ton, $\sigma_\$$ is the standard deviation of the cost per ton, $\bar{x}_\$$ is the mean cost per ton, and CV_n is the normalized coefficient of variation.

3.3 Results

Outputs from the model simulations included aqueous CO_2 mass fraction, gas pressure and saturation, precipitated salt saturation, aqueous salt mass fraction, node volume, x-coordinates, and diffusive porosity, which refers to all interconnected pore spaces. Only the first three of these datasets were considered in the sensitivity analyses. Aqueous CO_2 mass fraction, gas saturation, and gas pressure as a function of distance (radius) for the van Genuchten *m* parameter after 10,000 days (approximately 27 years) at an injection rate of 12.5 kg/s are shown as examples of the simulation outputs in Figures

11, 12, and 13, respectively. Results for the other parameters at the ~27 year time step are summarized in Appendix 3.

Aqueous CO_2 mass fraction represents the mass of CO_2 dissolved into the aquifer brine compared to the mass of the aquifer brine. For all parameters investigated there was a sharp increase near the injection well. The offset from the injection well represents a zone of brine dry out, where the only aqueous CO_2 was dissolved into brine trapped in small pores. This zone was followed by a fairly level phase extending out to about 3,500 m (except for very low values of intrinsic permeability and porosity, which showed a convex shape and extended out to 7,000 m respectively). At the gas front, which occurred between 3,000 and 4,000 m for most of the parameters at the ~27 year time step, the aqueous CO_2 mass fraction rapidly declined and asymptotically approached zero. At this point the aquifer was fully saturated with respect to brine and contains no dissolved CO_2. The van Genuchten residual liquid saturation and *m* parameter showed a slight increase in aqueous CO_2 mass fraction near the gas front; this was most likely related to dynamic mixing occurring at the leading edge of the CO_2 plume. The gas saturation for all parameters was unity near the injection site (complete gas saturation) and declined rapidly as distance from the injection well increased.

The mean gas pressure for each simulation was calculated and used to compare scenarios of differing parameter values. Table 7 shows the corresponding injection rates and the resulting cost per ton of CO_2 for each parameter. The following discussion considers the relationship between the change in injection rate and the resulting cost compared to the variation in mean gas pressure associated with each parameter range. As an example, Figure 14 shows the mean gas pressure as a function of injection rate for

various values of the van Genuchten *m* parameter. Results for the other parameters are summarized in Appendix 5.

The van Genuchten α parameter showed very little variation in mean gas pressure due to stepwise shifts from 0.5 to 3.0 m^{-1}. This was expressed as very small changes in the injection rate in order to maintain the same mean pressure as the base scenario. This shifted the amount of CO_2 sequestered per year only slightly and had almost no bearing on the final cost per ton of CO_2. As a result, the normalized coefficient of variation, CV_n, for α was 0.08 and ranked last among the parameters tested (see Table 8).

The default van Genuchten residual liquid saturation was zero. Increasing this value from 0.10 up to 0.30 by increments of 0.05 created only minor variations in the injection rate to maintain the base scenario mean pressure. As a result, variations in cost were minimal. This was expressed by the very low CV_n value of 1.24, slightly higher than the CV_n for alpha (see Table 8).

Pore compressibility values ranged from 2.5 x 10^{-10} to 7.5 x 10^{-10} Pa^{-1} and produced injection rates from 12.15 to 12.93 kg/s, respectively. The highest pore compressibility values resulted in the highest injection rates and the lowest cost per ton of CO_2 injected into the model aquifer with prices ranging from $2.25 to $2.40 (see Table 7). The CV_n for pore compressibility was 6.25, the sixth highest among the parameters tested (see Table 8).

The default porosity of the model formation was 0.12. This value was varied incrementally from 0.04 to 0.24 with lower porosity values requiring lower injection rates to produce mean gas pressure equal to the base scenario. This resulted in a higher price per ton of CO_2 injected. Prices ranged from $2.22 for the highest porosity value to $2.46 for the lowest (see Table 7). The CV_n for porosity was 7.88, ranking it fifth among the parameters

tested (see Table 8). It seems clear that the model is not as heavily influenced by shifts in the value of porosity as was originally anticipated. However, it should be noted that no connection between porosity and intrinsic permeability exists in the model. In other words, a change in porosity was not reflected in the value of intrinsic permeability despite the fact that in reality a connection may exist. This may explain in part the low sensitivity of the model to shifts in porosity.

The Brooks and Corey residual liquid saturation showed a similarly narrow spread in injection rates, from 11.05 to 14.20 kg/s, associated with parameter variation from 0.15 to 0.40. The resulting variations in cost were noticeable, ranging from $2.05 to $2.63 per ton of CO_2 (see Table 7). The CV_n for Brooks and Corey residual liquid saturation is 27.90, ranking it fourth among the parameters investigated (see Table 8).

The residual gas saturation was varied stepwise by a constant value of 0.05 from 0.05, the default value, to 0.30. This resulted in a range of injection rates from 5.91 to 12.50 kg/s. The lower S_{gr} values were associated with higher injection rates and lower cost per ton of CO_2 injected. Prices ranged from $2.33 to $4.93 per ton of injected CO_2 (see Table 7). The CV_n for S_{gr} was 54.69, the third highest variation among the parameters tested (see Table 8).

The van Genuchten *m* parameter, related to the pore size distribution, had an even higher CV_n, 89.37, demonstrating significant variations in cost associated with uncertainty of the parameter values (see Table 8). Injection rates ranging from 11.56 to 19.21 kg/s were required to produce the mean pressure associated with the base scenario, with higher m values associated with higher injection rates and lower cost per ton of CO_2 injected. The price per ton of CO_2 ranged from $1.52 to $2.52 (see Table 7).

Intrinsic permeability was varied stepwise, ranging from 1.0×10^{-12} to 1.0×10^{-15} m^2, with 1.0×10^{-13} m^2 being the model default. These values produced a wide range of injection rates from 0.17 kg/s for the lowest intrinsic permeability value to 119.20 kg/s for the highest intrinsic permeability value. Not surprisingly, the lowest intrinsic permeability value was associated with the highest cost per ton of CO_2 injected while the highest *k* value was associated with the lowest cost. Costs ranged from $0.24 to $168.50 per ton of injected CO_2 (see Table 7). The extreme fluctuations in cost demonstrate the sensitivity of the model to shifts in the values of intrinsic permeability and the importance of accurate measurement. The CV_n for intrinsic permeability was 121.69, the highest of all parameters tested (see Table 8). It should be noted that the CV_P for intrinsic permeability was also calculated based on the log of the parameter values due to the commonly accepted log-normal distribution of the parameter and it's tremendous variation. This produced a CV_n over an order of magnitude greater than the value listed above.

3.4 Conclusions

Using a model confined saline aquifer, multiple simulations were run with independently varied input parameters. The mean pressure in the aquifer for each scenario was computed and used to estimate the injection rate associated with the base scenario mean pressure. This injection rate was then used to calculate the cost per metric ton of CO_2 injected into the model aquifer, citing the rate used by Heath et al. (2012) as a rough estimate of the yearly cost of injection through a single well.

Intrinsic permeability, the van Genuchten *m* parameter, the residual gas saturation and the Brooks and Corey liquid saturation were the most influential input parameters.

While intrinsic permeability may be typically measured with acceptable accuracy, the capillary pressure-saturation variables are often only estimated. These results suggest the need for accurate measurements of these variables in order to correctly predict injection costs. Errors in measurement or imprecise estimation could result in inaccurate cost projections on the order of a few million to tens of millions of dollars over the life of the project (the time taken to inject 10,800,000 metric tons of CO_2 in this case).

Chapter 4 – General Conclusions

Porosity values were determined for 95 samples taken from the K-SR SAU carbonates in middle Tennessee. Data from these samples were non-normally distributed with a median value of 1.21 percent for all cores tested. Statistical analysis of the porosity values for individual formations showed the Wells Creek, Mascot, and Kingsport formations to be the most suitable for CO_2 sequestration in middle Tennessee in terms of available matrix pore volume, supporting our hypothesis that certain formations would have higher porosity than others. It should be noted that the majority of porosity values for the K-SR SAU were well below that which is desirable for a large-scale sequestration project. These data can be used to aid in the decision-making process concerning possible targets for CO_2 sequestration in Tennessee. However, the measurements of porosity in this document reflect only matrix porosity and do not take into account fractures and possible dissolution features that will contribute to total storage potential.

Future work in this area should include analysis of other petrophysical parameters including the capillary pressure-saturation variables for the Knox and Stones River groups. Additionally, other potential SAU's in Tennessee should be investigated, including the Mount Simon sandstone (Basal Sandstone in Figure 1).

Sensitivity analysis of the numerical simulations showed that some of the most influential petrophysical input parameters for modeling CO_2 sequestration are the van Genuchten *m* parameter and the Brooks and Corey residual gas and residual liquid saturations, though these are all outweighed by intrinsic permeability. Surprisingly, porosity did not play a crucial role in the model outcomes when using the mean gas pressure to compare scenarios, partially disproving our hypothesis that porosity would

have a significant influence in the model outcomes. However, our hypothesis that variation of influential parameters would greatly influence the cost per metric ton of CO_2 injection is supported by the simulation results, as variation of influential parameters, such as intrinsic permeability, the van Genuchten *m* parameter, and residual gas saturation, show a wide range in injection costs. These findings highlight the need for accurate measurement of the capillary pressure-saturation parameters and intrinsic permeability.

Future work in this area should include additional simulations varying parameters that are not necessarily petrophysical such as aquifer thickness, salinity, temperature, etc. Linking simulation parameters to real-world values could help to show how an aquifer behaves under differing petrophysical conditions when matched more closely to field conditions. Also, integration of parameter estimation software into STOMP-CO_2, such as the USGS program UCODE which can be used to perform sensitivity analyses, could substantially reduce the time required to set up and run the required simulations.

List of References

Andre, L., P. Audigane, et al. (2007). "Numerical modeling of fluid-rock chemical interactions at the supercritical CO2-liquid interface during CO2 injection into a carbonate reservoir, the Dogger aquifer (Paris Basin, France)." Energy Conversion and Management **48**(6): 1782-1797.

Bachu, S. (2000). "Sequestration of CO2 in geological media: criteria and approach for site selection in response to climate change." Energy Conversion and Management **41**(9): 953-970.

Bacon, D. H. and E. M. Murphy (2011). "Managing chemistry underground: Is co-sequestration an option in selected formations?" Energy Procedia **4**(0): 4457-4464.

Bacon, D. H., B. M. Sass, et al. (2009). "Reactive transport modeling of CO2 and SO2 injection into deep saline formations and their effect on the hydraulic properties of host rocks." Energy Procedia **1**(1): 3283-3290.

Birkholzer, J. T., Q. Zhou, et al. (2009). "Large-scale impact of CO2 storage in deep saline aquifers: A sensitivity study on pressure response in stratified systems." International Journal of Greenhouse Gas Control **3**(2): 181-194.

Bowersox, J., D. Williams, et al. (2011). "CO2 storage in U.S. Midcontinent Cambro-Ordovician carbonates: Implications of the Western Kentucky Carbon Storage Test." Geological Society of America 2011 Annual Meeting. Minneapolis, Minnesota, USA, October 9-12, 2011.

Bradshaw, J., S. Bachu, et al. (2007). "CO2 storage capacity estimation: Issues and development of standards." International Journal of Greenhouse Gas Control **1**(1): 62-68.

Brennan, S. T., R. C. Burruss, et al. (2010). A probabilistic assessment methodology for the evaluation of geologic carbon dioxide storage: U. S. Geological Survey, Open-File Report 2010-1127**:** 31.

Celia, M. A. and J. M. Nordbotten (2009). "Practical modeling approaches for geological storage of carbon dioxide." Ground Water **47**(5): 627-638.

Cheng, C. L., E. Perfect, et al. (2011). "Effects of average and point capillary pressure-saturation function parameters on multiphase flow simulations." AGU 2011 Fall Meeting. San Francisco, California, USA, Dec. 5-9, 2011.

Cinar, Y., O. Bukhteeva, et al. (2008). CO2 Storage in Low Permeability Formations. SPE/DOE Symposium on Improved Oil Recovery. Tulsa, Oklahoma, April 19-23, 2008. Society of Petroleum Engineers.

Cropper, S. C., E. Perfect, et al. (2011). "Comparison of average and point capillary pressure-saturation functions determined by steady-state centrifugation." Soil Sci. Soc. Am. J. **75**(1): 17-25.

Dorsch, J. (1997). "Effective porosity and density of carbonate rocks (Maynardville Limestone and Copper Ridge Dolomite) within Bear Creek Valley on the Oak Ridge Reservation based on modern petrophysical techniques." ORNL/GWPO-026. Oak Ridge Y-12 Plant, Oak Ridge, Tenn. 70 p.

Doughty, C. (2010). "Investigation of CO2 Plume Behavior for a Large-Scale Pilot Test of Geologic Carbon Storage in a Saline Formation." Transport in Porous Media **82**(1): 49-76.

Doughty, C., B. Freifeld, et al. (2008). "Site characterization for CO2 geologic storage and vice versa: the Frio brine pilot, Texas, USA as a case study." Environmental Geology **54**(8): 1635-1656.

Eiken, O., P. Ringrose, et al. (2011). "Lessons learned from 14 years of CCS operations: Sleipner, In Salah and Snøhvit." Energy Procedia **4**(0): 5541-5548.

Frailey, S. M., J. Damico, et al. (2011). "Reservoir characterization of the Mt. Simon Sandstone, Illinois Basin, USA." Energy Procedia **4**(0): 5487-5494.

Frailey, S. M. and R. J. Finley (2010). "Overview of the Midwest Geologic Sequestration Consortium Pilot Projects." SPE International Conference on CO2 Capture, Storage, and Utilization. New Orleans, Louisiana, USA, November 10-12, 2010. Society of Petroleum Engineers.

Franklin, J. (1972). "Suggested Methods for Determining Water Content, Porosity, Density, Absorption and Related Properties. Suggested Methods for Determining Swelling and Slake-durability Index Properties." International Society for Rock Mechanics. Commission on Standardization of Laboratory Field Tests.

Gherardi, F., T. Xu, et al. (2007). "Numerical modeling of self-limiting and self-enhancing caprock alteration induced by CO2 storage in a depleted gas reservoir." Chemical Geology **244**: 103-129.

Goldstrand, P. M., L. S. Menefee, et al. (1995). "Porosity development in the Copper Ridge Dolomite and Maynardville Limestone, Bear Creek Valley and Chestnut Ridge, Tennessee." Y/SUB95-SP912V/1-1093. Oak Ridge Y-12 Plant, Oak Ridge, Tenn. 57 p.

Gragg, M. and E. Perfect (2011). Rock core sample porosity testing for the Knox Group – Stones River Group carbon dioxide storage assessment unit in Tennessee. Tennessee Division of Geology Report. Knoxville, TN, University of Tennessee.

Gupta, N. (2008). "The Ohio River Valley CO2 Storage Project AEP Mountaineer Plant, West Virginia Numerical Simulation and Risk Assessment Report." U. S. D.O.E., Battelle. Contract No. DE-AC26-98FT40418.

Han, W., K.-Y. Kim, et al. (2011). "Sensitivity Study of Simulation Parameters Controlling CO2 Trapping Mechanisms in Saline Formations." Transport in Porous Media **90**(3): 807-829.

Heath, J. E., P. H. Kobos, et al. (2012). "Geologic Heterogeneity and Economic Uncertainty of Subsurface Carbon Dioxide Storage." SPE Econ & Mgmt. **4**(1): 32-41. SPE-158241-PA.

Izgec, O., B. Demiral, et al. (2005). Experimental and Numerical Investigation of Carbon Sequestration in Saline Aquifers. Exploration and Production Environmental Conference. Galveston, Texas, March 7-9, 2005. Society of Petroleum Engineers.

Juanes, R., E. J. Spiteri, et al. (2006). "Impact of relative permeability hysteresis on geological CO2 storage." Water Resour. Res. **42**(12): W12418.

Kazimierz, T., T. Jacek, et al. (2004). "Evaluation of Rock Porosity Measurement Accuracy with a Helium Porosimeter." Acta Montanistica Slovaca **9**(3): 316-318.

King, C., S. Coleman, et al. (2011). "The economics of an integrated CO2 capture and sequestration system: Texas Gulf Coast case study." Energy Procedia **4**(0): 2588-2595.

Klara, S. M., R. D. Srivastava, et al. (2003). "Integrated collaborative technology development program for CO2 sequestration in geologic formations - United States Department of Energy R&D." Energy Conversion and Management **44**(17): 2699-2712.

Kongsjorden, H., O. Karstad, et al. (1998). "Saline aquifer storage of carbon dioxide in the Sleipner project." Waste Management **17**(5-6): 303-308.

Koperna, G. J., D. E. Riestenberg, et al. (2012). The SECARB Anthropogenic Test: The First US Integrated Capture, Transportation, and Storage Test. Carbon Management Technology Conference. Orlando, Florida, USA, February 7-9, 2012. Carbon Management Technology Conference.

McCoy, S. T. and E. S. Rubin (2009). "Variability and uncertainty in the cost of saline formation storage." Energy Procedia **1**(1): 4151-4158.

Middleton, R. S., G. N. Keating, et al. (2012). "Effects of geologic reservoir uncertainty on CO2 transport and storage infrastructure." International Journal of Greenhouse Gas Control **8**(0): 132-142.

Mo, S. and I. Akervoll (2005). "Modeling Long-Term CO2 Storage in Aquifer With a Black-Oil Reservoir Simulator." SPE/EPA/DOE Exploration and Production Environmental Conference. Galveston, Texas, USA. March 7-9, 2005. Society of Petroleum Engineers.

Ogden, J. (2002). "Modeling infrastructure for a fossil hydrogen energy system with CO2 sequestration." 6th International Conference on Greenhouse Gas Control Technologies. Kyoto, Japan, September 30 - October 4, 2002.

Pacala, S. and R. Socolow (2004). "Stabilization Wedges: Solving the Climate Problem for the Next 50 Years with Current Technologies." Science **305**(5686): 968-972.

Poiencot, B. K., C. J. Brown, et al. (2012). "Feasibility of Transportation and Geologic Sequestration of Carbon in the Florida Panhandle." Carbon Management Technology Conference. Orlando, Florida, USA, Carbon Management Technology Conference.

Pruess, K., J. Garcia, et al. (2002). "Intercomparison of numerical simulation codes for geologic disposal of CO2." NETL, LBNL-51813**:** 104 pages.

Pruess, K., T. Xu, et al. (2003). "Numerical Modeling of Aquifer Disposal of CO2." SPE Journal **8**(1): 49-60.

Rossi, A. M. and R. C. Graham (2010). "Weathering And Porosity Formation In Subsoil Granitic Clasts, Bishop Creek Moraines, California." Soil Sci. Soc. Am. J. **74**(1): 172-185.

Sakurai, S., T. S. Ramakrishnan, et al. (2005). “Monitoring Saturation Changes for CO2 Sequestration: Petrophysical Support of the Frio Brine Pilot Experiment.” 46th Annual Logging Symposium. New Orleans, Louisiana, USA. Society of Petrophysicists & Well Log Analysts**:** 16.

Schnaar, G. and D. C. Digiulio (2009). "Computational Modeling of the Geologic Sequestration of Carbon Dioxide." Vadose Zone Journal **8**(2): 389-403.

Sifuentes, W. F., M. A. Giddins, et al. (2009). “Modeling CO2 Storage in Aquifers: Assessing the Key Contributors to Uncertainty.” Offshore Europe. Aberdeen, UK, Society of Petroleum Engineers.

Solomon, S., M. Carpenter, et al. (2008). "Intermediate storage of carbon dioxide in geological formations: A technical perspective." International Journal of Greenhouse Gas Control **2**(4): 502-510.

Sundquist, E. T., R. C. Burruss, et al. (2008). "Carbon sequestration to mitigate climate change." U.S. Geological Survey Fact Sheet 2008-3097.

Szulczewski, M. and R. Juanes (2009). "A simple but rigorous model for calculating CO2 storage capacity in deep saline aquifers at the basin scale." Energy Procedia **1**(1): 3307-3314.

van Genuchten, M. T. (1980). "A Closed-form Equation for Predicting the Hydraulic Conductivity of Unsaturated Soils." Soil Sci. Soc. Am. J. **44**(5): 892-898.

White, M. and M. Oostrom (2006). “STOMP subsurface transport over multiple phases, version 4.0, user guide.” Richland, Washington, Pacific Northwest National Laboratory.

Yang, F., B. Bai, et al. (2010). "Characteristics of CO2 sequestration in saline aquifers." Petroleum Science **7**(1): 83-92.

Zhang, Z. and R. Agarwal (2012, Article in Press). "Numerical simulation and optimization of CO2 sequestration in saline aquifers." Computers & Fluids (Article In Press).

Appendices

Appendix 1. Tables

Table 1. Characteristics, time frames, and potential sizes of trapping mechanisms for CO_2 sequestration in saline aquifers (modified from Bradshaw et al., 2007).

Trapping Mechanism	Characteristics of Trapping Mechanism	Time Frame	Potential Size
Structural/Stratigraphic	Trapping within folds, anticlines, faults, etc. due to buoyancy of CO_2.	Immediate	Significant
Residual Gas	CO_2 becomes trapped in pore spaces of reservoir rock as plume migrates.	Immediate to thousands of years	Very large
Solubility	CO_2 eventually dissolves into the formation brine.	Hundreds to thousands of years	Very large
Mineral	CO_2 reacts with minerals in reservoir rock to form new minerals.	Tens to thousands of years	Significant

Table 2. Three samples of Berea sandstone (A9, A3, and O3) were sequentially oven-dried for 24 hours at 105°C (a) and then vacuum-saturated for 17 hours (b) and their masses determined gravimetrically.

(a) Oven-dried Measurements				**(b) Vacuum-saturated Measurements**			
Sample ID	A9	A3	O3	Sample ID	A9	A3	O3
Mass (g)	53.76	52.22	52.22	-	-	-	-
Mass (g)	53.73	52.23	52.18	Mass (g)	58.68	57.17	57.17
Mass (g)	53.73	52.19	52.17	Mass (g)	58.85	57.31	57.32
Mass (g)	53.72	52.19	52.16	Mass (g)	58.96	57.39	57.39
Average	53.74	52.21	52.18	Average	58.83	57.29	57.29
Standard dev.	0.02	0.02	0.03	Standard dev.	0.14	0.11	0.11
CV (%)	0.03	0.04	0.05	CV (%)	0.24	0.19	0.20

Table 3. Multiple measurements of a cylindrical sandstone core using the NextEngine imaging software and digital caliper. Note that the coefficient of variation for the caliper data is over three times higher than that of the NextEngine software.

NextEngine software volume (cm^3)		**Caliper volume (cm^3)**
1	25.88	26.10
2	25.83	26.23
3	25.90	26.10
4	25.90	26.00
5	25.89	25.97
Average	25.88	26.08
Standard dev.	0.03	0.10
CV (%)	0.11	0.39

Table 4. Porosity values for the K-SR SAU (predominantly carbonate rocks) at depths above and below 800 m.

Depth	n	Minimum (%)	Maximum (%)	Median (%)
All	95	0.21	10.67	1.21
≤ 800 m	69	0.21	10.67	1.22
> 800 m	26	0.65	5.73	1.21

Table 5. Porosity values by formation along with totals.

Formation ‡	n	Minimum (%)	Maximum (%)	Median (%)	Geometric Mean (%)†
O - Carters	7	0.60	4.91	0.99	1.20^{ABC}
O - Lebanon	3	0.64	2.30	1.05	1.16^{ABC}
O - Ridley	9	0.44	2.91	0.94	0.96^{BC}
O - Murfreesboro	15	0.21	3.17	1.00	0.82^{C}
O – Wells Creek	6	1.02	6.29	1.47	2.10^{A}
O - Mascot	20	0.44	10.67	1.44	1.85^{AB}
O - Kingsport	10	0.98	6.50	1.33	1.89^{AB}
O - Longview	4	0.63	1.24	1.20	1.03^{ABC}
O - Chepultepec	6	0.89	1.61	1.16	1.15^{ABC}
Є – Copper Ridge	15	0.65	5.73	1.14	1.25^{ABC}

† Note: geomteric mean values with the same superscript letter are not significantly different at the 95% confidence level according to a protected t-test in SAS.

‡ Note: O: Ordovician, Є: Cambrian.

Table 6. STOMP-CO2 simulation default input values.

Parameter	Value	Parameter	Value
Intrinsic Permeability	10^{-13} m^2	***Brooks and Corey Residual Gas Sat.***	0.05
Porosity	0.12	***Brooks and Corey Residual Liquid Sat.***	0.3
Pore Compressibility	4.5 x 10^{-10} Pa^{-1}	***van Genuchten Residual Liquid Sat.***	0.0
Initial Aquifer Temp.	45° C	Initial Aquifer Pressure	1.2 x 10^7 Pa
van Genuchten m Parameter	0.457	Initial Aquifer Salinity	15 wt.-% NaCl
van Genuchten α Parameter	0.5 m^{-1}	***CO_2 Injection Rate***	12.5 kg/s

Note: The parameters in bold italics were varied while all other parameters were held constant.

Table 7. Parameter values, injection rates, volume of CO_2 injected per year, and the resulting costs per metric ton of CO_2.

Parameter Type	**Parameter Value**	**Injection Rate (kg/s)**	**Volume of CO_2 (metric tons/yr)**	**$/metric ton (2012 USD)**
Intrinsic Permeability (m^2)	1.00×10^{-15}	0.17	5447	$168.40
	5.00×10^{-15}	1.19	37391	$24.53
	1.00×10^{-14}	1.46	45980	$19.95
	5.00×10^{-14}	6.55	206447	$4.44
	1.00×10^{-13}	12.50	394200	$2.33
	5.00×10^{-13}	59.08	1863077	$0.49
	1.00×10^{-12}	119.20	3759011	$0.24
van Genuchten *m* paramter	0.426	11.56	364643	$2.52
	0.438	11.93	376327	$2.44
	0.457	12.50	394200	$2.33
	0.516	14.33	452053	$2.03
	0.537	14.68	462873	$1.98
	0.547	15.07	475212	$1.93
	0.556	15.27	481689	$1.90
	0.600	16.34	515141	$1.78
	0.672	17.79	561164	$1.63
	0.696	18.17	572883	$1.60
	0.708	18.32	577888	$1.59
	0.772	19.21	605714	$1.52
Residual Gas Saturation	0.05	12.50	394200	$2.33
	0.10	11.24	354442	$2.59
	0.15	10.01	315587	$2.91
	0.20	8.58	270627	$3.39
	0.25	7.09	223595	$4.10
	0.30	5.91	186356	$4.93

Table 7. Continued.

Parameter Type	Parameter Value	Injection Rate (kg/s)	Volume of CO_2 (metric tons/yr)	$/metric ton (2012)
Residual Liquid Saturation (Brooks and Corey)	0.15	14.20	447803	$2.05
	0.20	13.69	431762	$2.12
	0.25	13.13	414048	$2.22
	0.30	12.50	394200	$2.33
	0.35	11.81	372583	$2.46
	0.40	11.05	348470	$2.63
Porosity (%)	0.04	11.81	372408	$2.46
	0.08	12.23	385599	$2.38
	0.12	12.50	394200	$2.33
	0.16	12.95	408533	$2.25
	0.20	13.05	411479	$2.23
	0.24	13.10	413217	$2.22
Pore Compressibility (Pa^{-1})	2.50×10^{-10}	12.15	383179	$2.40
	3.50×10^{-10}	12.33	388983	$2.36
	4.50×10^{-10}	12.50	394200	$2.33
	5.50×10^{-10}	12.65	399052	$2.30
	6.50×10^{-10}	12.80	403521	$2.27
	7.50×10^{-10}	12.93	407672	$2.25
Residual Liquid Saturation (van Genuchten)	0.00	12.50	394200	$2.33
	0.10	12.64	398475	$2.30
	0.15	12.68	399898	$2.30
	0.20	12.72	401143	$2.29
	0.25	12.76	402473	$2.28
	0.30	13.02	410725	$2.23
van Genuchten α paramter (m^{-1})	0.50	12.50	394200	$2.33
	1.00	12.51	394480	$2.33
	1.50	12.51	394572	$2.33
	2.00	12.51	394620	$2.33
	2.50	12.51	394651	$2.33
	3.00	12.51	394672	$2.33

Table 8. Coefficents of variation for each petrophysical parameter tested.

Parameter	**CV_P**	**$CV_\$$**	**CV_n**	**Rank**
Intrinsic Permeability	159.64	194.26	121.69	1
van Genuchten *m* Parameter	17.60	19.69	89.37	2
Residual Gas Saturation	53.45	29.23	54.69	3
Residual Liquid Saturation (Brooks and Corey)	34.02	9.49	27.90	4
Porosity	53.45	4.21	7.88	5
Pore Compressibility	37.42	2.32	6.20	6
Residual Liquid Saturation (van Genuchten)	64.81	1.36	2.09	7
van Genuchten α Paramter	53.45	0.04	0.08	8

Appendix 2. Figures

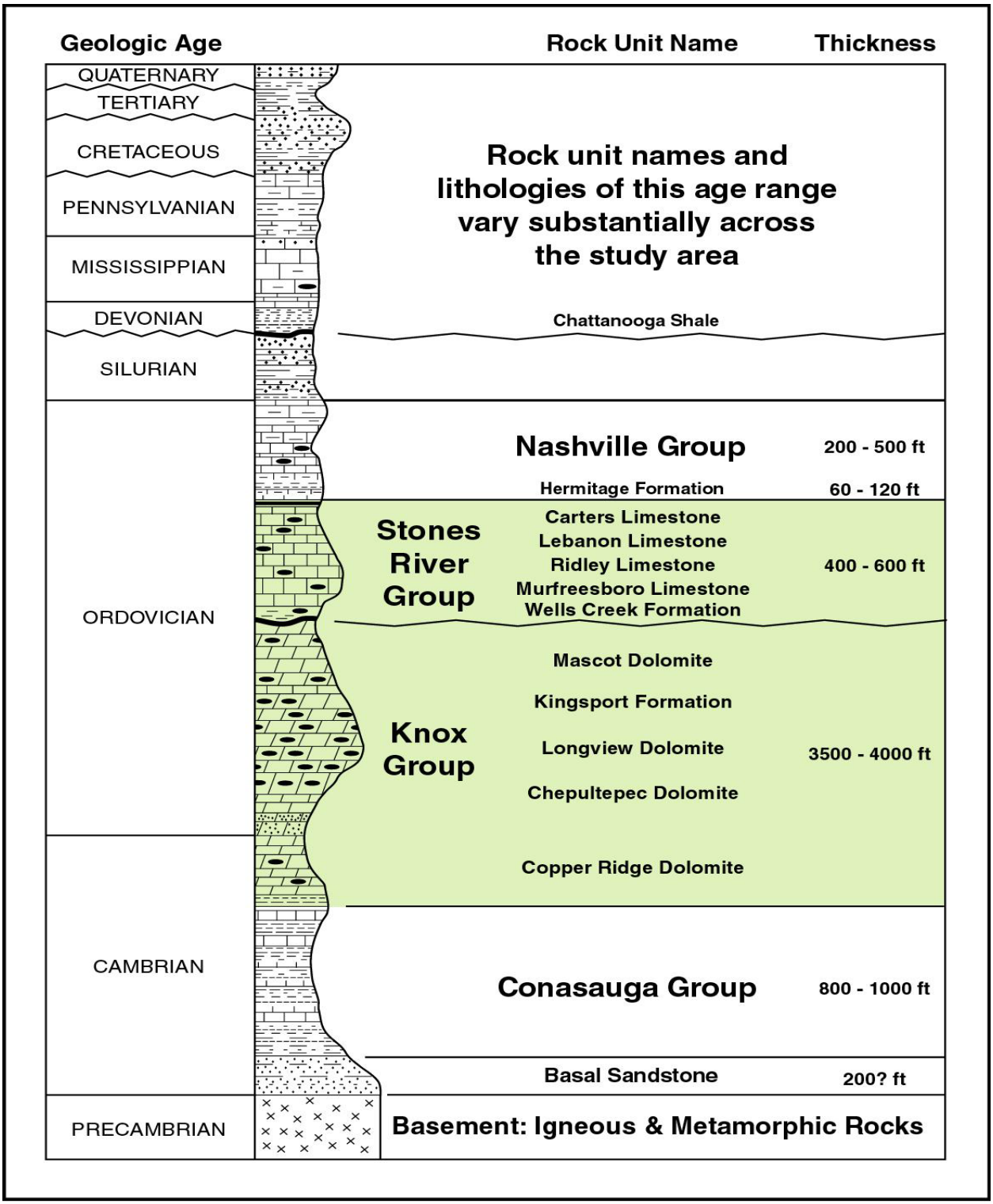

Figure 1. Stratigraphic column of the study area with units of interest highlighted (Gragg and Perfect, 2011).

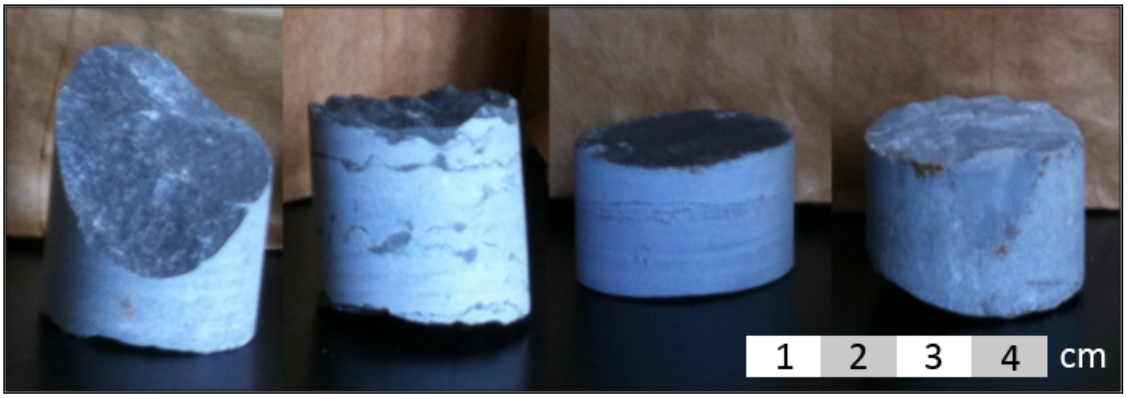

Figure 2. Four samples taken from the Exxon CU-30 core.

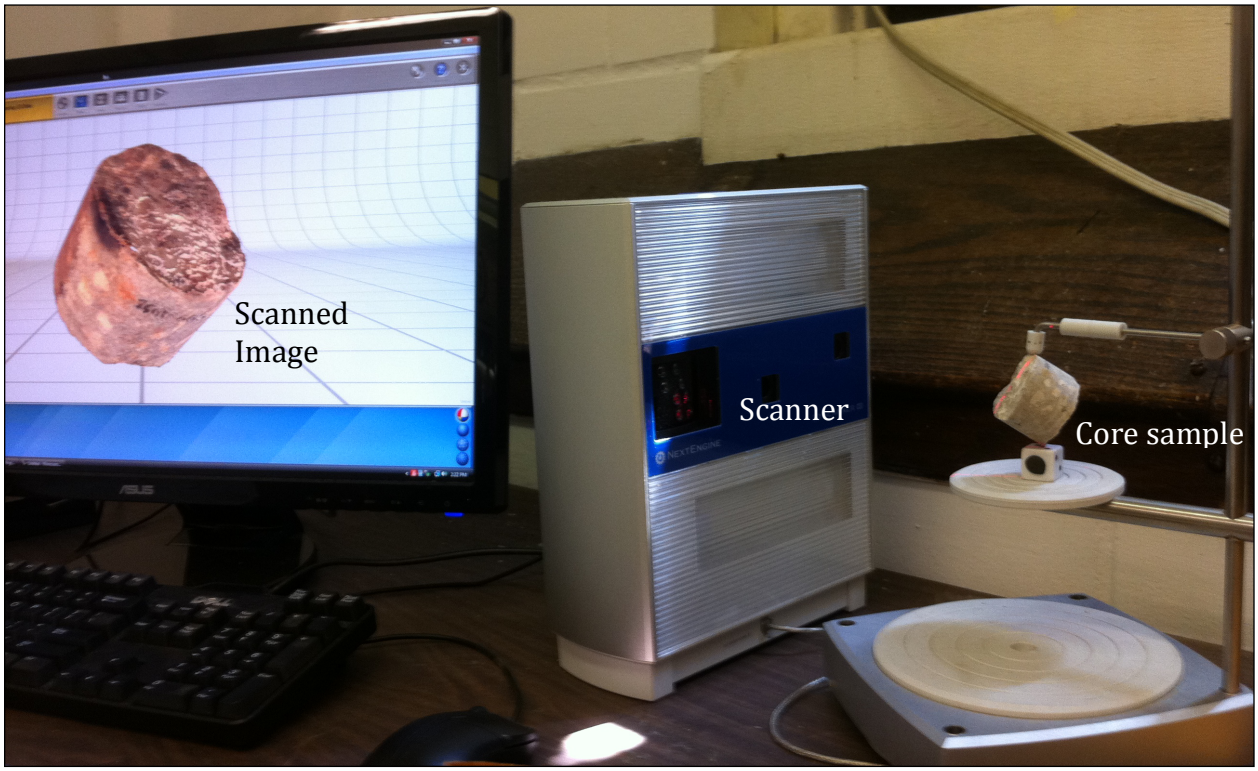

Figure 3. NextEngine Desktop 3D Scanner and scanned 3D image.

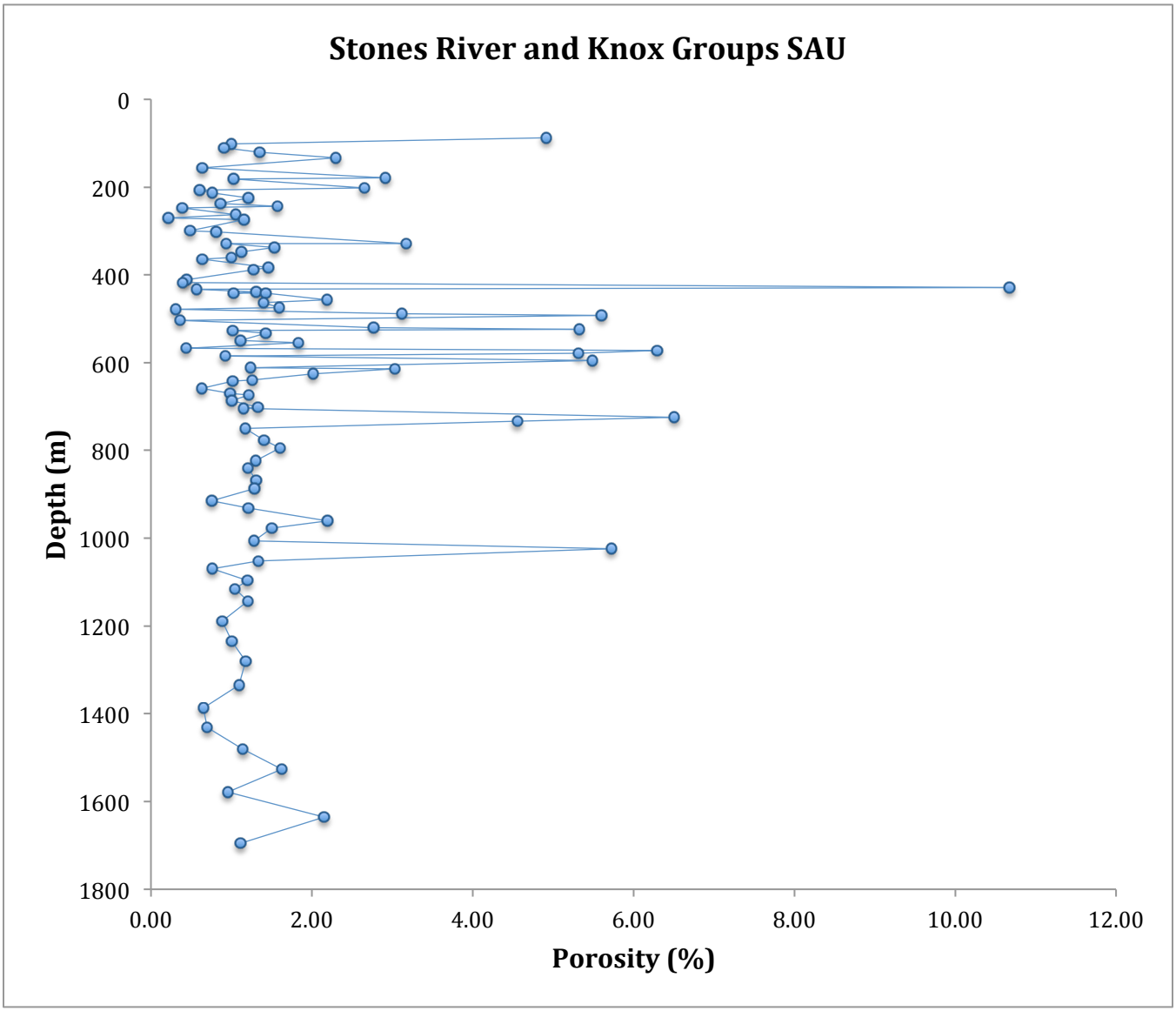

Figure 4. Porosity trend with depth for all cores.

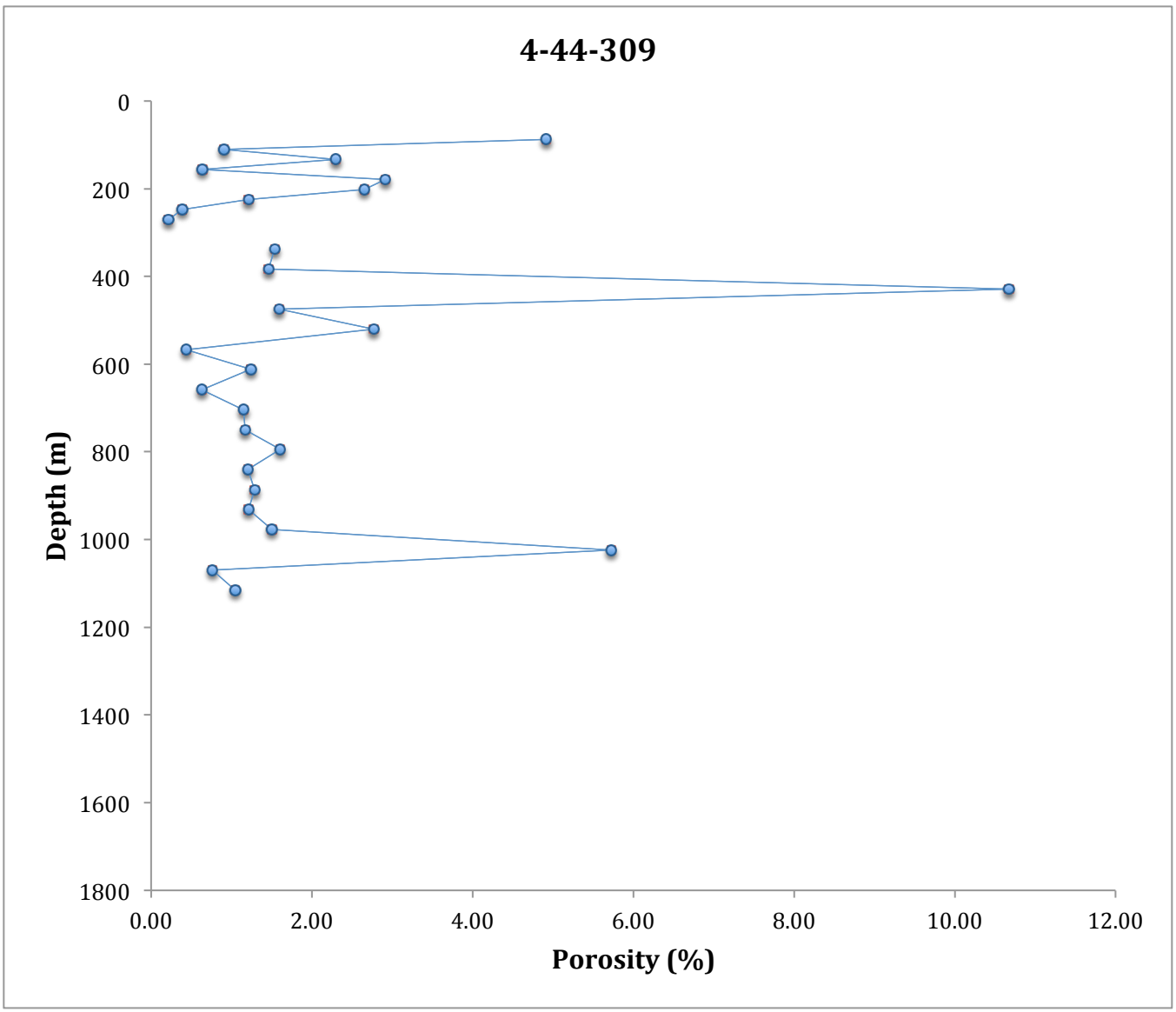

Figure 5. Porosity trend with depth for the 4-44-309 basement test core (Smith County, Tennessee), covering both the Knox and Stones River groups.

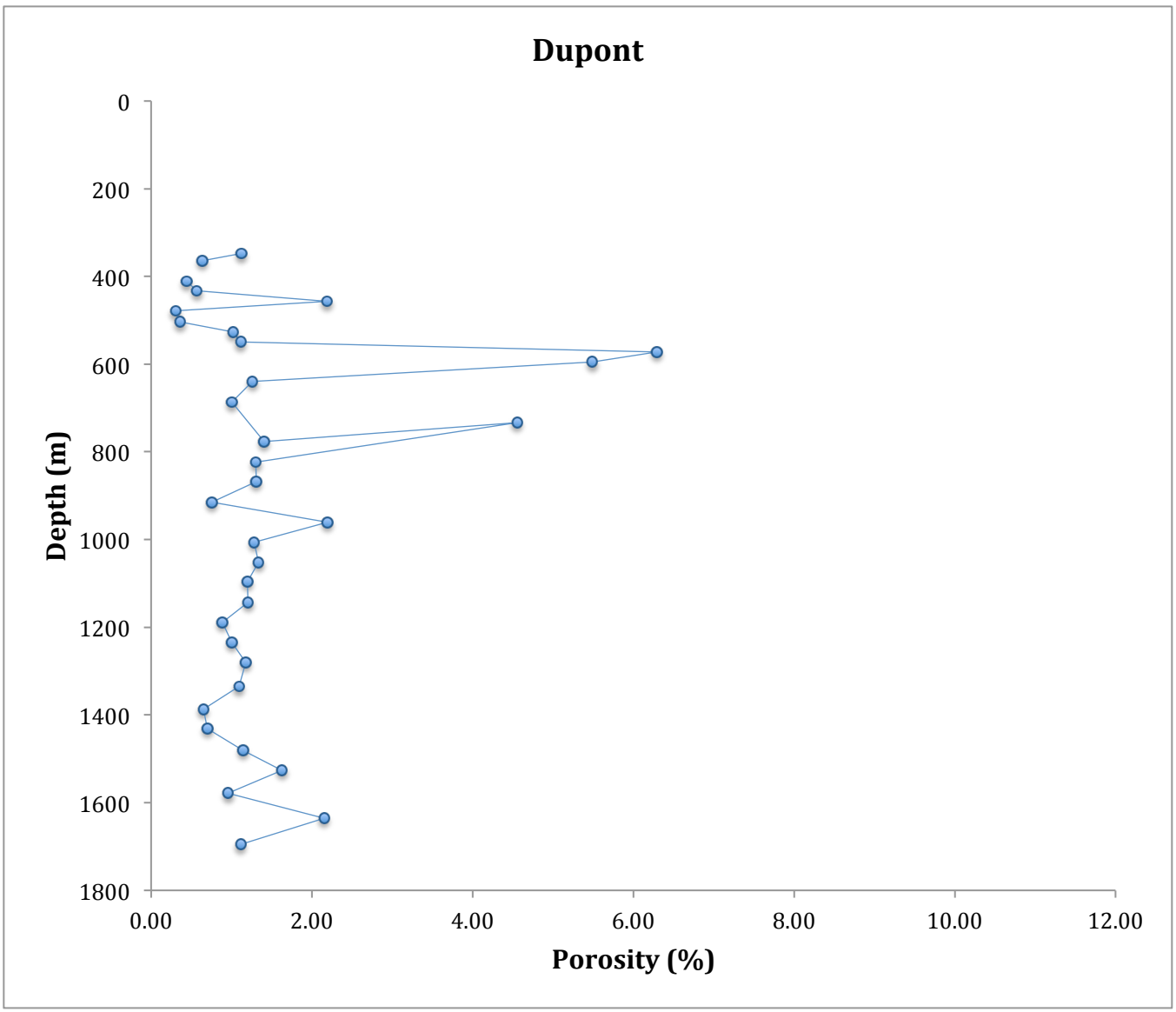

Figure 6. Porosity trend with depth for the Dupont geohydrological survey well core (Humphreys County, Tennessee), covering both the Knox and Stones River groups.

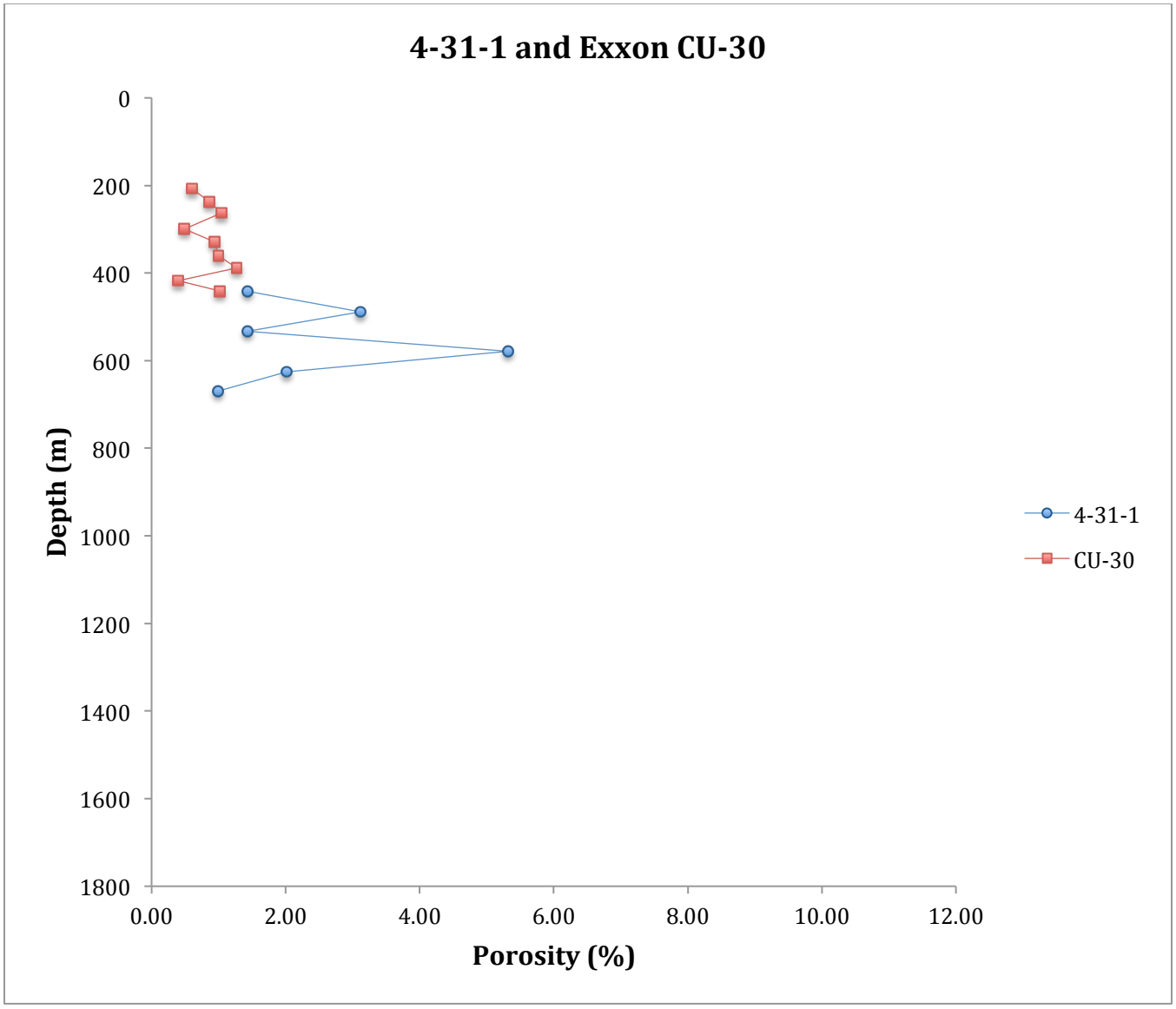

Figure 7. Porosity trends with depth for the 4-31-1 core (Davidson County, Tennessee), covering a portion of the Knox group, and the Exxon CU-30 core (Jackson County, Tennessee), covering most of the Stones River group. Note that these cores do not necessarily correlate to create a continuous stratigraphic sequence.

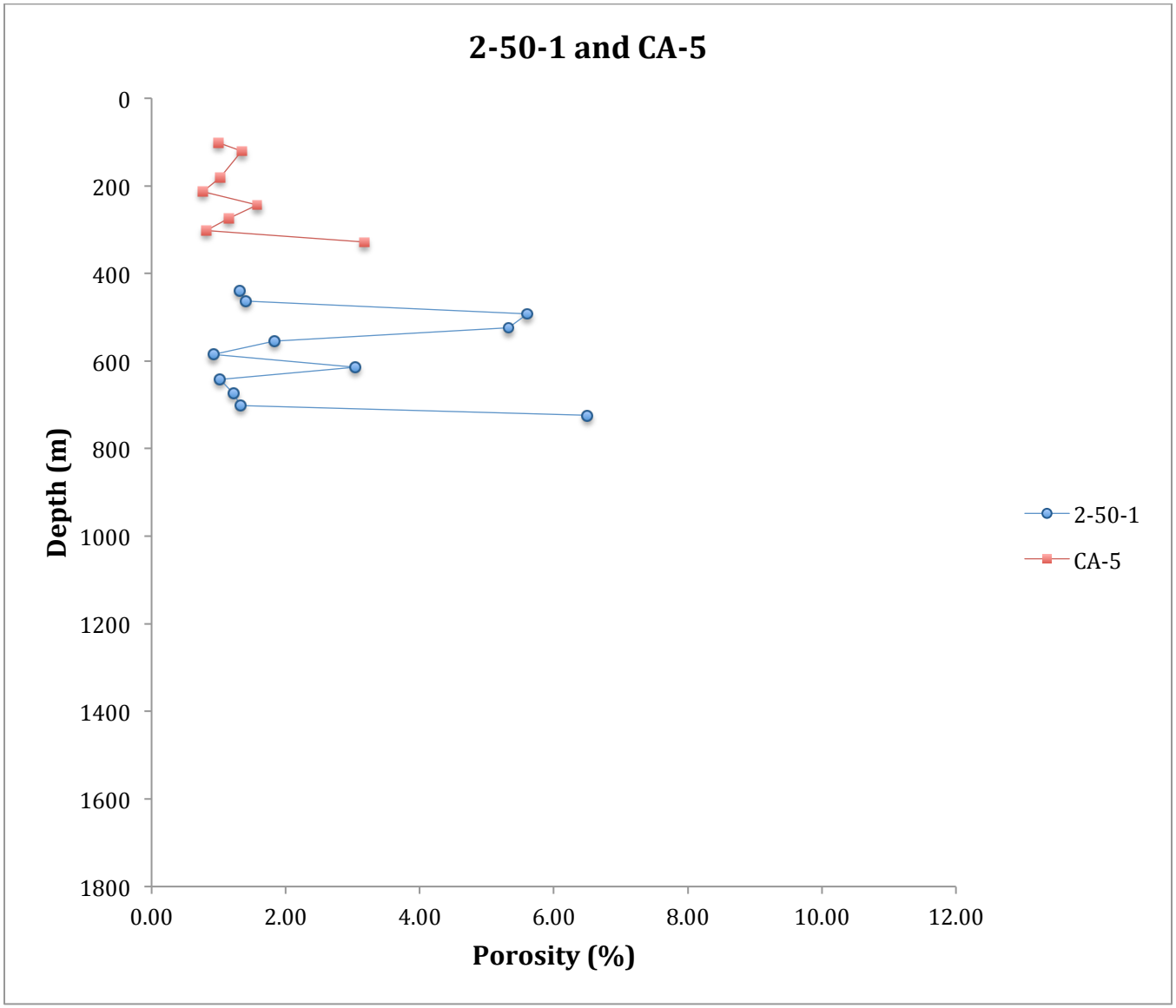

Figure 8. Porosity trends with depth for the 2-50-1 core (Overton County, Tennessee), covering portions of the Knox and Stones River groups, and the CA-5 core (Cannon, County, Tennessee), covering a portion of the Stones River group. Note that these cores do not necessarily correlate to create a continuous stratigraphic sequence.

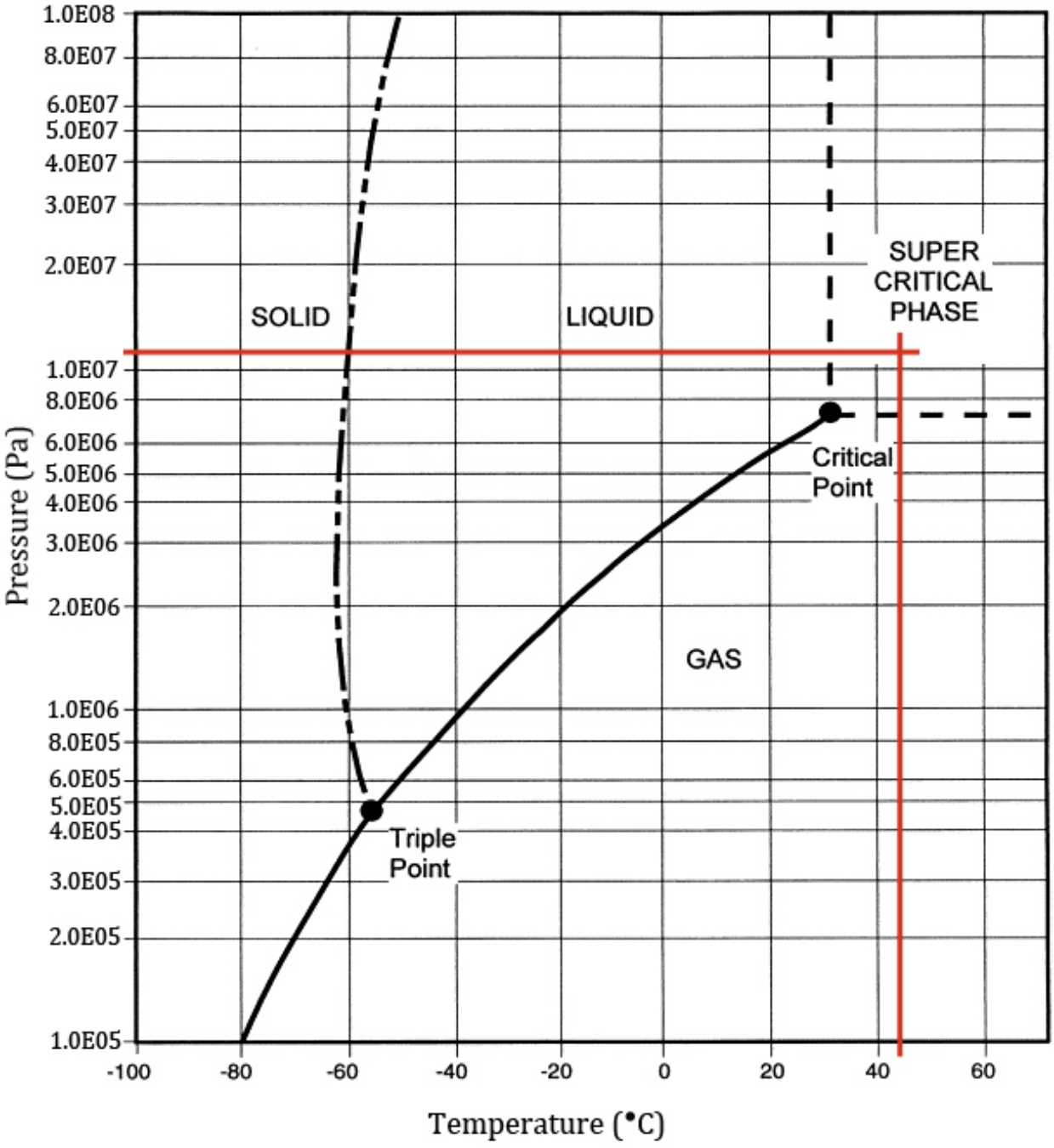

Figure 9. Phase diagram for CO_2 with red lines showing the default temperature, 45°C, and pressure, 1.2e7 Pa, for the model aquifer (modified from Bachu, 2000). Note that the default temperature and pressure values are adequate to maintain supercritical CO_2.

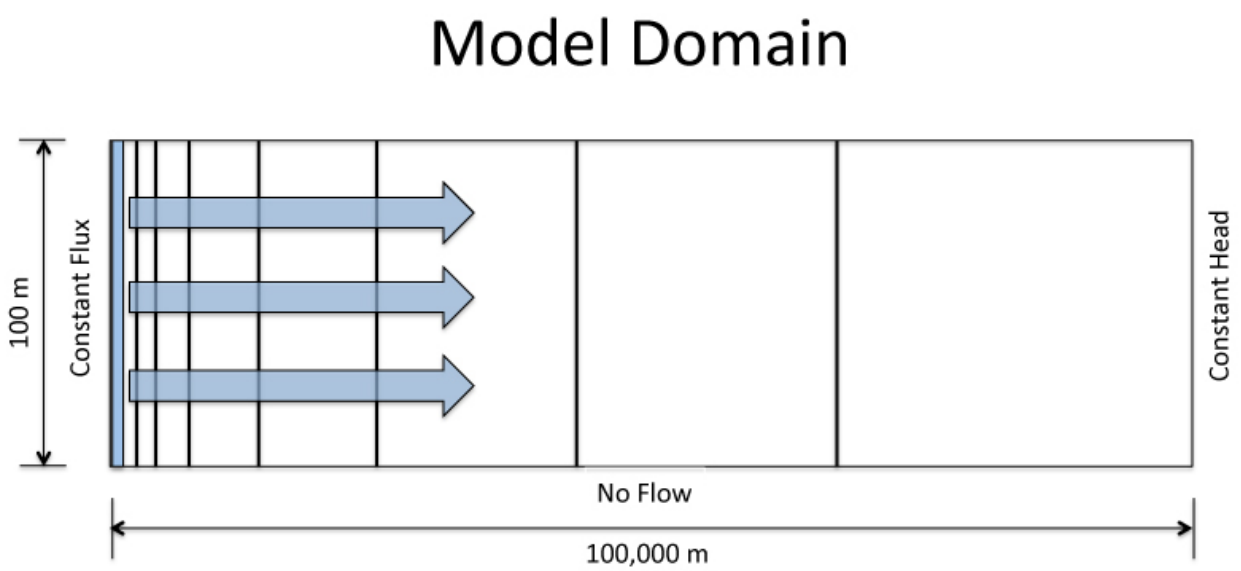

Figure 10. A schematic visual representation of the model domain. One hundred grid cells were used with spacing increasing exponentially with distance from the injection well at the west border. Arrows indicate injected CO_2. This model domain is based on a model created by Pruess et al. (2002).

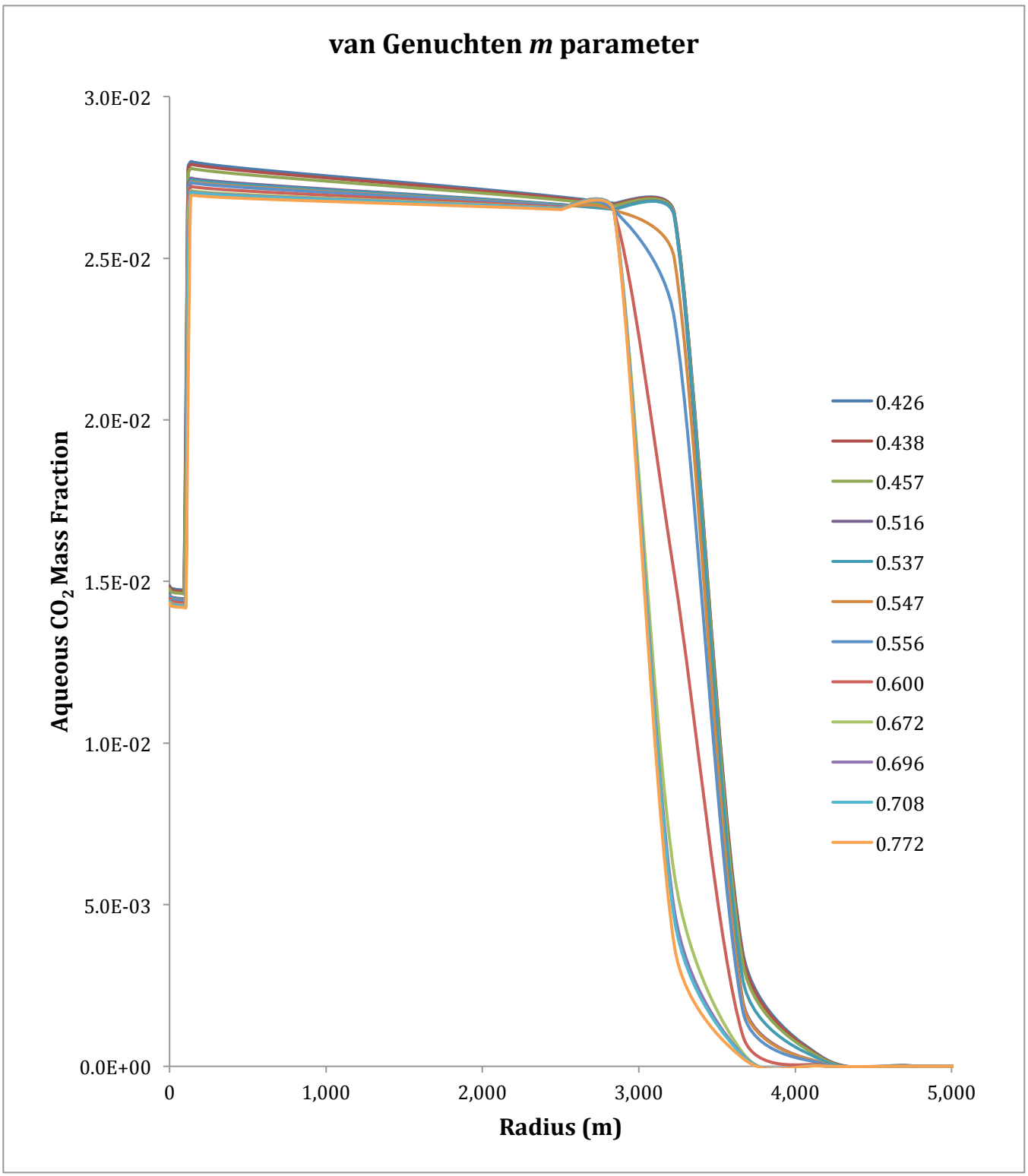

Figure 11. Aqueous CO_2 mass fraction as a function of radial distance from the injection well for various values of the van Genuchten *m* parameter after approximately 27 years at an injection rate of 12.5 kg/s.

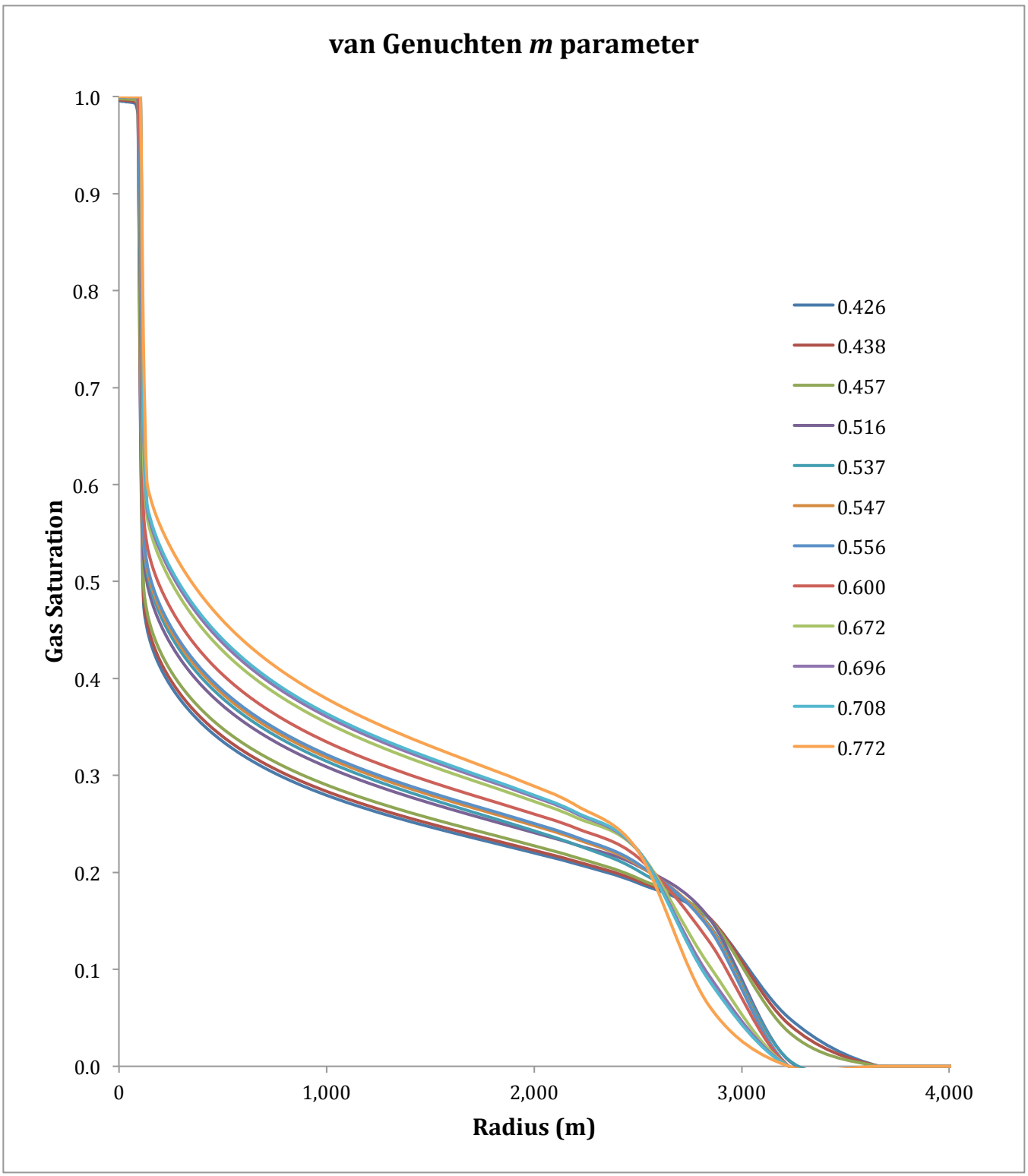

Figure 12. Gas saturation as a function of radial distance from injection well for various values of the van Genuchten *m* parameter after approximately 27 years at an injection rate of 12.5 kg/s.

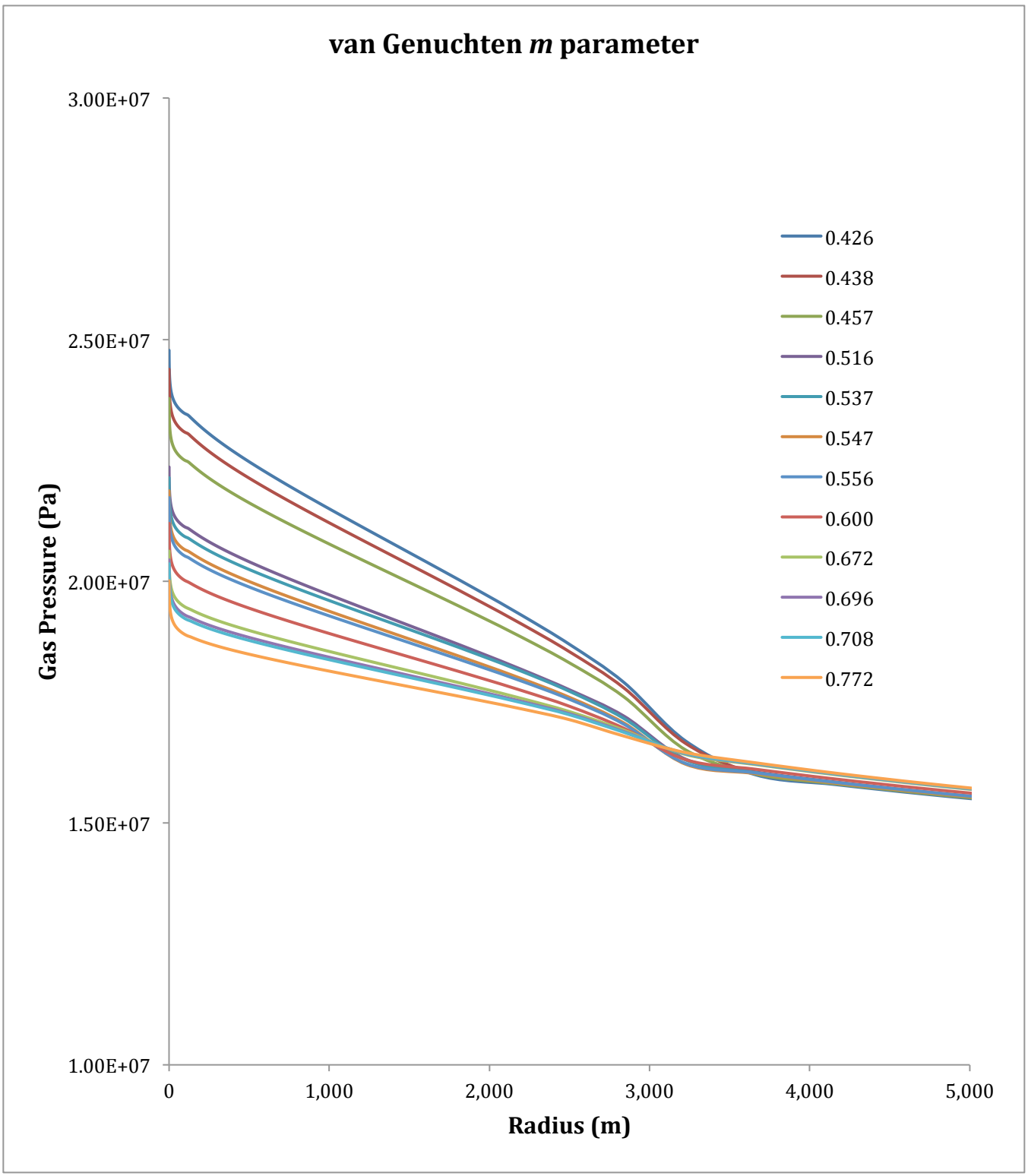

Figure 13. Gas pressure as a function of radial distance from injection well for various values of the van Genuchten *m* parameter after approximately 27 years at an injection rate of 12.5 kg/s.

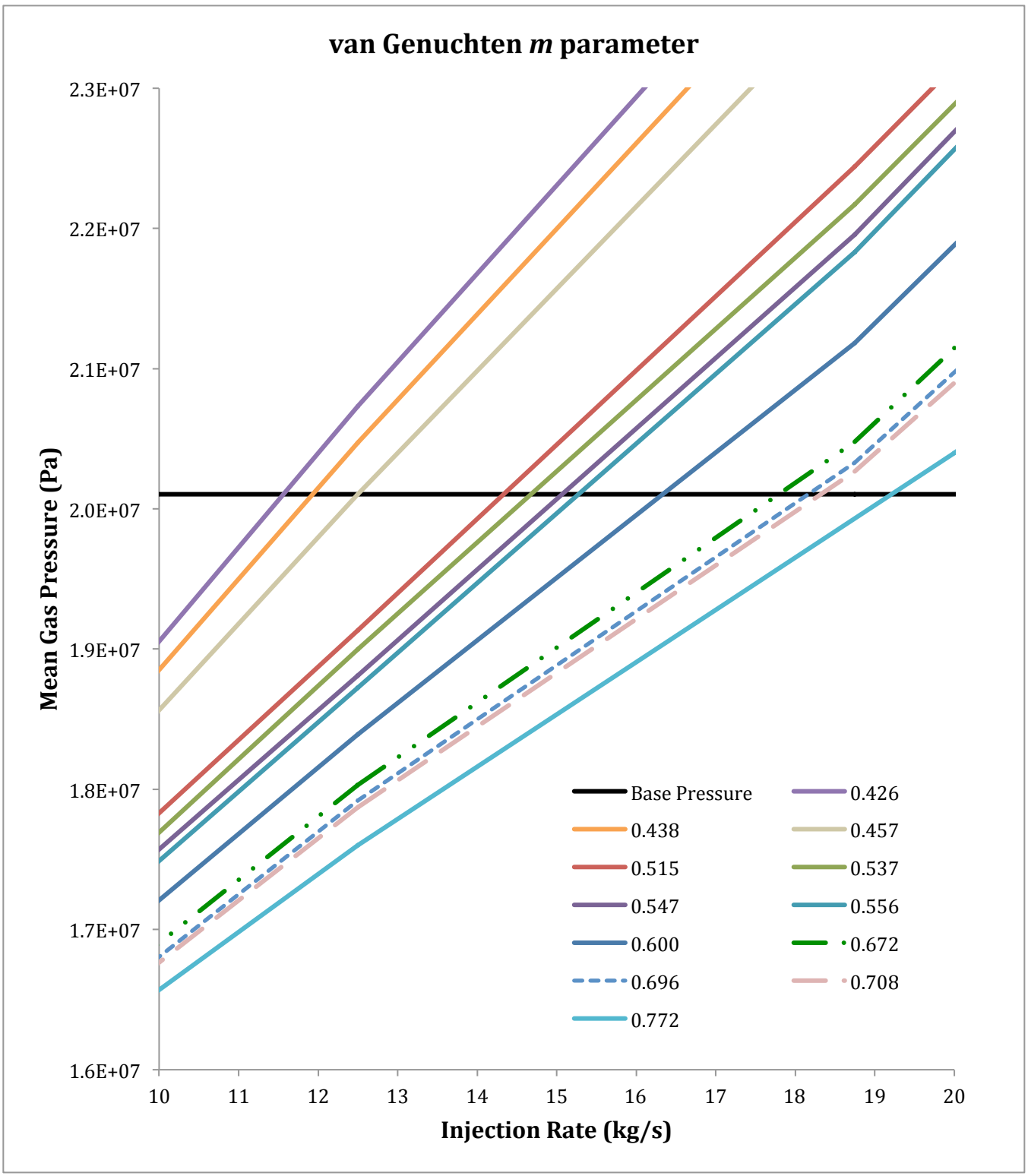

Figure 14. Mean gas pressure as a function of injection rate for various values of the van Genuchten *m* parameter. The horizontal line represents the mean gas pressure associated with the base scenario.

Appendix 3. Raw Porosity Data

Sample ID	Depth (ft)	Depth (m)	Formation	Group	Porosity
4-31-1-01	2197.0	669.6	Ok	OЄK	0.98
4-31-1-02	2051.0	625.1	Ok	OЄK	2.01
4-31-1-03	1898.0	578.5	Ok	OЄK	5.32
4-31-1-04	1748.0	532.8	Oma	OЄK	1.43
4-31-1-05	1603.3	488.7	Oma	OЄK	3.12
4-31-1-06	1450.0	442.0	Oma	OЄK	1.43
H 01	286.3	87.3	Oca	OSR	4.91
H 02	361.3	110.1	Oca	OSR	0.91
H 03	436.7	133.1	Olb	OSR	2.30
H 04	513.0	156.4	Ord	OSR	0.63
H 05	586.2	178.7	Ord	OSR	2.91
H 06	661.4	201.6	Ord	OSR	2.65
H 07	736.1	224.4	Ord	OSR	1.21
H 08	813.0	247.8	Om	OSR	0.39
H 09	886.7	270.3	Om	OSR	0.21
H 11	1108.8	337.9	Owc	OSR	1.54
H 12	1257.7	383.3	Oma	OЄK	1.46
H 13	1408.0	429.2	Oma	OЄK	10.67
H 14	1557.9	474.9	Oma	OЄK	1.60
H 15	1708.0	520.6	Oma	OЄK	2.77
H 16	1859.6	566.8	Oma	OЄK	0.44
H 17	2007.7	611.9	Olv	OЄK	1.24
H 18	2159.3	658.2	Olv	OЄK	0.63
H 19	2308.4	703.6	Oche	OЄK	1.15
H 20	2458.3	749.3	Oche	OЄK	1.17
H 21	2607.8	794.9	Oche	OЄK	1.61
H 22	2757.7	840.5	Єcr	OЄK	1.21
H 23	2910.6	887.1	Єcr	OЄK	1.29
H 24	3056.2	931.5	Єcr	OЄK	1.21
H 25	3206.2	977.2	Єcr	OЄK	1.50
H 26	3360.6	1024.3	Єcr	OЄK	5.73
H 27	3508.7	1069.4	Єcr	OЄK	0.76
H 28	3660.3	1115.6	Єcr	OЄK	1.05
D 01	5562.4	1695.4	Єcr	OЄK	1.12
D 02	5365.5	1635.4	Єcr	OЄK	2.16
D 03	5180.5	1579.0	Єcr	OЄK	0.95
D 04	5009.0	1526.7	Єcr	OЄK	1.63
D 05	4859.0	1481.0	Єcr	OЄK	1.14
D 06	4694.7	1430.9	Єcr	OЄK	0.70

D 07	4552.0	1387.4	Ecr	OEK	0.65
D 08	4378.0	1334.4	Ecr	OEK	1.09
D 09	4199.3	1279.9	Oche	OEK	1.17
D 10	4052.0	1235.0	Oche	OEK	1.00
D 11	3898.8	1188.3	Oche	OEK	0.89
D 12	3750.3	1143.1	Olv	OEK	1.21
D 13	3598.1	1096.7	Olv	OEK	1.20
D 14	3449.1	1051.3	Ok	OEK	1.34
D 15	3301.0	1006.1	Ok	OEK	1.28
D 16	3149.5	960.0	Oma	OEK	2.20
D 17	3000.0	914.4	Oma	OEK	0.76
D 18	2845.7	867.4	Oma	OEK	1.31
D 19	2702.0	823.6	Oma	OEK	1.30
D 20	2406.6	733.5	Oma	OEK	4.55
D 21	2549.4	777.1	Oma	OEK	1.41
D 22	2250.5	686.0	Oma	OEK	1.01
D 23	2100.0	640.1	Oma	OEK	1.26
D 24	1951.4	594.8	Owc	OSR	5.49
D 25	1875.5	571.7	Owc	OSR	6.29
D 26	1800.8	548.9	Owc	OSR	1.12
D 27	1728.5	526.8	Om	OSR	1.02
D 28	1653.6	504.0	Om	OSR	0.36
D 29	1571.0	478.8	Om	OSR	0.31
D 30	1498.6	456.8	Om	OSR	2.19
D 31	1421.2	433.2	Ord	OSR	0.57
D 32	1350.0	411.5	Ord	OSR	0.44
D 34	1196.2	364.6	Olb	OSR	0.64
D 35	1141.8	348.0	Oca	OSR	1.12
2-50-1-001	1441.5	439.4	Om	OSR	1.31
2-50-1-002	1517.4	462.5	Owc	OSR	1.40
2-50-1-003	1614.3	492.0	Oma	OEK	5.60
2-50-1-004	1721.0	524.6	Oma	OEK	5.32
2-50-1-005	1818.5	554.3	Oma	OEK	1.83
2-50-1-006	1918.5	584.8	Oma	OEK	0.92
2-50-1-007	2014.5	614.0	Ok	OEK	3.03
2-50-1-008	2105.6	641.8	Ok	OEK	1.02
2-50-1-009	2209.5	673.5	Ok	OEK	1.22
2-50-1-010	2304.0	702.3	Ok	OEK	1.33
2-50-1-011	2375.0	723.9	Ok	OEK	6.50
CU30-001	677.5	206.5	Oca	OSR	0.60
CU30-002	778.0	237.1	Oca	OSR	0.87
CU30-003	862.0	262.7	Olb	OSR	1.05
CU30-004	981.4	299.1	Ord	OSR	0.49

CU30-005	1078.0	328.6	Ord	OSR	0.94
CU30-006	1180.5	359.8	Om	OSR	1.00
CU30-007	1275.5	388.8	Om	OSR	1.27
CU30-008	1369.0	417.3	Om	OSR	0.40
CU30-009	1447.0	441.0	Owc	OSR	1.02
CA5-001	1076.9	328.2	Om	OSR	3.17
CA5-002	799.0	243.5	Om	OSR	1.57
CA5-003	899.0	274.0	Om	OSR	1.16
CA5-004	989.0	301.4	Om	OSR	0.81
CA5-005	396.0	120.7	Oca	OSR	1.35
CA5-006	700.5	213.5	Om	OSR	0.76
CA5-007	594.0	181.1	Ord	OSR	1.02
CA5-008	332.0	101.2	Oca	OSR	0.99

Appendix 4. Example STOMP Input File

15 wt.-% Salinity Input File

~Simulation Title Card
1,
Problem 3,
M.D. White,
Pacific Northwest Laboratory,
21 May 2002,
09:45 AM PST,
10,
Intercomparison of simulation models for CO2 disposal in
underground storage reservoirs.
Test Problem 3: Radial Flow from a CO2 Injection Well
This problem addresses two-phase flow of CO2 and water
for simplified flow geometry and medium properties. The
aquifer into which injection is made is assumed infinite-acting,
homogeneous, and isotropic. Gravity and inertial effects are
neglected, injection is made at a constant mass rate, and flow
is assumed 1-D radial (line source). Under the conditions
stated the problem has a similarity solution where dependence on
radial distance R and time t occurs only through the similarity
variable x = R2/t (O'Sullivan 1981; Doughty and Pruess 1992).

~Solution Control Card
Normal,
H2O-NaCl-CO2,
1,
0,day,1.e+5,day,1.e-3,s,1.e+4,day,1.15,16,1.e-06,
10000,
Variable Aqueous Diffusion,
Variable Gas Diffusion,
0,

~Grid Card
Cylindrical,
100,1,1,
0.3,m,0.34068267,m,0.386882272,m,0.439346951,m,0.498926308,m,0.566585156,m,
0.643419145,m,0.730672508,m,0.829758203,m,0.9422808,m,1.070062462,m,
1.215172455,m,1.379960655,m,1.567095601,m,1.779607712,m,2.020938356,m,
2.294995583,m,2.606217409,m,2.959643684,m,3.360997708,m,3.81677891,m,
4.334368098,m,4.922146988,m,5.589633925,m,6.347638032,m,7.208434242,m,
8.185962079,m,9.296051391,m,10.55667869,m,11.98825828,m,13.61397279,m,
15.46014866,m,17.55668242,m,19.9375248,m,22.64123061,m,25.71158298,m,
29.19830246,m,33.15785213,m,37.65435198,m,42.76061723,m,48.55933748,m,

55.14441582,m,62.62248937,m,71.11465626,m,80.75843656,m,91.70999929,m,
104.1466914,m,118.2699096,m,134.308362,m,152.5217712,m,173.2050808,m,
196.6932312,m,223.3665839,m,253.6570806,m,288.0552382,m,327.1180922,m,
371.4782167,m,421.853969,m,479.0611216,m,544.0260733,m,617.8008506,m,
701.5801442,m,796.7206557,m,904.7630673,m,1027.456991,m,1166.789304,m,
1325.016317,m,1504.700323,m,1708.751078,m,1940.472932,m,2203.618331,m,
2502.448588,m,2841.802888,m,3227.176651,m,3664.810527,m,4161.79145,m,
4726.16741,m,5367.077773,m,6094.901285,m,6921.424143,m,7860.030856,m,
8925.920993,m,10136.35532,m,11510.93531,m,13071.92059,m,14844.58935,m,
16857.64778,m,19143.69485,m,21739.75025,m,24687.85387,m,28035.74657,m,
31837.64332,m,36155.1111,m,41058.06594,m,46625.90509,m,52948.79278,m,
60129.12031,m,68283.16417,m,77542.96894,m,88058.48564,m,100000,m,100000,m,
0.0,deg,45.0,deg,
0.0,m,100.0,m,

~Rock/Soil Zonation Card
1,
Aquifer,1,100,1,1,1,1,

~Mechanical Properties Card
Aquifer,2650,kg/m^3,0.12,0.12,Compressibility,4.5e-10,1/Pa,100.0,bar,Millington and Quirk,

~Hydraulic Properties Card
Aquifer,1.0e-13,m^2,,,,,0.8,0.8,

~Saturation Function Card
Aquifer,van Genuchten,0.5,1/m,1.84162,0.0,0.457,,

~Aqueous Relative Permeability Card
Aquifer,Mualem Irreducible,0.457,0.30,

~Gas Relative Permeability Card
Aquifer,Corey,0.05,0.30,

~Salt Transport Card
Aquifer,0.0,m,0.0,m,

~Initial Conditions Card
Gas Pressure,Aqueous Pressure,
4,
Gas Pressure,120.0,Bar,,,,,,1,100,1,1,1,1,
Aqueous Pressure,120.0,Bar,,,,,,1,100,1,1,1,1,
Temperature,45.0,C,,,,,,1,100,1,1,1,1,
Salt Mass Fraction,0.15,,,,,,,1,100,1,1,1,1,

~Source Card
1,
Gas Mass Rate,Water-Vapor Mass Fraction,1,1,1,1,1,1,1,
0,s,120.0,bar,12.5,kg/s,0.0,

~Boundary Conditions Card
1,
East,Aqu. Dirichlet,Gas Dirichlet,Aqu. Mass Frac.,
100,100,1,1,1,1,1,
0,s,120.0,bar,0.0,120.0,bar,1.0,0.15,,

~Output Options Card
1,
64,1,1,
1,1,s,m,deg,6,6,6,
6,
Gas Saturation,,
Salt Saturation,,
Salt Aqueous Mass Fraction,,
CO2 Aqueous Mass Fraction,,
Gas Pressure,Pa,
Diffusive Porosity,,
4,
30,day,
100,day,
1000,day,
10000,day,
6,
Gas Saturation,,
Salt Saturation,,
Salt Aqueous Mass Fraction,,
CO2 Aqueous Mass Fraction,,
Gas Pressure,Pa,
Diffusive Porosity,,

Appendix 5. Supplimentary Figures

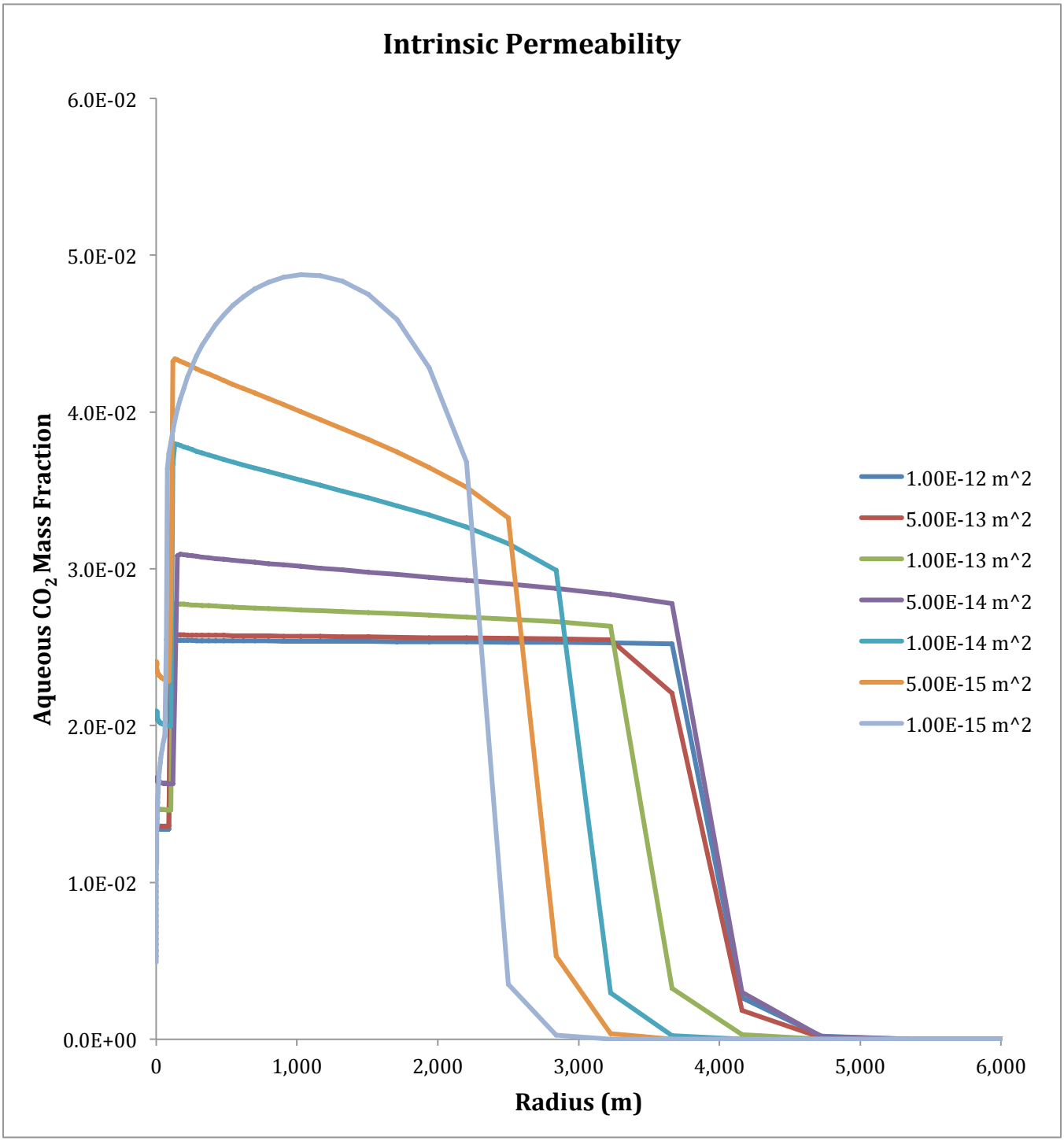

Aqueous CO_2 mass fraction as a function of radial distance from the injection well for various values of intrinsic permeability after approximately 27 years at an injection rate of 12.5 kg/s.

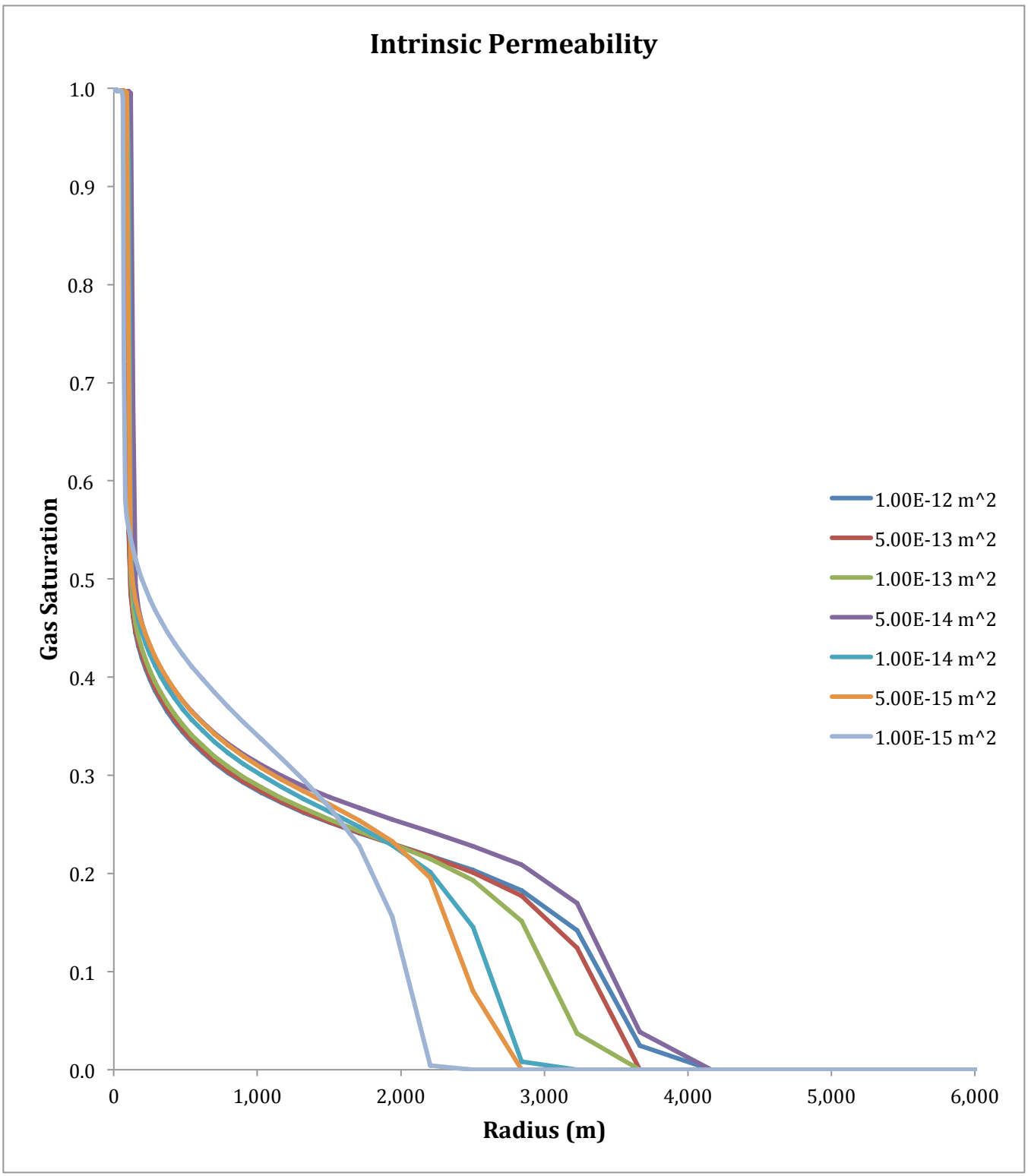

Gas saturation as a function of radial distance from injection well for various values of intrinsic permeability after approximately 27 years at an injection rate of 12.5 kg/s.

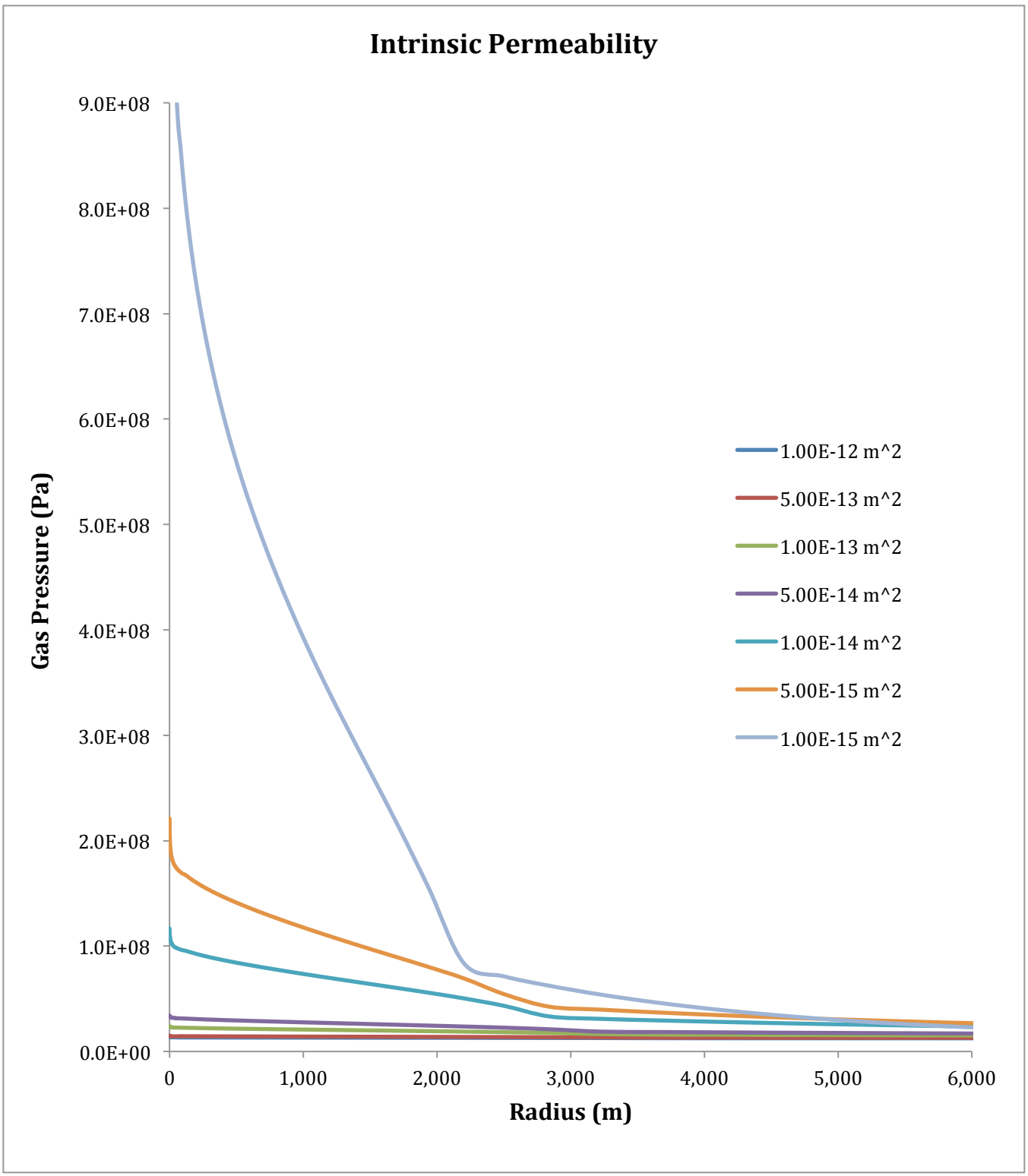

Gas pressure as a function of radial distance from injection well for various values of intrinsic permeability after approximately 27 years at an injection rate of 12.5 kg/s.

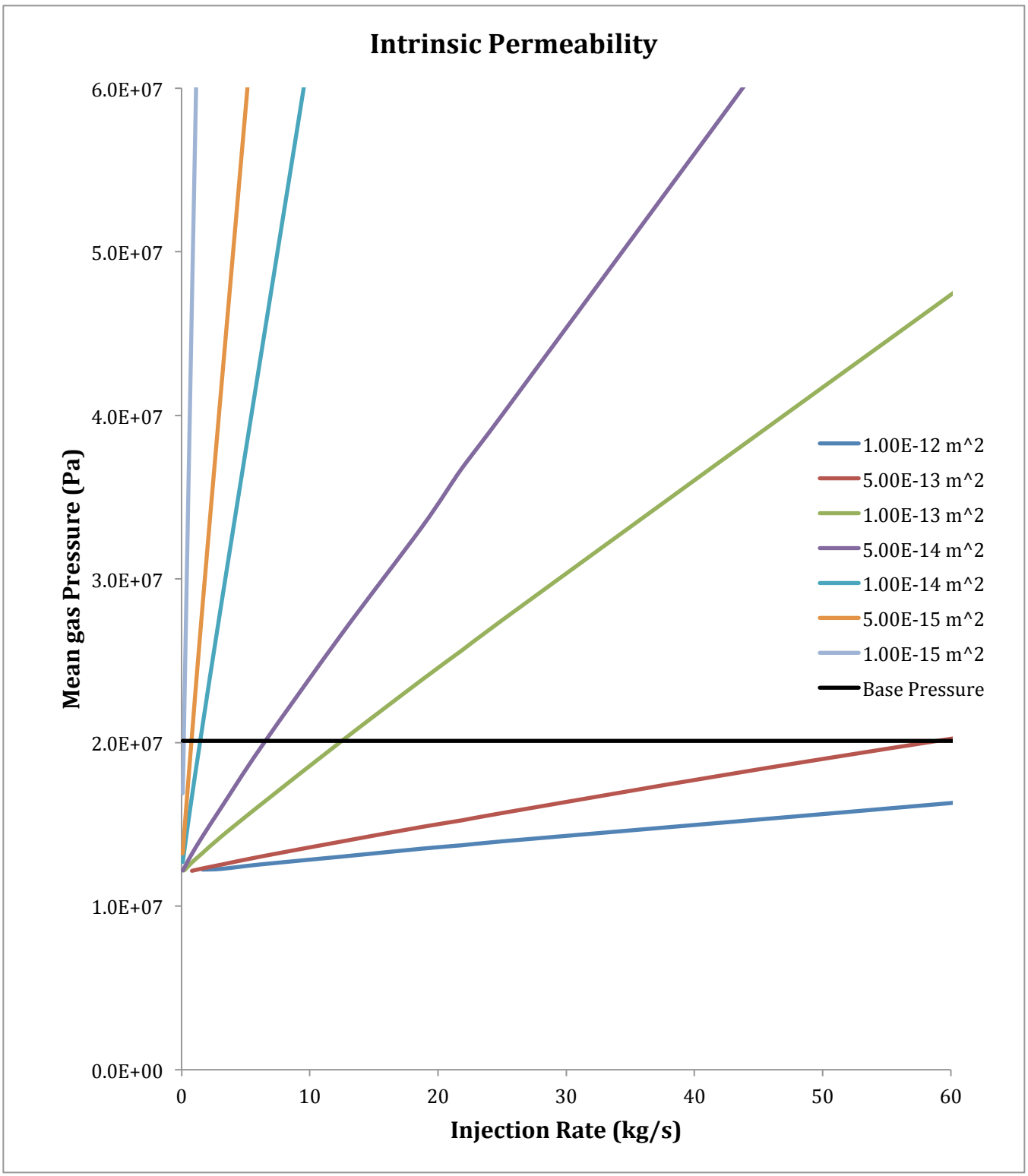

Mean gas pressure as a function of injection rate for various values of intrinsic permeability. The horizontal line represents the mean gas pressure associated with the base scenario.

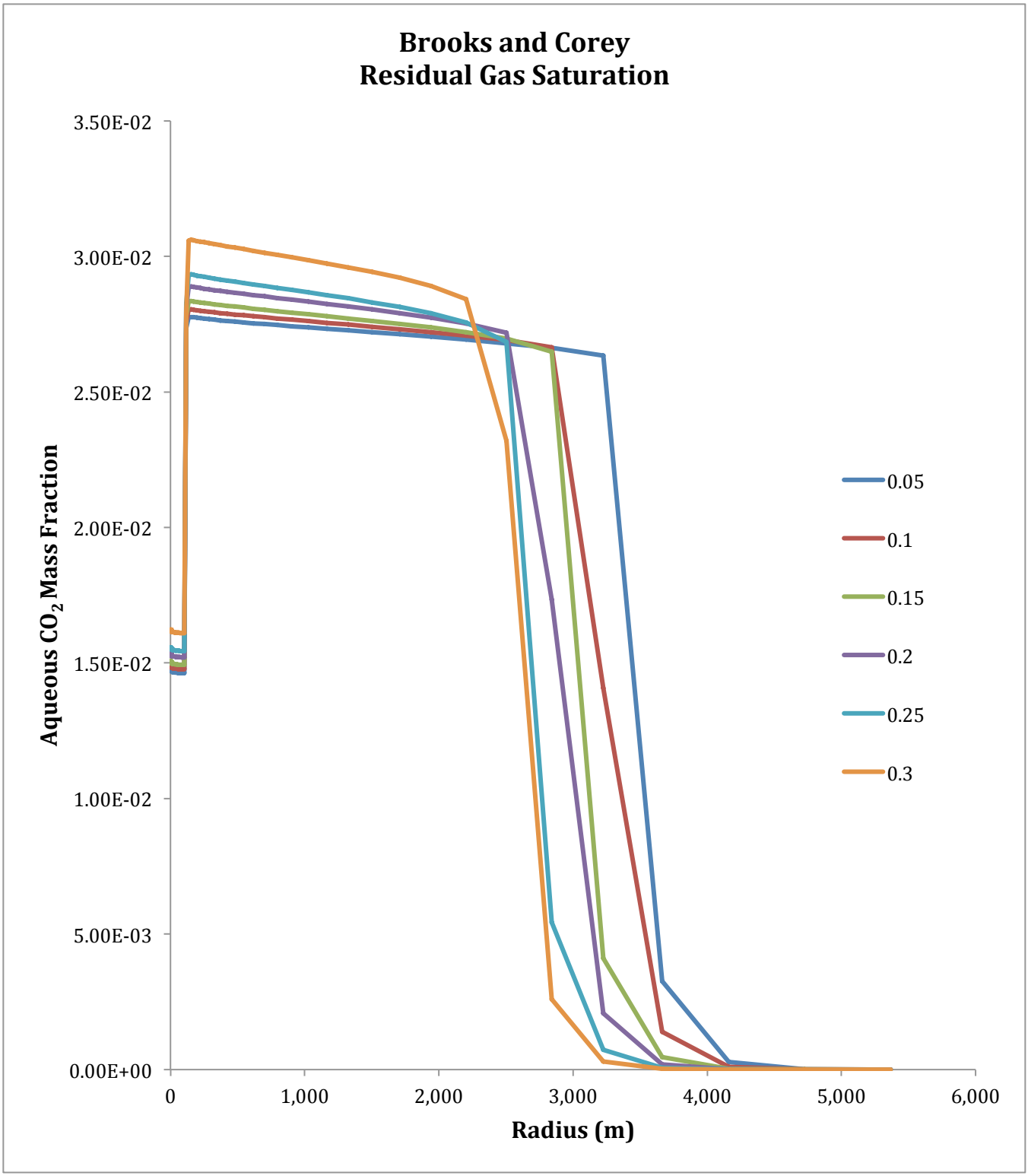

Aqueous CO_2 mass fraction as a function of radial distance from the injection well for various values of the Brooks and Corey residual gas saturation after approximately 27 years at an injection rate of 12.5 kg/s.

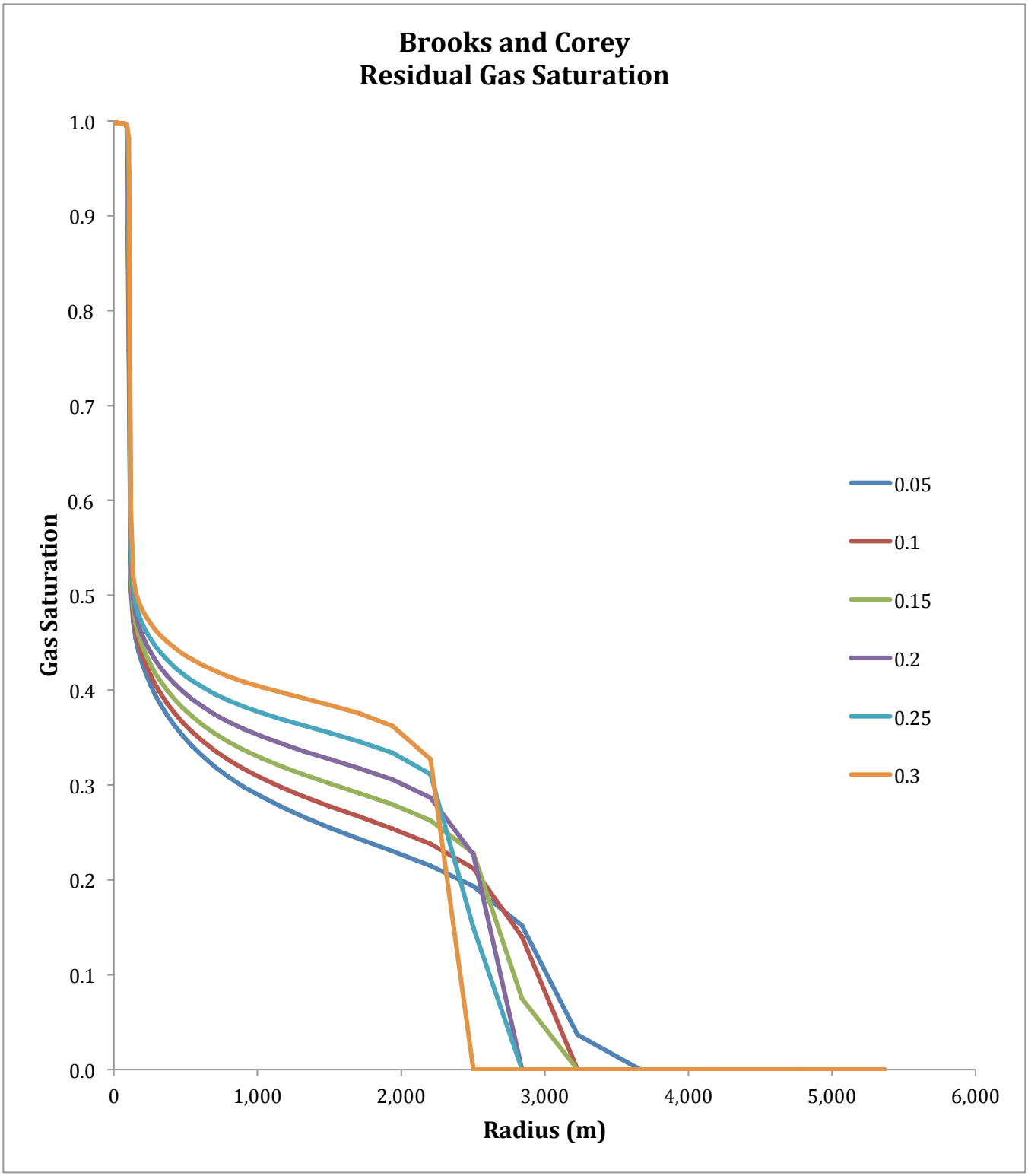

Gas saturation as a function of radial distance from injection well for various values of the Brooks and Corey residual gas saturation after approximately 27 years at an injection rate of 12.5 kg/s.

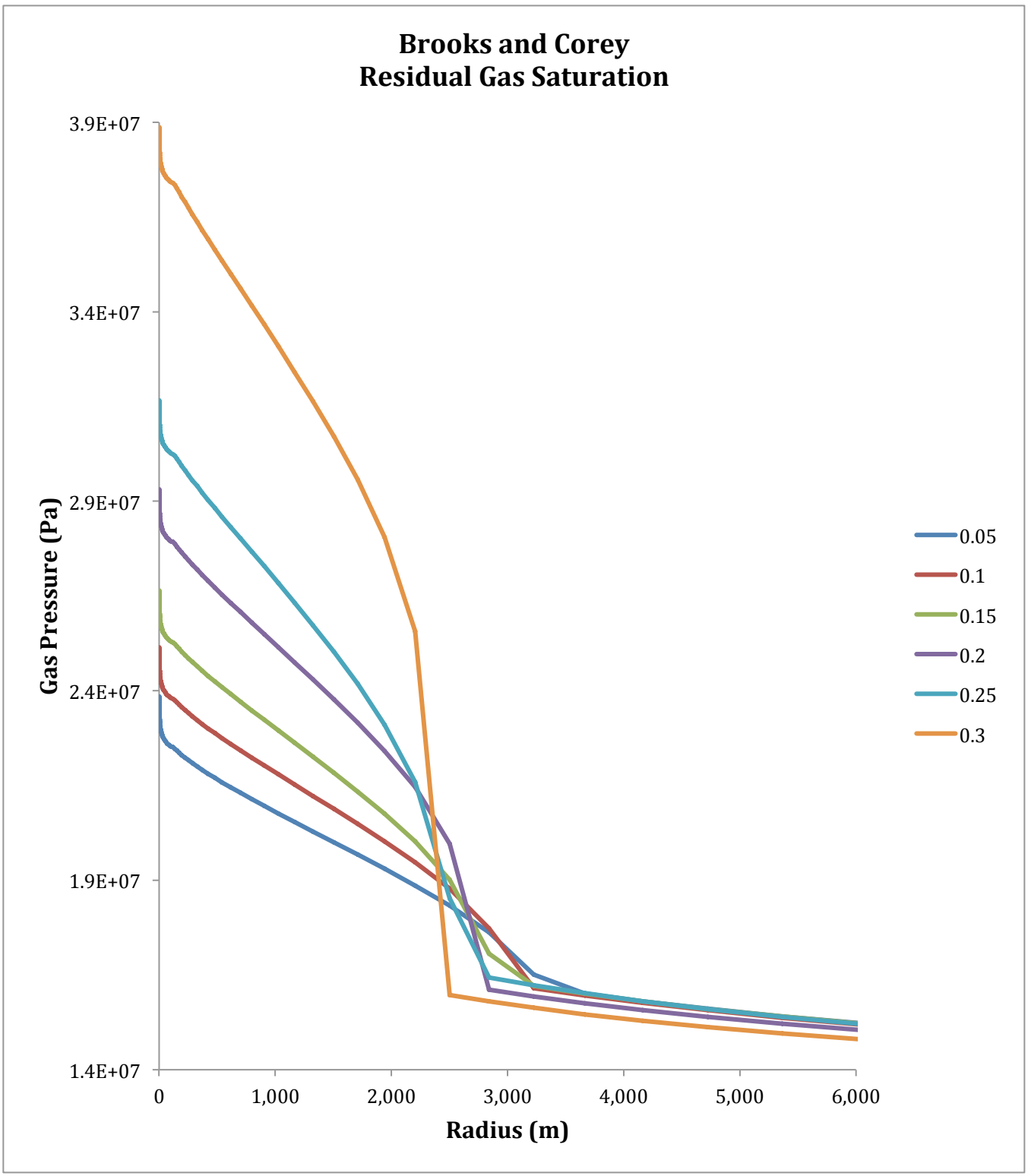

Gas pressure as a function of radial distance from injection well for various values of the Brooks and Corey residual gas saturation after approximately 27 years at an injection rate of 12.5 kg/s.

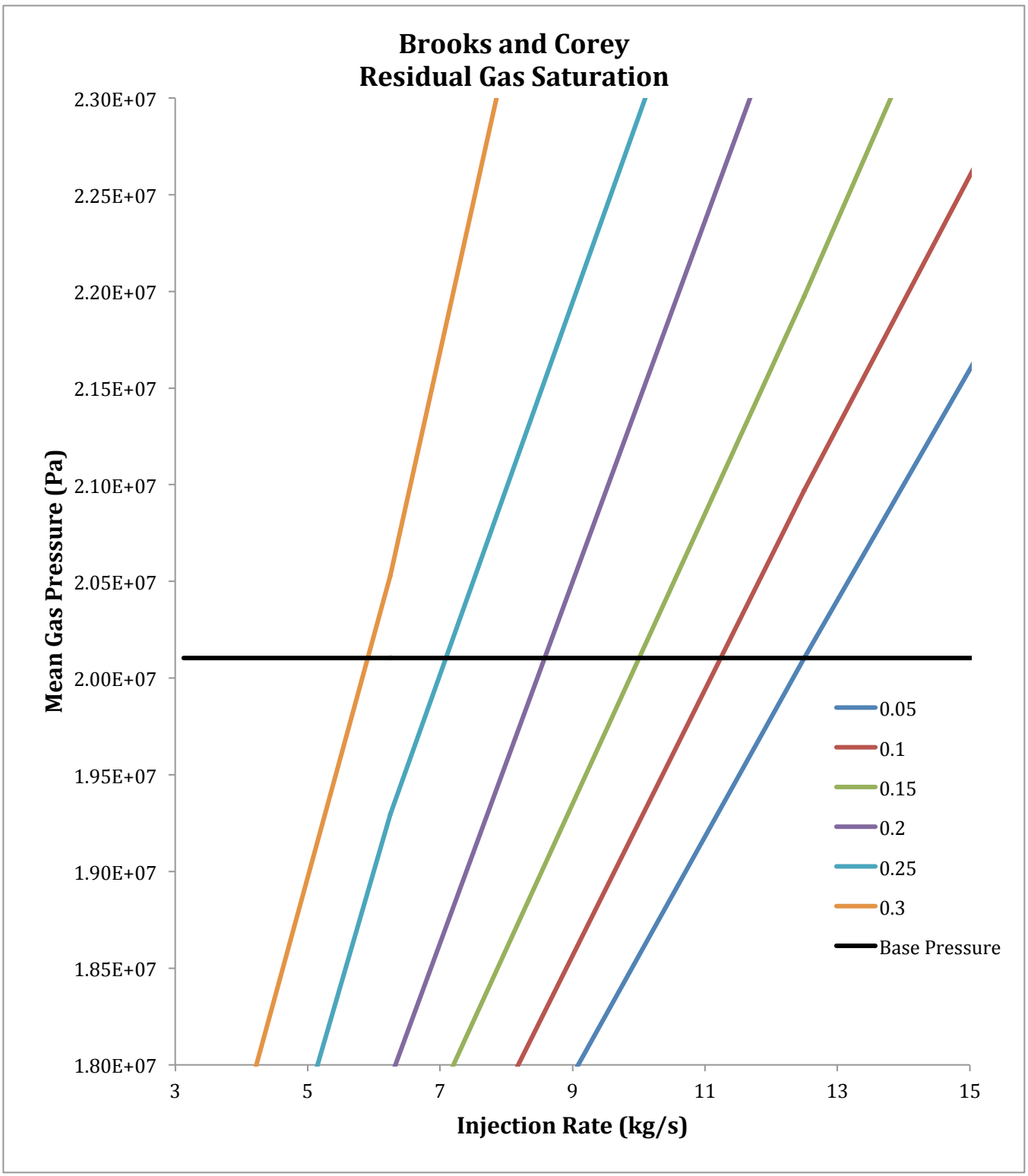

Mean gas pressure as a function of injection rate for various values of the Brooks and Corey residual gas saturation. The horizontal line represents the mean gas pressure associated with the base scenario.

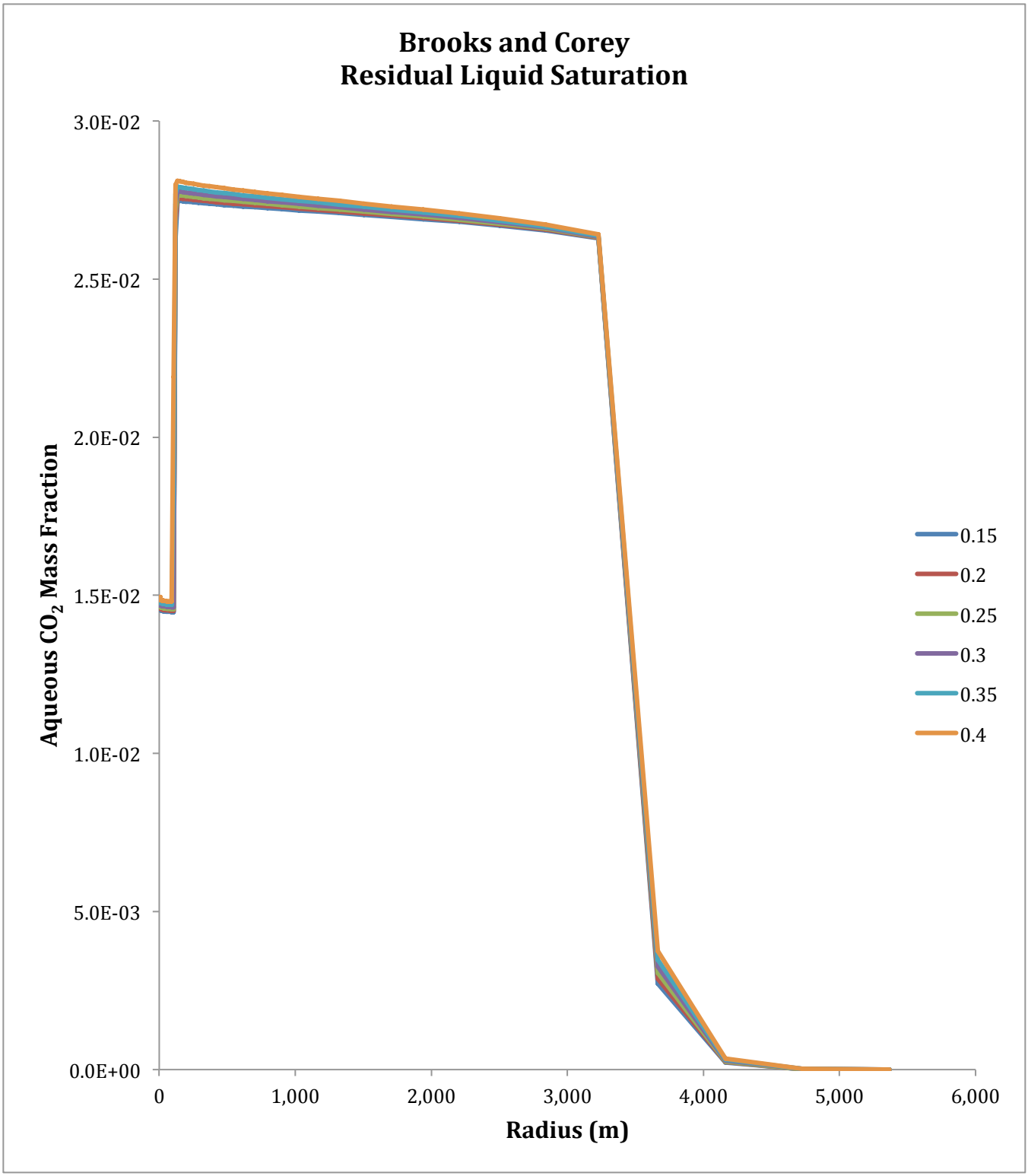

Aqueous CO_2 mass fraction as a function of radial distance from the injection well for various values of the Brooks and Corey residual liquid saturation after approximately 27 years at an injection rate of 12.5 kg/s.

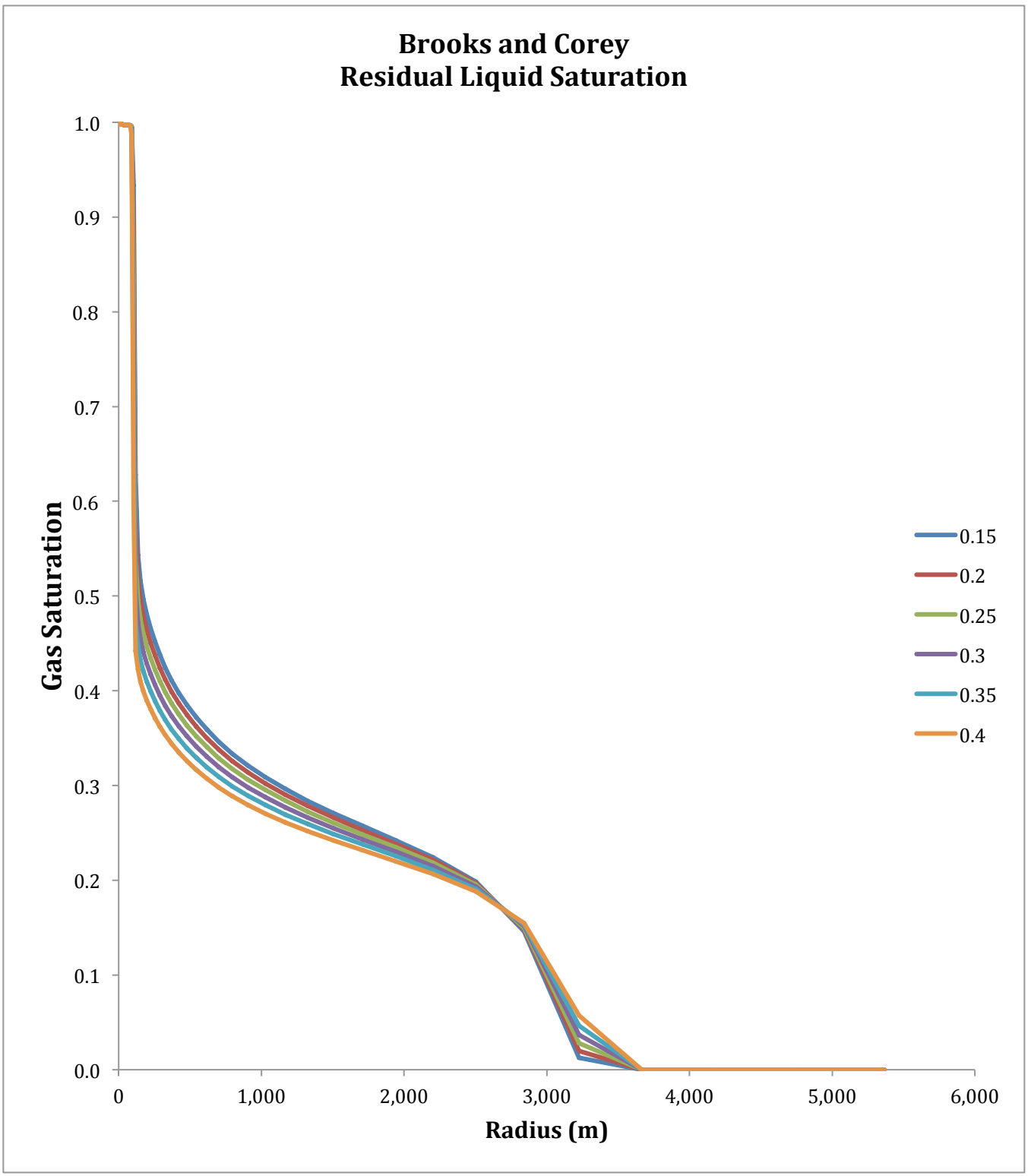

Gas saturation as a function of radial distance from injection well for various values of the Brooks and Corey residual liquid saturation after approximately 27 years at an injection rate of 12.5 kg/s.

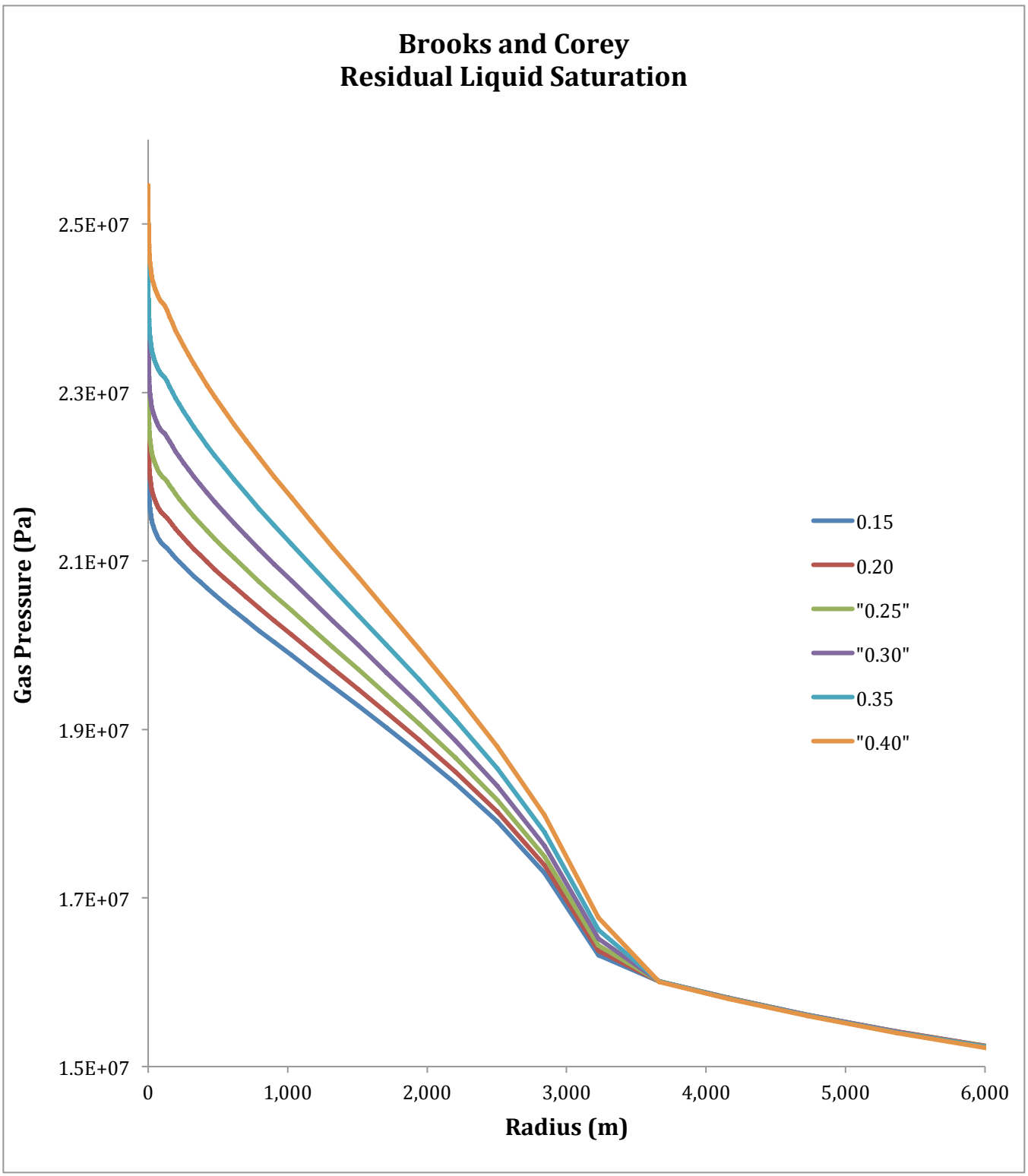

Gas pressure as a function of radial distance from injection well for various values of the Brooks and Corey residual liquid saturation after approximately 27 years at an injection rate of 12.5 kg/s.

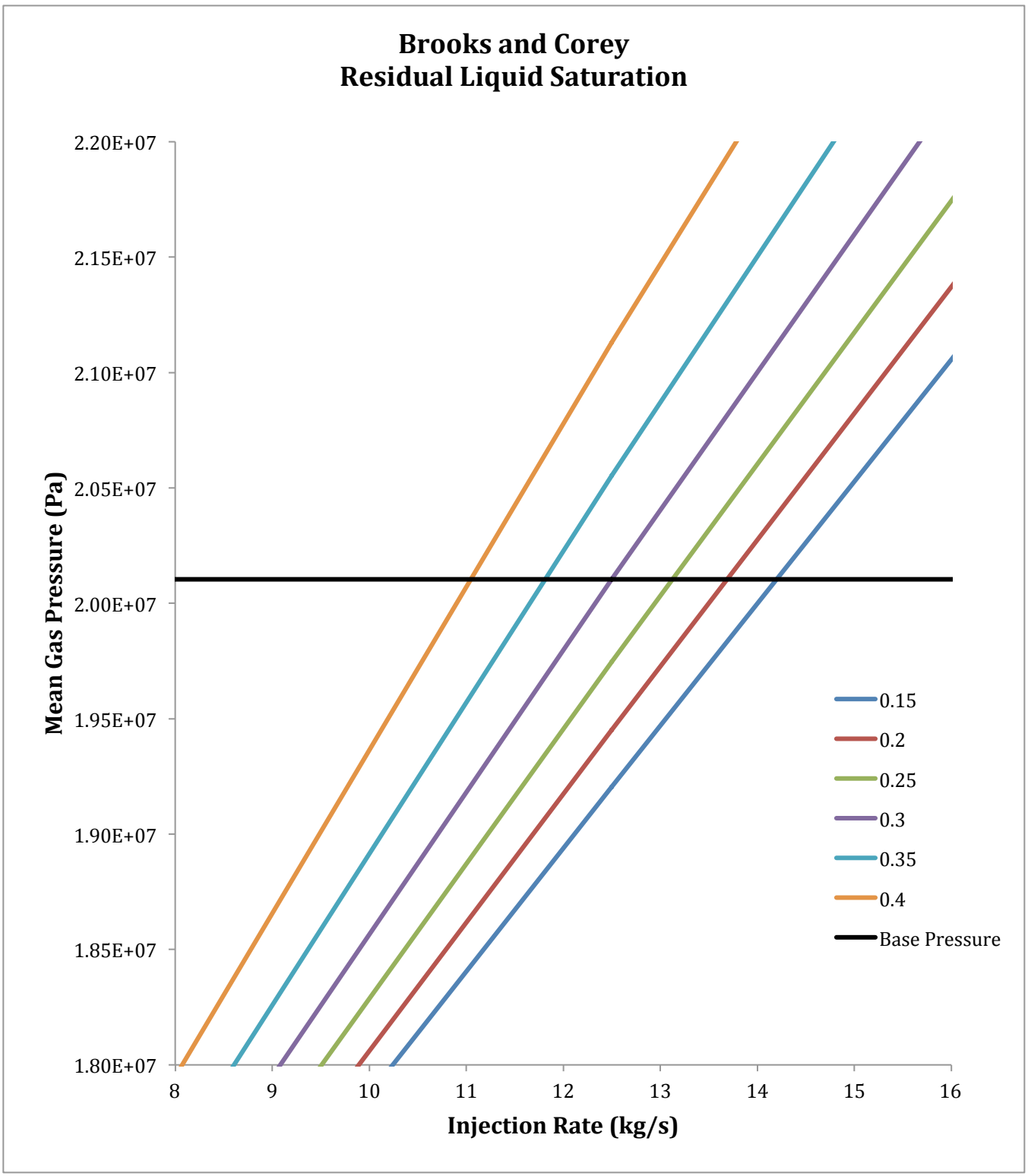

Mean gas pressure as a function of injection rate for various values of the Brooks and Corey residual liquid saturation. The horizontal line represents the mean gas pressure associated with the base scenario.

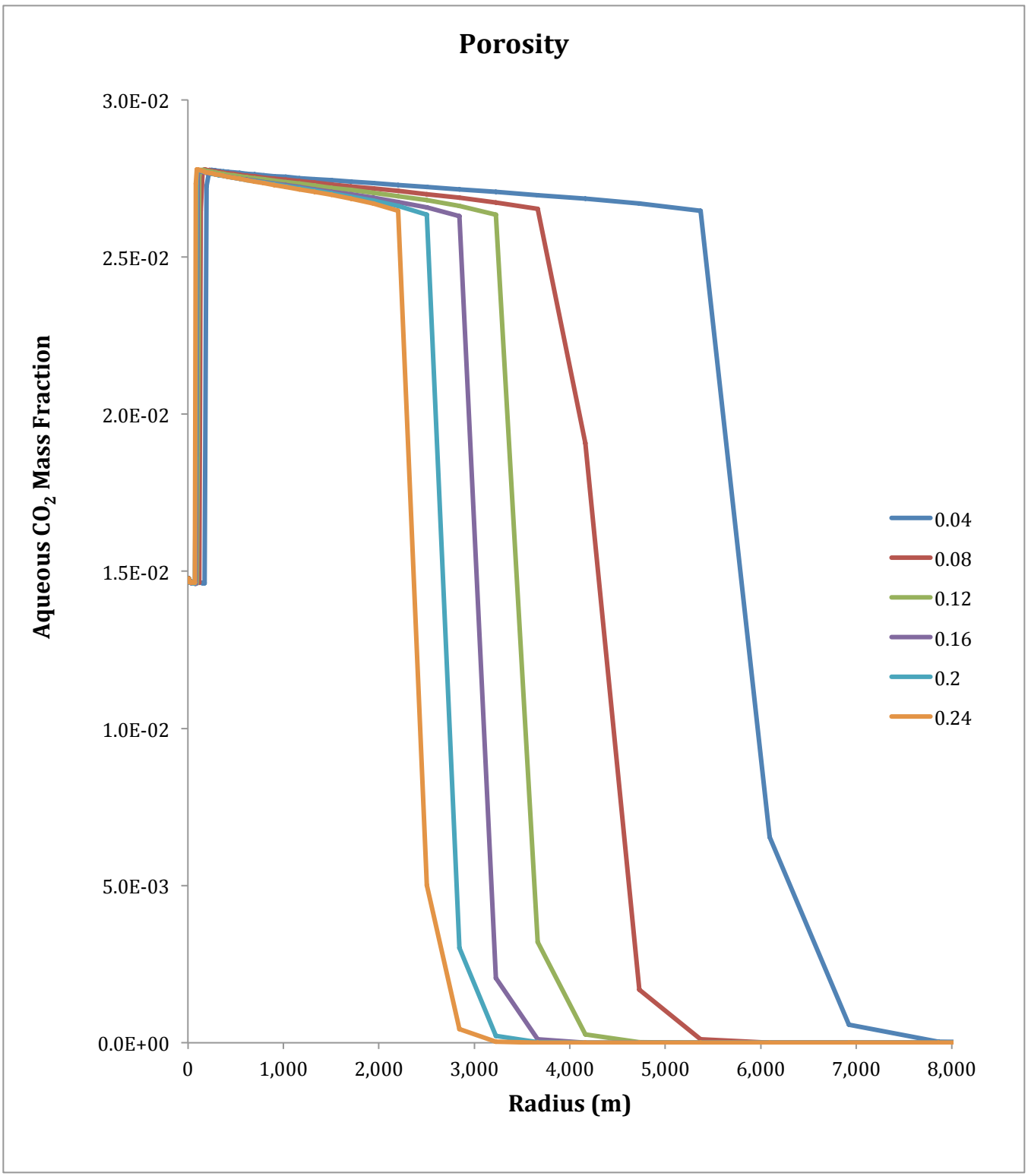

Aqueous CO_2 mass fraction as a function of radial distance from the injection well for various porosity values after approximately 27 years at an injection rate of 12.5 kg/s.

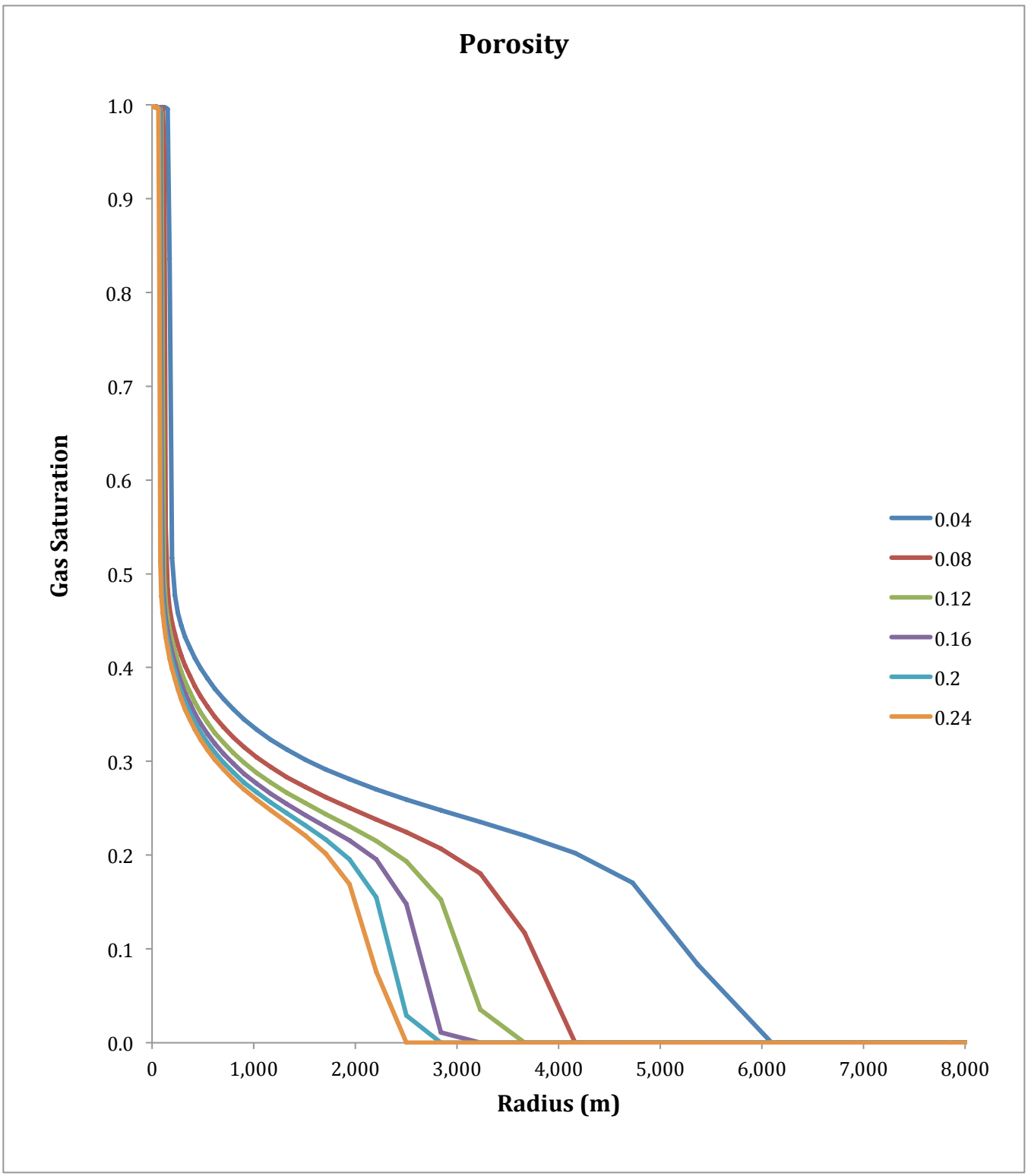

Gas saturation as a function of radial distance from injection well for various porosity values after approximately 27 years at an injection rate of 12.5 kg/s.

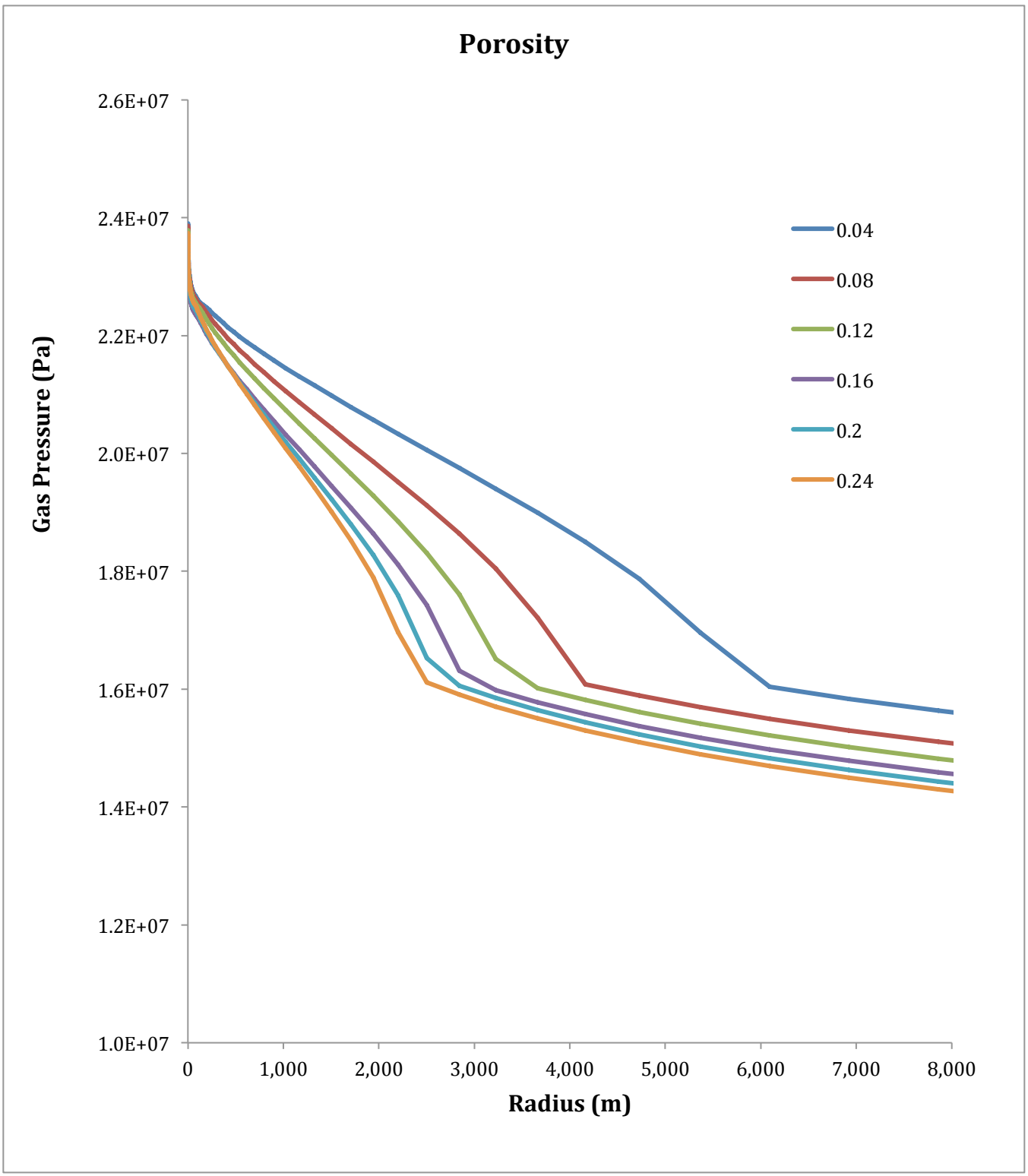

Gas pressure as a function of radial distance from injection well for various porosity values after approximately 27 years at an injection rate of 12.5 kg/s.

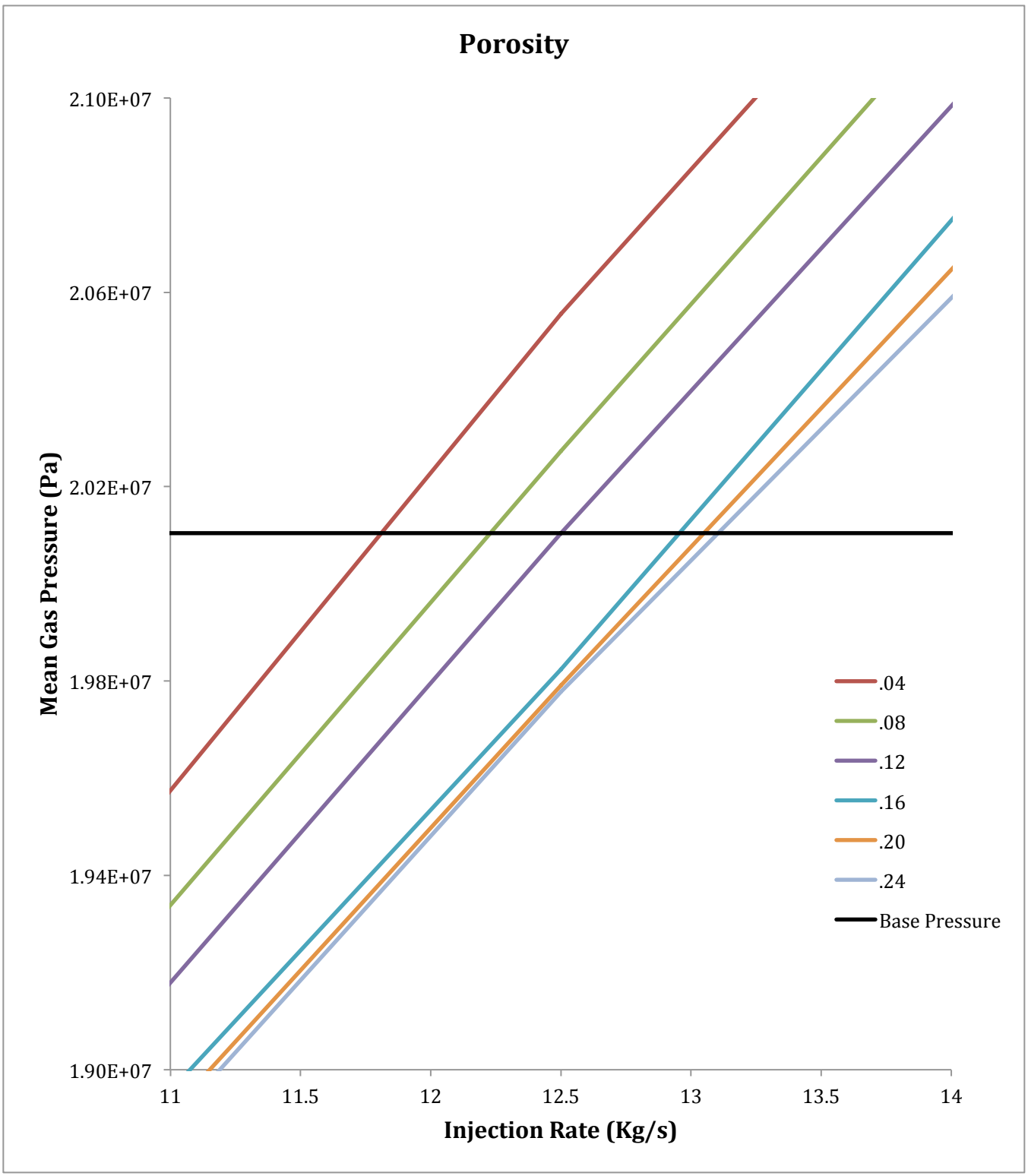

Mean gas pressure as a function of injection rate for various porosity values. The horizontal line represents the mean gas pressure associated with the base scenario.

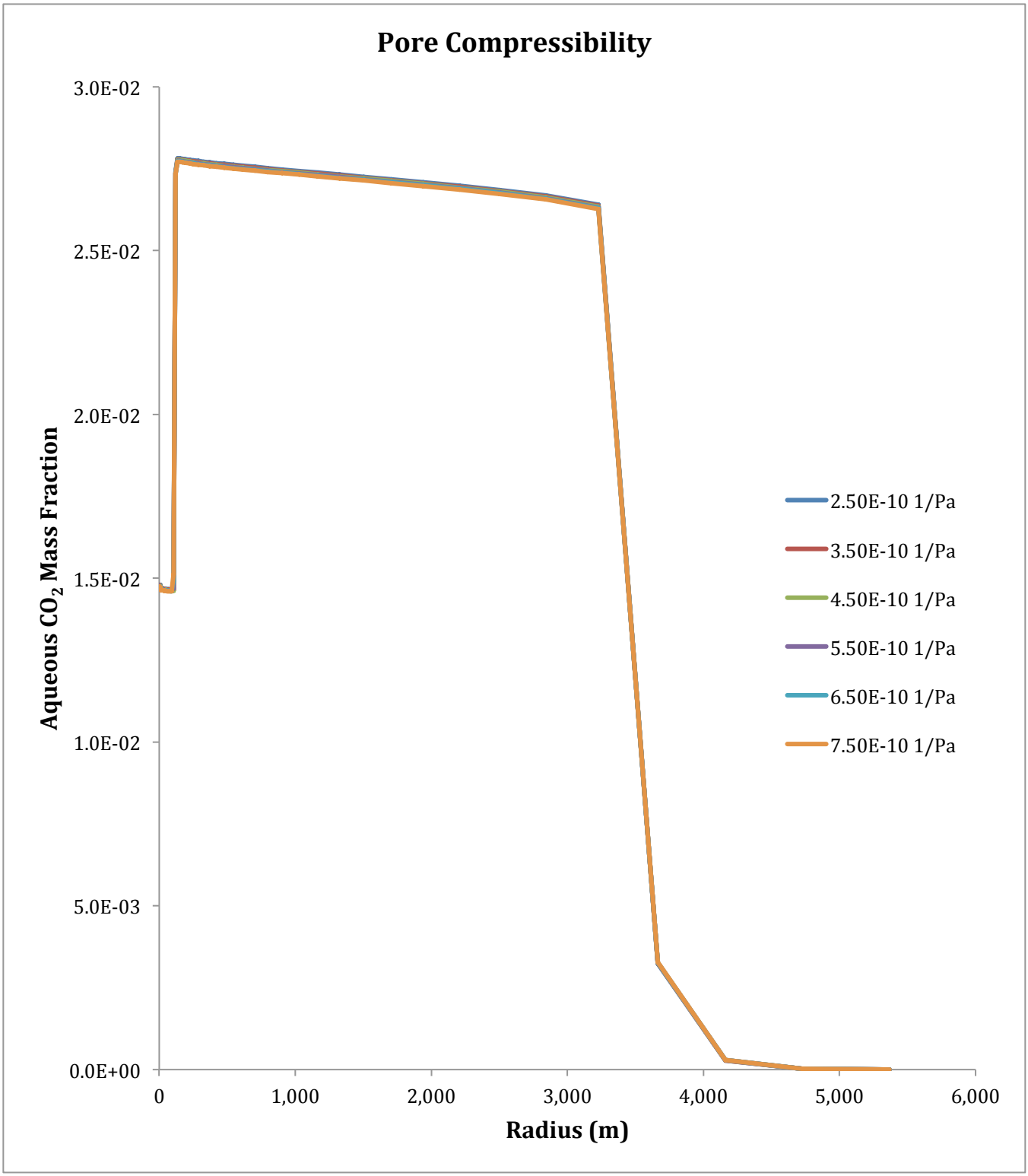

Aqueous CO_2 mass fraction as a function of radial distance from the injection well for various values of pore compressibility after approximately 27 years at an injection rate of 12.5 kg/s.

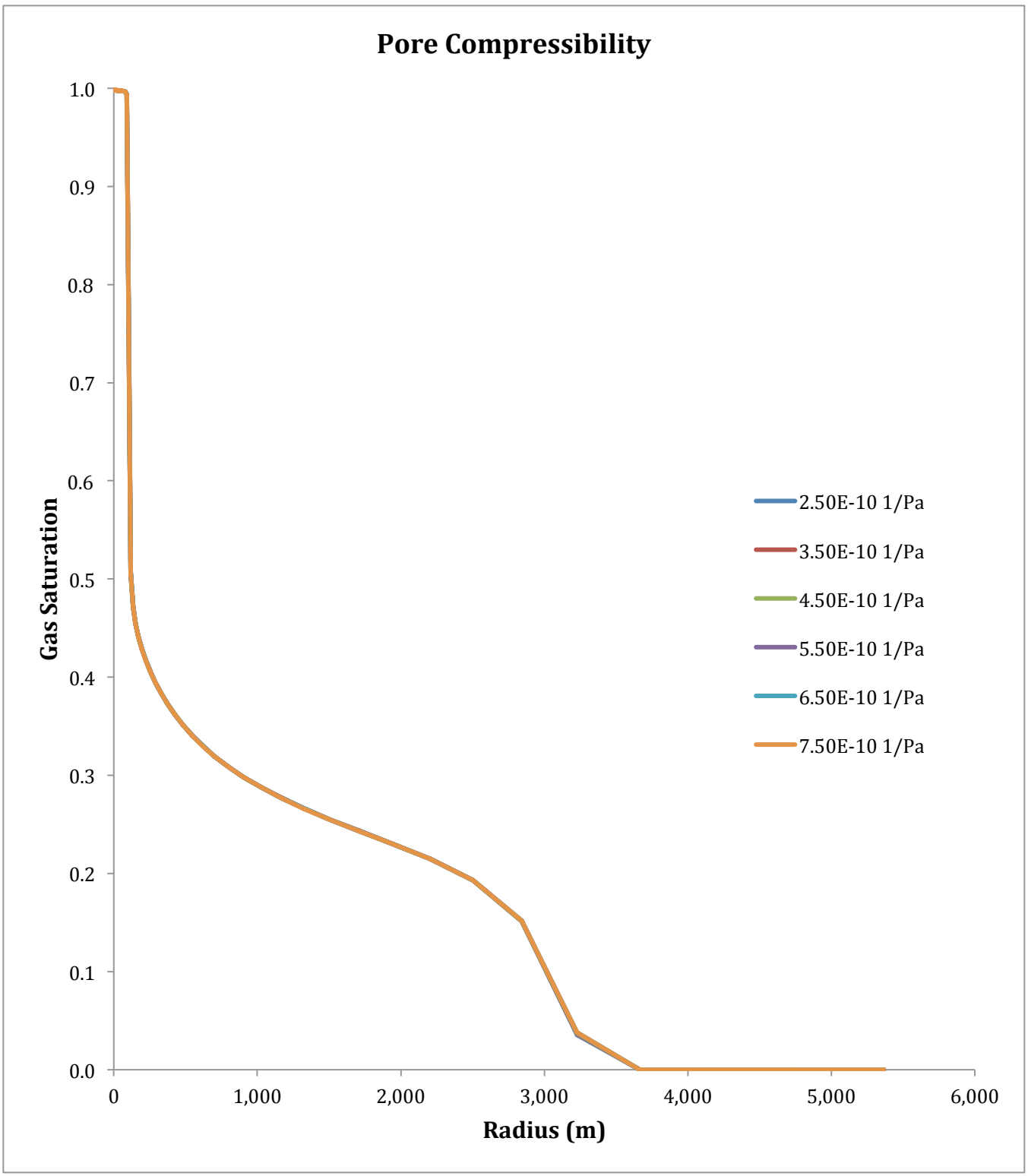

Gas saturation as a function of radial distance from injection well for various values of pore compressibility after approximately 27 years at an injection rate of 12.5 kg/s.

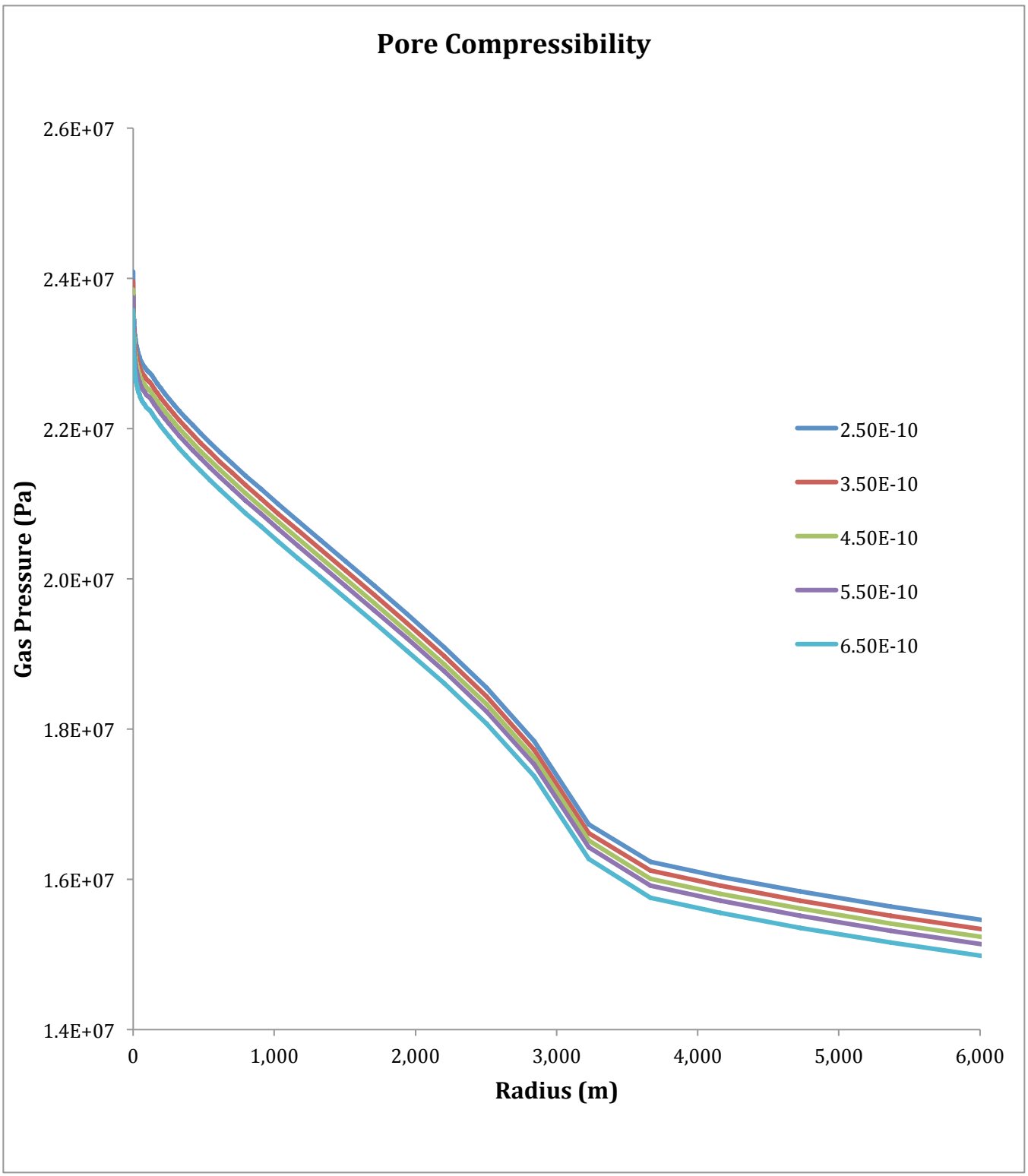

Gas pressure as a function of radial distance from injection well for various pore compressibility values after approximately 27 years at an injection rate of 12.5 kg/s.

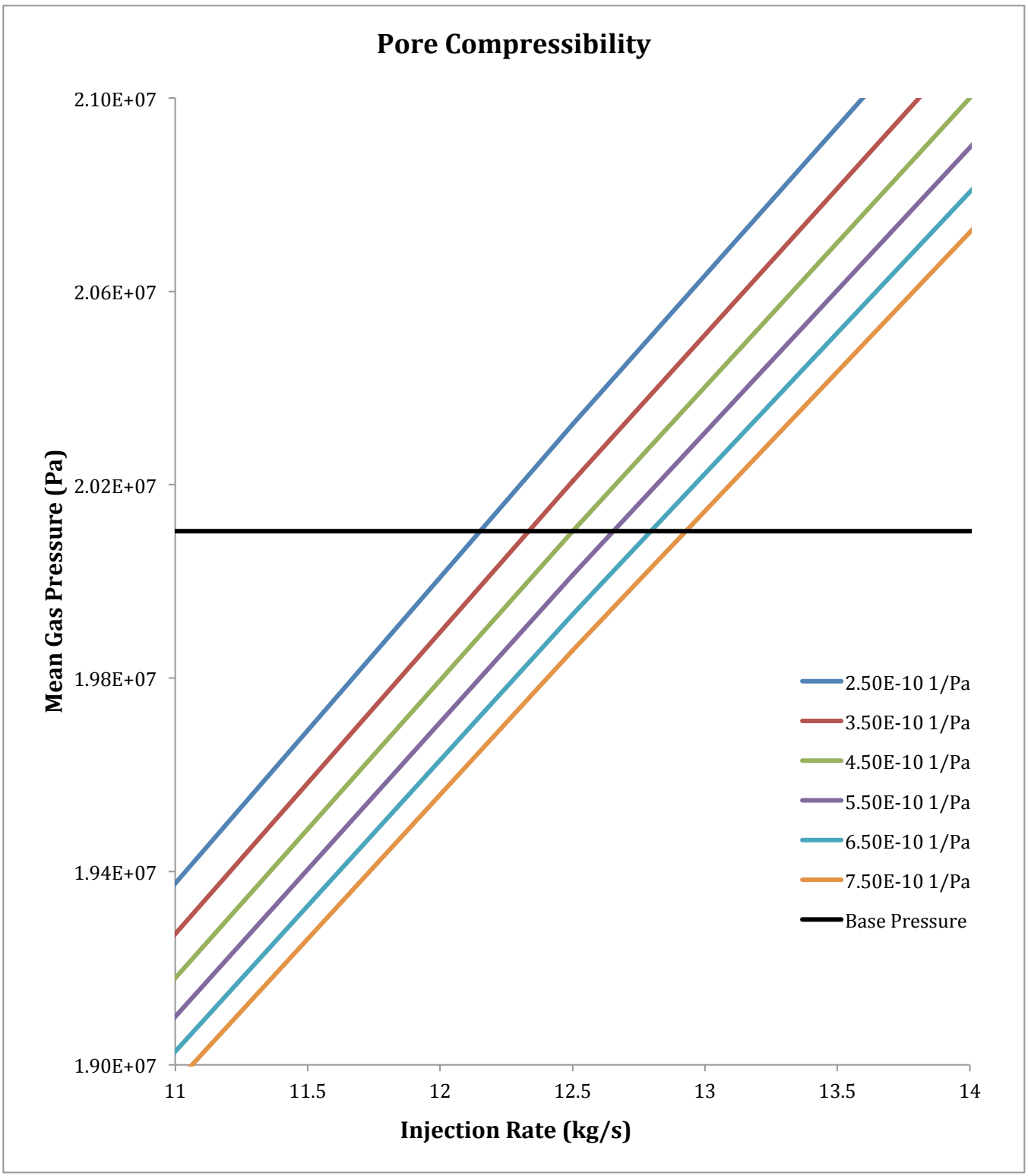

Mean gas pressure as a function of injection rate for various values of pore compressibility. The horizontal line represents the mean gas pressure associated with the base scenario.

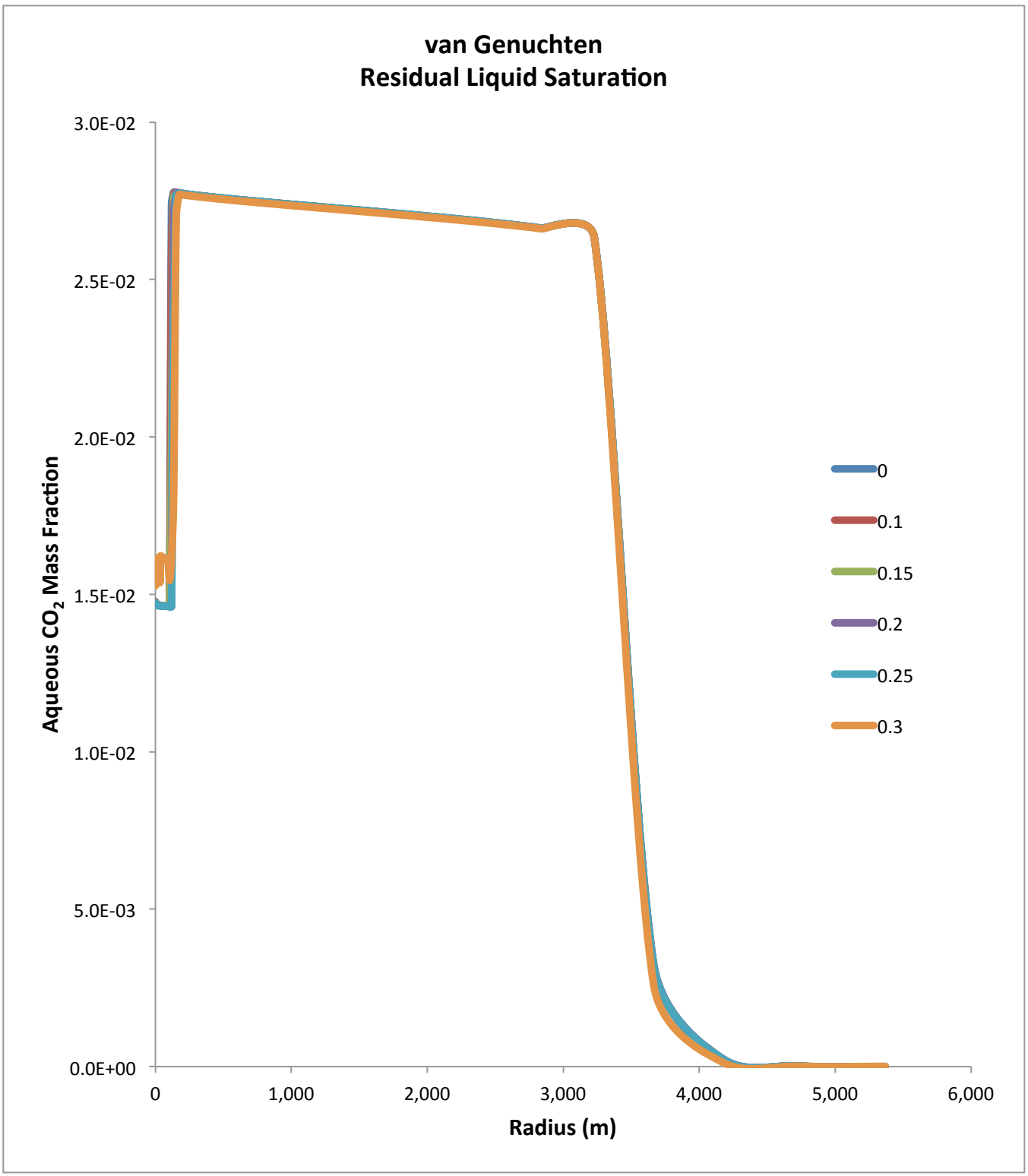

Aqueous CO_2 mass fraction as a function of radial distance from the injection well for various values of the van Genuchten residual liquid saturation after approximately 27 years at an injection rate of 12.5 kg/s.

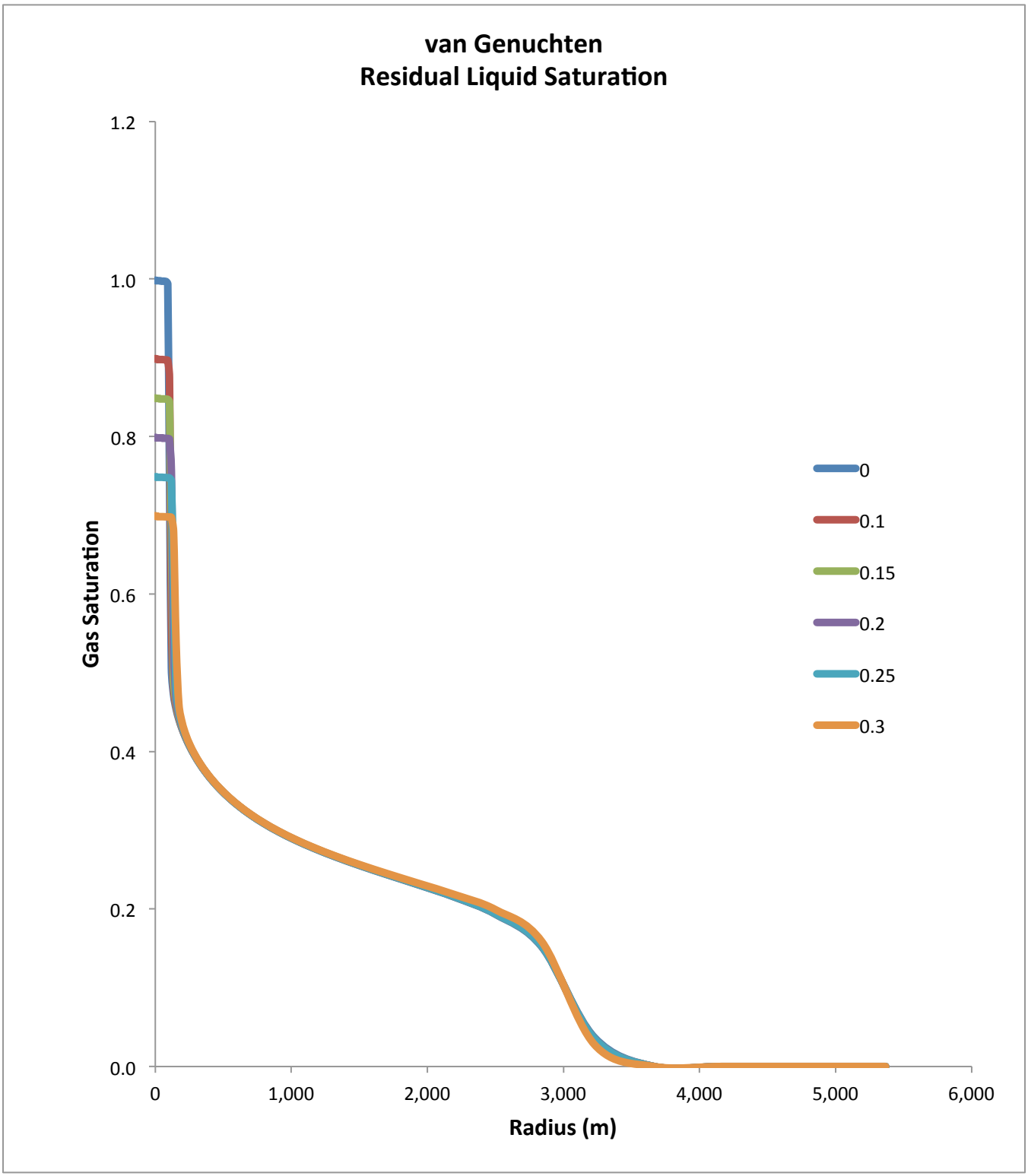

Gas saturation as a function of radial distance from injection well for various values of the van Genuchten residual liquid saturation after approximately 27 years at an injection rate of 12.5 kg/s.

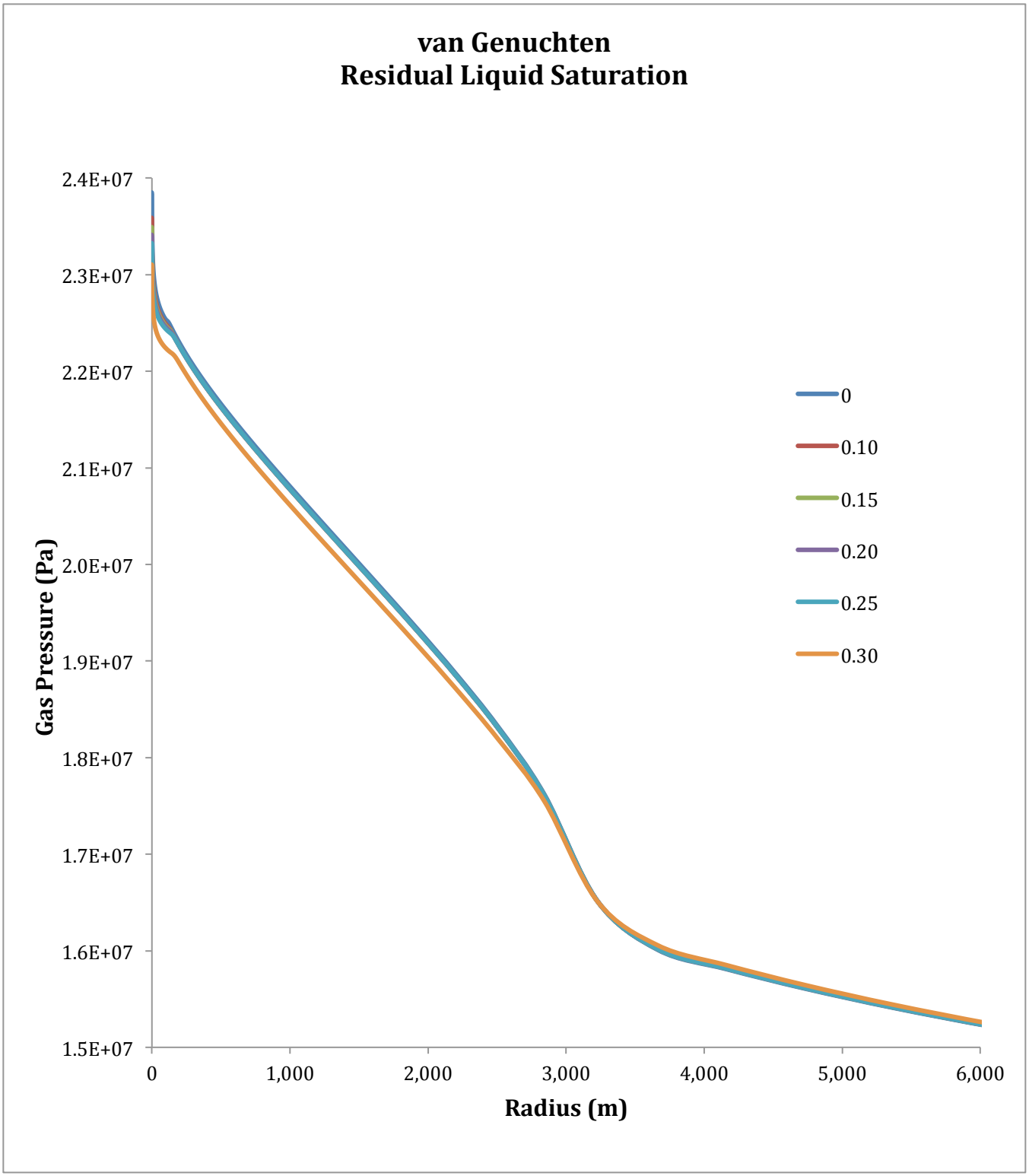

Gas pressure as a function of radial distance from injection well for various values of the van Genuchten residual liquid saturation after approximately 27 years at an injection rate of 12.5 kg/s.

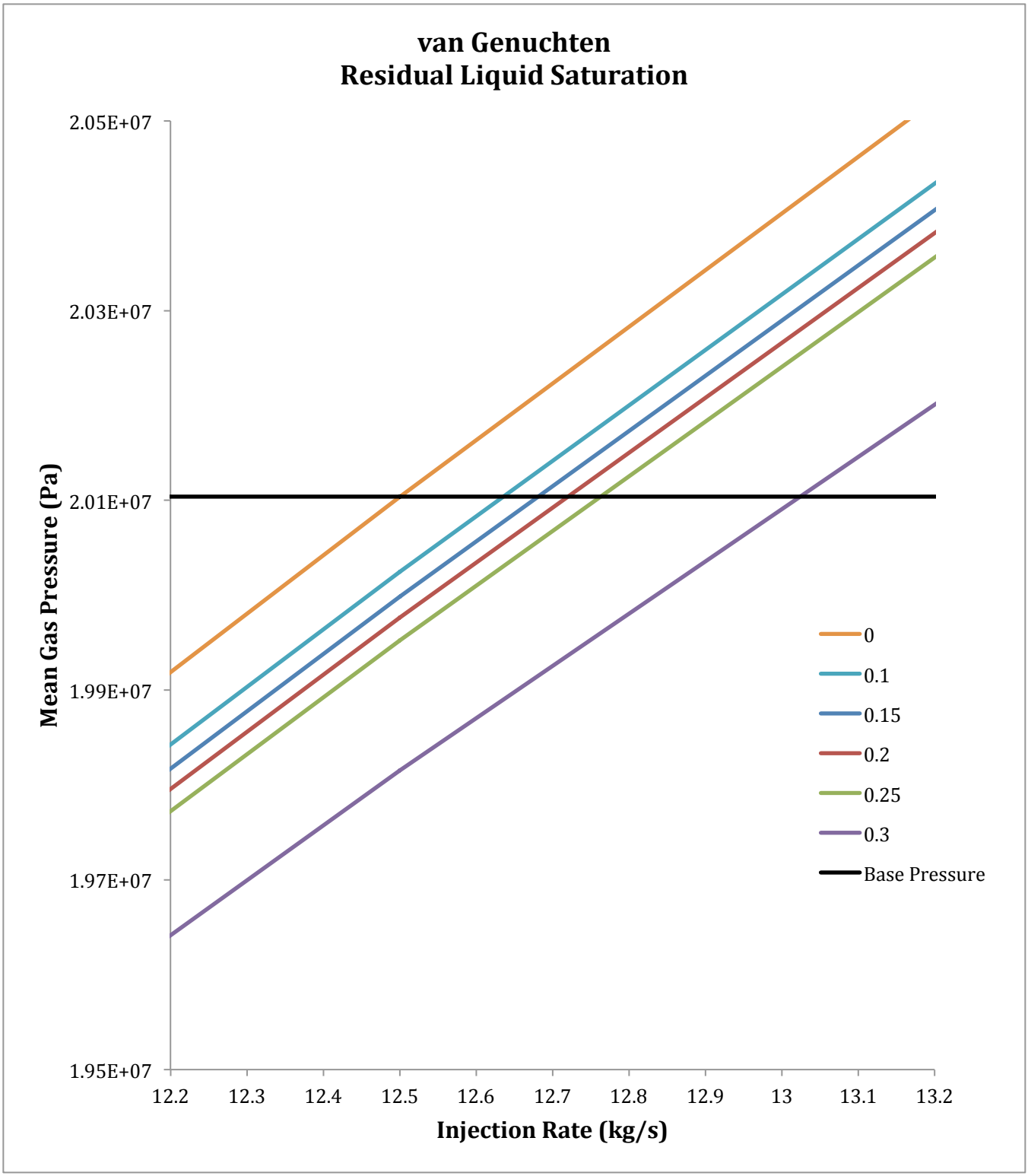

Mean gas pressure as a function of injection rate for various values of the van Genuchten residual liquid saturation. The horizontal line represents the mean gas pressure associated with the base scenario.

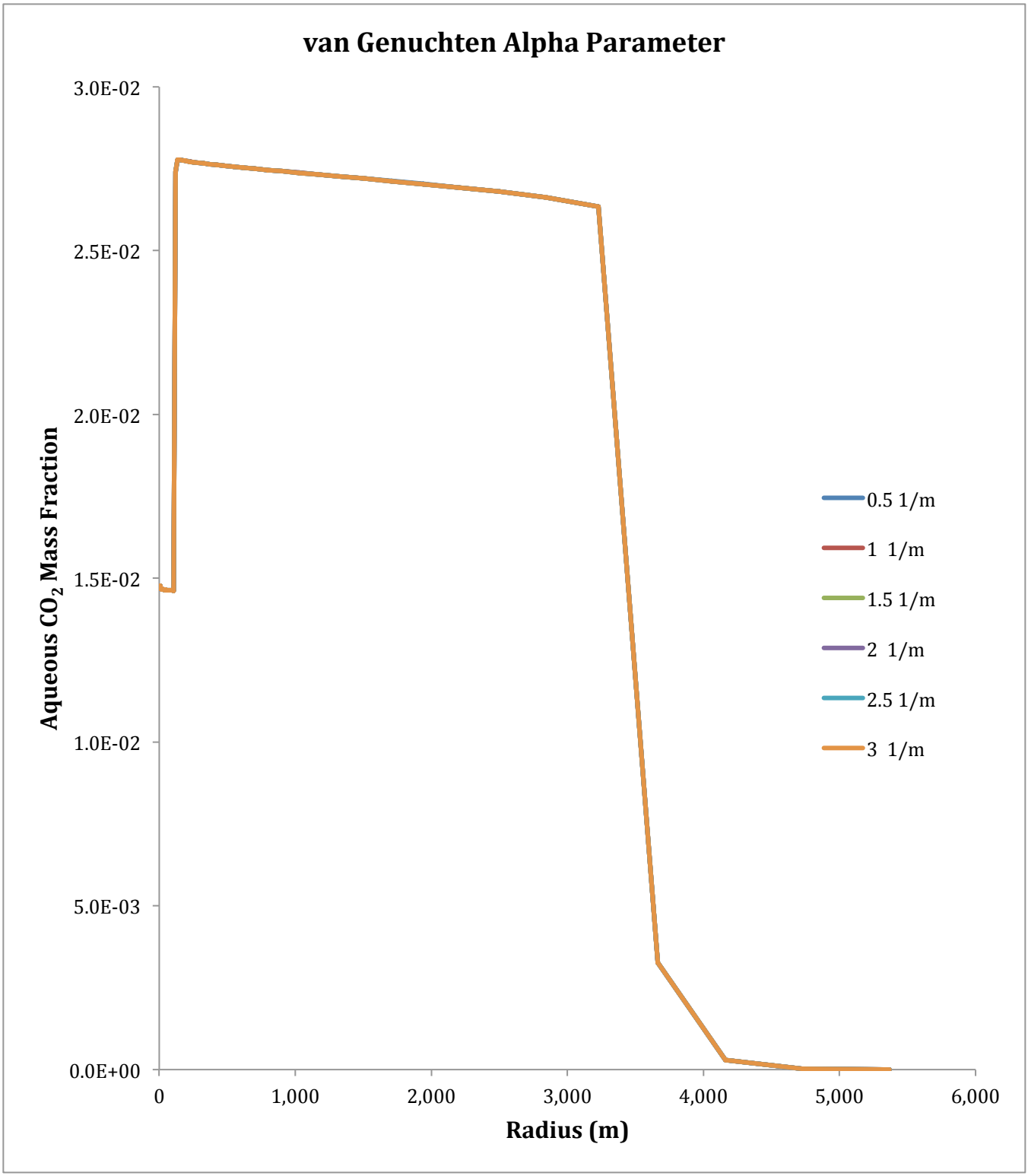

Aqueous CO_2 mass fraction as a function of radial distance from the injection well for various values of the van Genuchten α parameter after approximately 27 years at an injection rate of 12.5 kg/s.

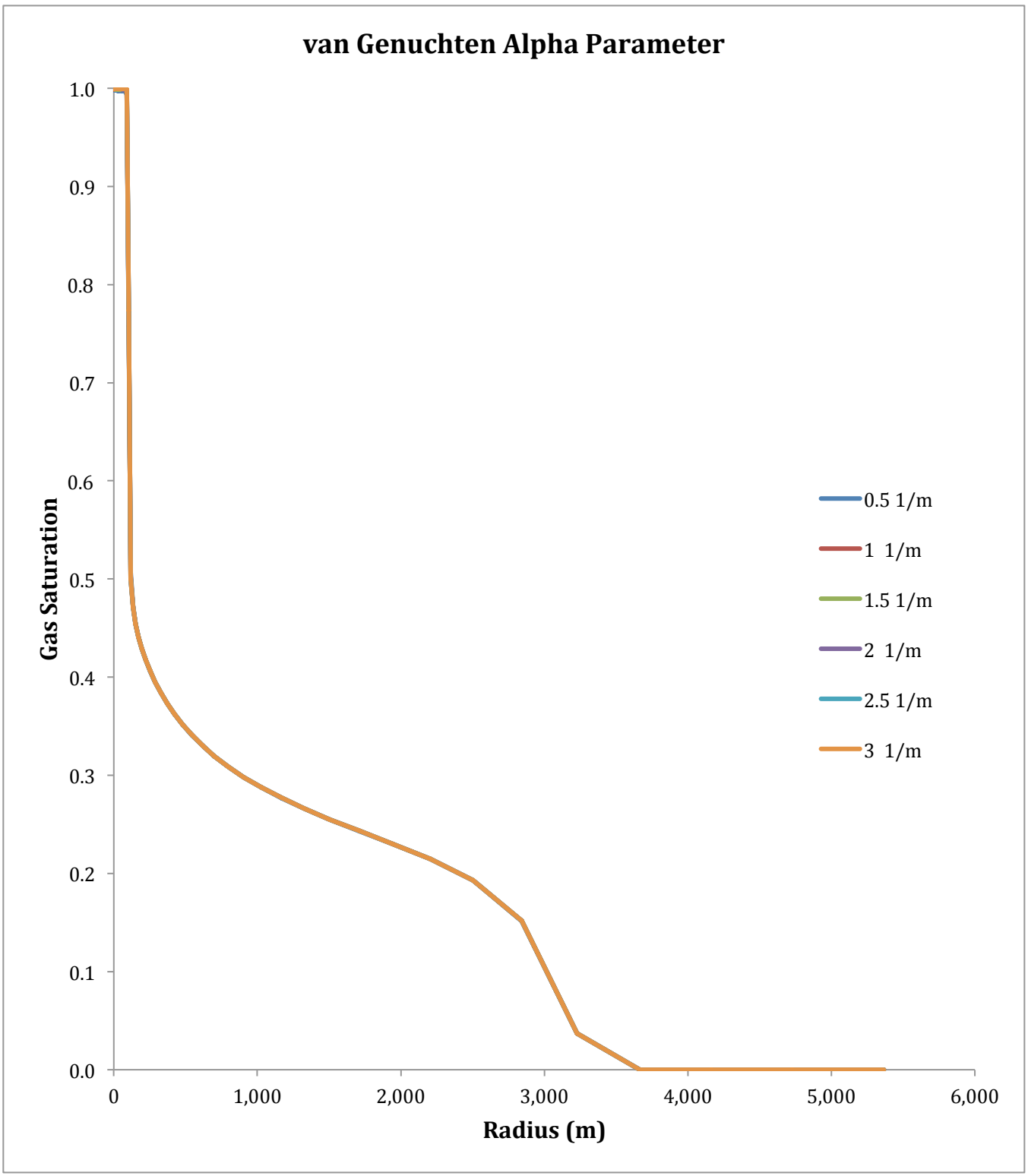

Gas saturation as a function of radial distance from injection well for various values of the van Genuchten α parameter after approximately 27 years at an injection rate of 12.5 kg/s.

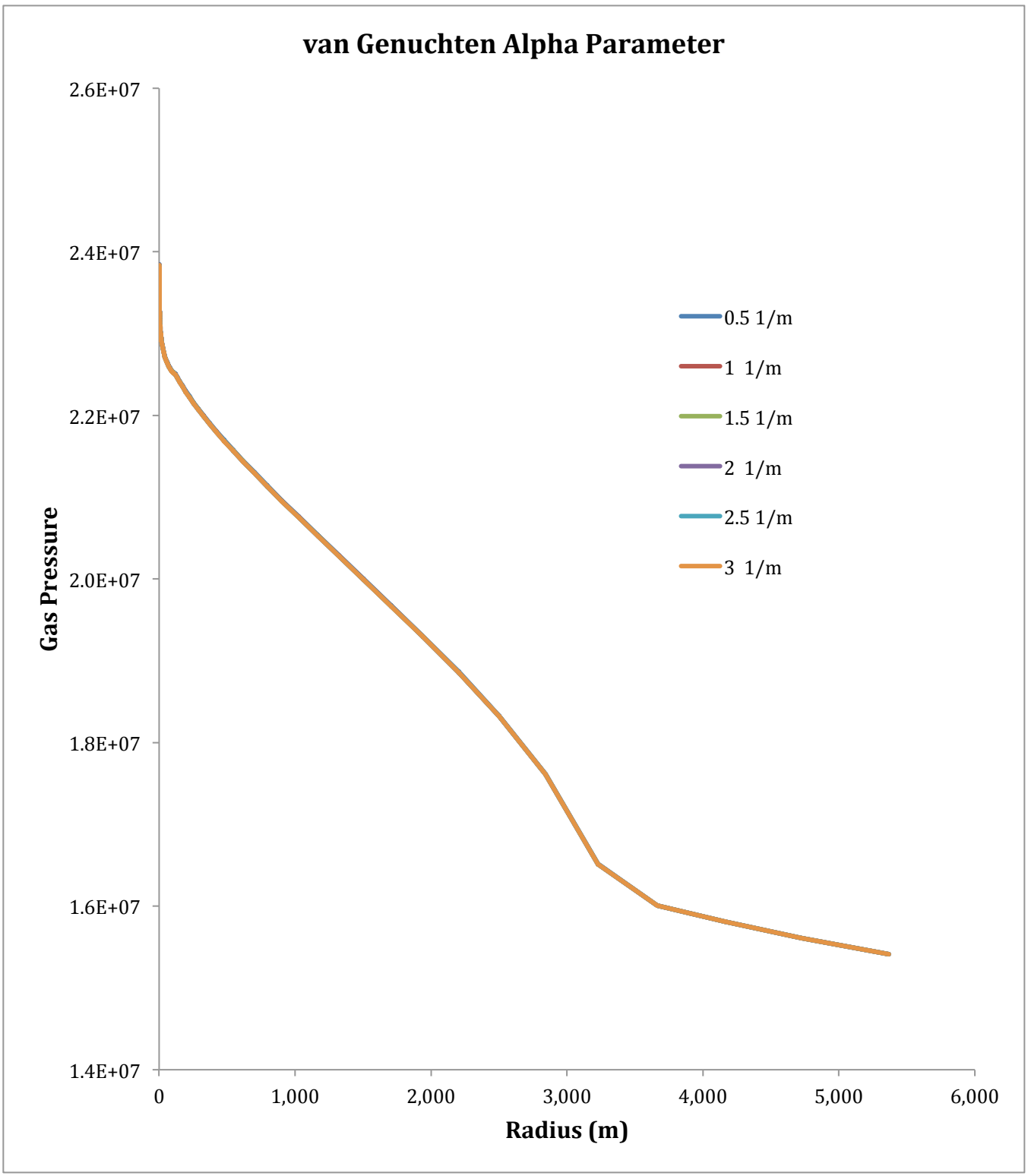

Gas pressure as a function of radial distance from injection well for various values of the van Genuchten α parameter after approximately 27 years at an injection rate of 12.5 kg/s.

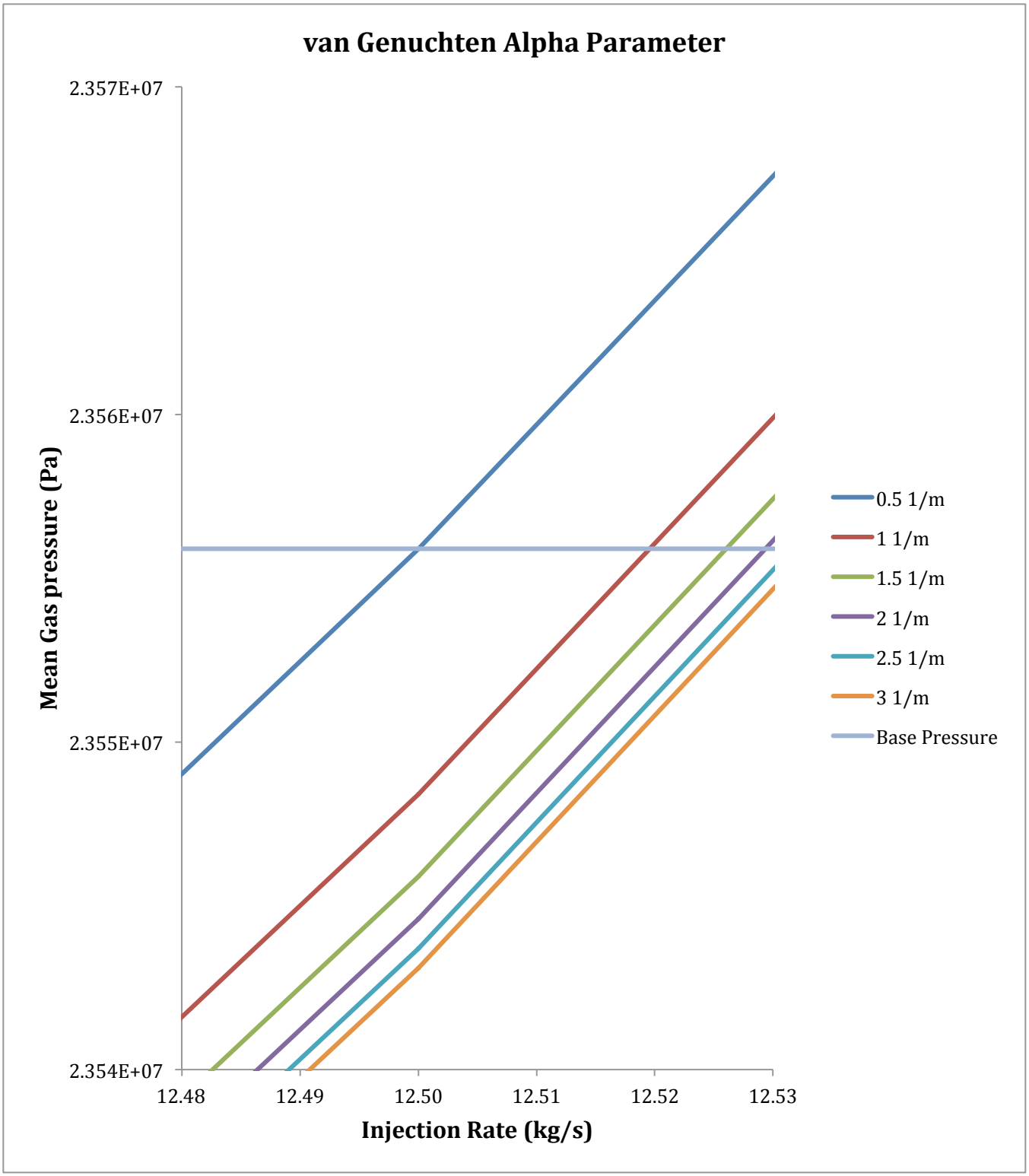

Mean gas pressure as a function of injection rate for various values of the van Genuchten α parameter. The horizontal line represents the mean gas pressure associated with the base scenario.

Vita

Michael Gragg was born in Sandpoint, Idaho, to John and Elizabeth Gragg, and has two younger brothers, Nickolus and Timothy. He attended several elementary schools but graduated from East Bakersfield High School in Bakersfield, California. After graduation he attended Bakersfield Community College, receiving his Associates of Arts degree in Liberal Arts. He and his wife, Gretchen, and their first born son, Elijah, moved to Nashville, Tennessee, where Michael attended and graduated Magna Cum Laude from Austin Peay State University with a Bachelor's of Science degree in geoscience with an emphasis in geology. He and his family then moved to Knoxville, Tennessee, for graduate studies at the University of Tennessee, Knoxville. Michael's thesis topic was carbon sequestration in deep saline aquifers and focused on porosity measurements, numerical modeling, and fluctuations in costs associated with uncertainty of petrophysical parameters. Michael will be graduating with is Master's of Science in geology December of 2012 and plans to enter the environmental consulting field.